# PROTEASOME ACTIVATION BY THE 19S REGULATORY PARTICLE: STRUCTURAL DYNAMICS OF 26S ASSEMBLY AND SUBSTRATE RECOGNITION

A DISSERTATION
SUBMITTED TO THE FACULTY OF THE
UNIVERSITY OF MINNESOTA
BY

**AARON CHRISTOPHER EHLINGER**

IN PARTIAL FULFILLMENT OF THE REQUIREMENTS
FOR THE DEGREE OF
DOCTOR OF PHILOSOPHY

KYLIE J. WALTERS, PhD
ADVISOR

JUNE 2013

# Acknowledgements

I am foremost grateful to Kylie for her tireless work, insights, and perspectives that she has imparted over the course of my work. Simply studying the subject matter had given me a micro-scale perception of research, but Kylie forced me to think beyond what assay to use or how the experiments are run. Instead, she helped me never lose sight of what this data contributes to the project, the system, and potentially even the larger society. The scientific process will always be about people and personalities, and for teaching me to think about research and science in this way, I am supremely thankful.

None of my research would be possible without technical and personal support from members of the Walters Lab. I am indebted to Naixia Zhang and Xiang Chen for teaching me to acquire and interpret NMR data. Xiang was especially helpful for imparting his technical knowledge of many elements of biophysics, bioinformatics, and data presentation. I am similarly grateful to Leah Randles for her exhaustive knowledge of the wet lab and an incredible array of techniques, as well as her empathy for the challenges of being a graduate student. Fen Liu, Yang Kang, Bala Medicherla, Kim Wadsworth, and Fahu He each brought their incredible expertise to the lab, and I thank them for their eagerness to help.

I would also like to acknowledge my thesis committee: Professors Doug Ohlendorf, Gianluigi Veglia, Deanna Koepp and Lincoln Potter. They went to my

*For Dad*

# Abstract

Since its discovery in the late 1970s, the ubiquitin-proteasome system (UPS) has become recognized as the major pathway for regulated cellular proteolysis. Processes ranging from cell cycle control, pathogen resistance, and protein quality control rely on selective protein degradation at the proteasome for homeostatic function. Perhaps as a consequence of the importance of this pathway, and the genesis of severe diseases upon its dysregulation, protein degradation by the UPS is highly controlled from the level of substrate recognition to proteolysis. Technological advances over the last decade have created an explosion of structural and mechanistic information that has underscored the complexity of the proteasome and its upstream regulatory factors. Significant insights have come from study of the 19S proteasome regulatory particle (RP) responsible for recognition and processing of ubiquitinated substrates destined for proteolysis. Established as a highly dynamic proteasome activator, a large number of both permanent and transient RP components with specialized functional roles are critical for proteasome function. This research investigates the dynamic nature of protein-protein interactions involved in proteasome assembly and substrate recruitment, and how they provide context to our current understanding of proteasome activation by the RP.

The RP can exist juxtaposed to either or both ends of the proteasome core particle (CP). RP triphosphatase proteins (Rpt1-Rpt6), which form a

heterohexameric ring and are critical for substrate translocation into the CP, bind chaperone-like proteins (Hsm3, Nas2, Nas6, Rpn14) implicated in RP assembly. NMR and other biophysical methods reveal that the *S. cerevisiae* Rpt6 C-terminal domain undergoes dynamic helix-coil transitions enabled by helix-destabilizing glycines within its two most C-terminal $\alpha$-helices. Rpn14 binds selectively to Rpt6's 4-helix bundle, with surprisingly high affinity. Loss of the Rpt6 partially unfolded state by glycine to alanine substitution (Rpt6 $G^{360,387}A$) disrupts holoenzyme formation *in vitro*, an effect enhanced by Rpn14. *S. cerevisiae* lacking Rpn14 and with Rpt6 $G^{360,387}A$ incorporated demonstrate hallmarks of defective proteasome assembly and synthetic growth defects. Rpt4 and Rpt5 also exchange, suggesting that conserved structural heterogeneity among Rpt proteins may facilitate RP-CP assembly.

Degradation by the RP canonically requires substrate ubiquitination. At least two ubiquitin receptors exist in the RP, S5a/Rpn10 and Rpn13. Whereas Rpn13 has only one ubiquitin-binding surface, S5a binds ubiquitin with two independent ubiquitin interacting motifs (UIMs). The NMR experiments described here reveal that Rpn13 and S5a bind K48-linked diubiquitin simultaneously with subunit specificity, and a model structure of S5a and Rpn13 bound to K48-linked polyubiquitin is provided. Altogether, these data demonstrate that S5a is highly adaptive and cooperative towards binding ubiquitin chains, and dynamics may facilitate substrate recognition coordinately through multireceptor avidity-mediated effects.

# Table of Contents

# List of Tables

# List of Figures

# Introduction[‡]

A major aspect of eukaryotic cell maintenance and viability is the rapid and selective turnover of misfolded, exogenous, or down-regulated proteins. As a culmination of cell signaling events, these proteins are frequently targeted to the 26S proteasome, a 2.5 MDa protease responsible for catalyzing the decomposition of proteins into short peptides. Proteasome substrates are typically marked by covalent attachment of ubiquitin polymers, which are recognized by 26S machinery as a signal for destruction. Together, the ubiquitin-proteasome system (UPS; see Table 1 for abbreviations) constitutes a major and highly conserved pathway for targeted protein degradation[1–3]. Improper function of the UPS can result in a variety of human pathologies, including autoimmunity and inflammation, neurodegeneration, and cancer[4]; thus the proteasome is a promising therapeutic target. bortezomib (Velcade®) and carfilzomib (Kyprolis™) are proteasome inhibitors used to treat certain hematological cancers, and other inhibitors are in clinical trials[5,6].

---

**Table 1.** Abbreviations of the ubiquitin-proteasome system

| Abbreviation | Description |
| --- | --- |
| 26S | 19S Regulatory Particle with the 20S Core Particle |
| AAA ATPases | ATPases Associated with diverse Activities |
| Ar-φ | Aromatic-Hydrophobic |
| CC | Coiled Coil |
| CP | 20S Core Particle |
| DUB | Deubiquitinating Enzyme |
| HbYX | Hydrophobic–Tyrosine–Any Amino Acid |
| MPN | Mpr1, Pad1, N-terminal |
| OB | Oligonucleotide/oligosaccharide-Binding |
| PAN | Proteasome Activating Nucleotidase |
| PC | Proteasome, Cyclosome |
| PCI | Proteasome, COP9, Initiation factor 3 |
| Pru | Pleckstrin-like Receptor of Ubiquitin |
| RP | 19S Regulatory Particle |
| Rpn | Regulatory Particle Non-ATPase |
| Rpt | Regulatory Particle Triphosphatase |
| Ub | Ubiquitin |
| UBL-UBA | Ubiquitin-like – Ubiquitin-associating |
| UIM | Ubiquitin Interacting Motif |
| UPS | Ubiquitin-Proteasome System |
| VWA | von Willebrand factor type A |

A highly regulated enzymatic cascade coordinates the recognition of protein substrates, as reviewed[7–9]. These enzymes are responsible for both selection of proteasome targets and catalyzing the attachment of ubiquitin polypeptides. Ubiquitin moieties are typically conjugated through an isopeptide bond between their C-terminal glycine carboxylate and a free amine on another protein. Ubiquitination may occur either on a substrate or on another ubiquitin to form a polymeric chain. Ubiquitinating enzymes can function with strict chemical specificity for one of ubiquitin's seven lysines or its N-terminal methionine. Different linkage types confer unique chain topologies that are recognized by ubiquitin-binding proteins to select for substrates with a particular chain length or structure[10–12]. Some types, such as K63-linked chains, can signal for non-degradative events like cell trafficking, activation of NF-κB signaling, and DNA damage response[13,14]. Each of ubiquitin's seven lysines appear to target substrates for proteasomal degradation in yeast except K63[15], whose extended chain conformation[16,17] binds factors that prevent proteasome association[18]. K48 and K11 constitute the largest relative cellular abundance of chains in yeast at ~30% each, with K63 third at slightly more than half that amount[15]. A similar study in human embryonic kidney 293 cells observed a higher relative proportion of K48- and K63-linked chains at 52% and 38%, respectively[19].

The basic component of the proteasome is the 20S core particle (CP)[20], a barrel-shaped protease composed of four heptameric rings of $\alpha$ and $\beta$ subunits

3

that stack in a $\alpha_7\beta_7\beta_7\alpha_7$ structure[21]; these subunits are related but unique in eukaryotes[22] (Figure 1A). Three interior chambers are formed at ring interfaces, including two antechambers at the $\alpha_7\beta_7$ ring interfaces and a catalytic chamber at the $\beta_7\beta_7$ ring interface (Figure 1B). The catalytic chamber contains the proteolytic activity of the proteasome[23], whereas the antechamber maintains substrates in an unfolded state prior to their proteolysis[24]. Peptide hydrolysis is catalyzed by conserved threonines at the N-termini of the eukaryotic $\beta1$, $\beta2$, and $\beta5$ subunits with a caspase, trypsin, and chymotrypsin-like specificity, respectively[25]. bortezomib inhibits proteolysis through its ability to bind all three catalytic pockets, with highest affinity for $\beta5$[26,27] (Figure 1C). The CP is competent to cleave unstructured proteins in a ubiquitin-independent pathway accounting for up to 20% of cellular targets[28], but this process provides little means for substrate specificity and is ineffective for folded proteins, as the N-terminal region of the $\alpha$ ring subunits contain an axial gate that sterically occludes folded proteins from entering[29]. Upon CP activation by native proteins or chemical agents, the gating residues shift to a conformation that provides access to the CP interior[30,31].
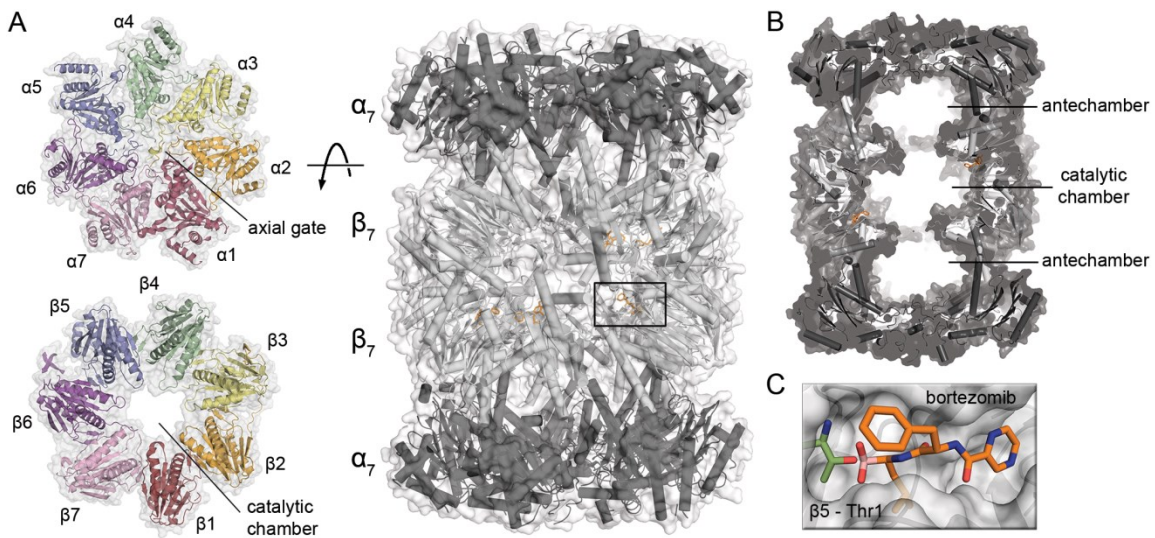
**Figure 1.** Structure of the 20S core particle

**(A)** Structure of the *Saccharomyces cerevisiae* CP ($\alpha$ rings in dark gray, $\beta$ rings in light gray) bound to bortezomib (orange; PDB entry 2F16), as well as a view of the $\alpha$- and $\beta$- rings that highlight the axial gate and catalytic chamber. The unique subunits of the eukaryotic CP are indicated.
**(B)** A cross-section of the CP illustrating the catalytic chamber and both antechambers.
**(C)** A zoomed view of the catalytic pocket of the $\beta5$ subunit showing its N-terminal threonine bound to bortezomib.

## Proteasome activation

Cells use a variety of proteins or protein complexes, known as activators, that dock into the CP, open its gate, and make it accessible for proteolysis[32]. Structural data have yielded insights into mechanisms of activator action on the CP[33], although their substrate specificity, biological relation to each other, and the cellular triggers for their interaction with CP remain under intense scrutiny.

## Diversity of activators

Endogenous CP activators include Blm10 (PA200)[34,35], 11S (PA28 or REG)[36,37], the RP (PA700)[38], and Cdc48 (p97)[39,40]. Multiple activators share a common mechanism for CP binding in which a hydrophobic residue–tyrosine–any amino acid (HbYX) C-terminal motif docks into cavities formed at the $\alpha$ ring subunit interfaces and induces gate opening[41,42]. Blm10[43] contains a single C-terminal HbYX, whereas Cdc48[39] and the RP[41] contain a ring of six AAA+ ATPases that use HbYX motifs to dock into the CP's $\alpha$ ring pockets. The RP ATPase ring is composed of unique Regulatory Particle Triphosphatase (Rpt) proteins, and the strict HbYX motifs of Rpt2, Rpt3, and Rpt5 dock the RP into the CP in mature holoenzymes[44,45]. PI31 and the Pba1-Pba2 (PAC1-PAC2) heterodimer also use HbYX motifs to dock into the CP, although these interactions lead to its inhibition[46,47]. Pba1-Pba2 promotes CP maturation[48], and in contrast to activators, binding of its HbYX motif to CP leads to a gate configuration that is not sufficiently

opened for proteolysis of even small peptides[49]. Whereas PI31 inhibits CP[46], it stimulates proteolysis by CP-RP complexes[50].

Studies in archaea, have revealed a similar role for the HbYX motif of RP functional homolog Proteasome Activating Nucleotidase (PAN)[41,51], but neither its HbYX motif nor that of archaeal Cdc48 are required for CP binding and activation[39,40]. Archaeal Cdc48 uses a bipartite binding mode to bind CP that includes its HbYX and a conserved AAA loop that is expected to be proximal to CP $\alpha$ ring gating residues[40]. A similar motif exists at this location in PAN and the Rpts[51], and in PAN, these loops appear to enable CP binding when its HbYX is deleted[40].

The RP is a ~19 subunit complex of stably and transiently associated proteins that caps the CP to form the 26S proteasome used by the UPS. It includes ubiquitin receptors to recognize substrates, deubiquitinating enzymes to remove ubiquitin, and its six Rpt proteins to facilitate substrate unfolding and translocation into the CP (Figure 2). The Rpts contain an N-terminal coiled-coil (CC) that engages in extensive Rpt-Rpt contacts, an oligomer-binding (OB) domain, an ATPase domain, and a C-terminal domain (CTD) (Figure 3). Currently, no high resolution structure is available for a full Rpt molecule. Cryoelectron microscopy (EM) data combined with cross-linking and interaction studies, as well as experimentally determined or modeled structures of RP components, have enabled production of full RP models to ~7-9 Å resolution[44,45,52–55]. In these models, the Rpts adopt a Rpt1-Rpt2-Rpt6-Rpt3-Rpt4-Rpt5[56] arrangement that

forms an asymmetrical lock washer-like structure relative to the CP with Rpt2 at the lowest end and Rpt3 at the highest end; Rpt6 is at their interface in an intermediate configuration[45].

PAN similarly forms an AAA+ hexameric ring structure, although a homohexamer. A crystal structure of an 11S fusion protein containing the PAN HbYX motif bound to CP illustrates CP-HbYX contacts[57] that are critical for PAN activation[42] and are expected to be conserved in Rpt2, Rpt3, and Rpt5. Although not docked into the CP $\alpha$ ring in mature proteasomes, Rpt6 contains a non-canonical HbYX variant that binds with high specificity to the $\alpha2\alpha3$ CP pocket during RP assembly, suggesting that the Rpt proteins are reconfigured during proteasome maturation[58]. Their reorganization may be facilitated by their own dynamic behavior, as EM variability maps demonstrate a high degree of heterogeneity in the Rpt region of mature proteasome[52], and ATP binding and hydrolysis elicit conformational changes in the ring[55]. ATP$\gamma$S-binding to subunits within PAN similarly induces conformational changes in the unbound subunits that reduce their ATP$\gamma$S affinity[59].
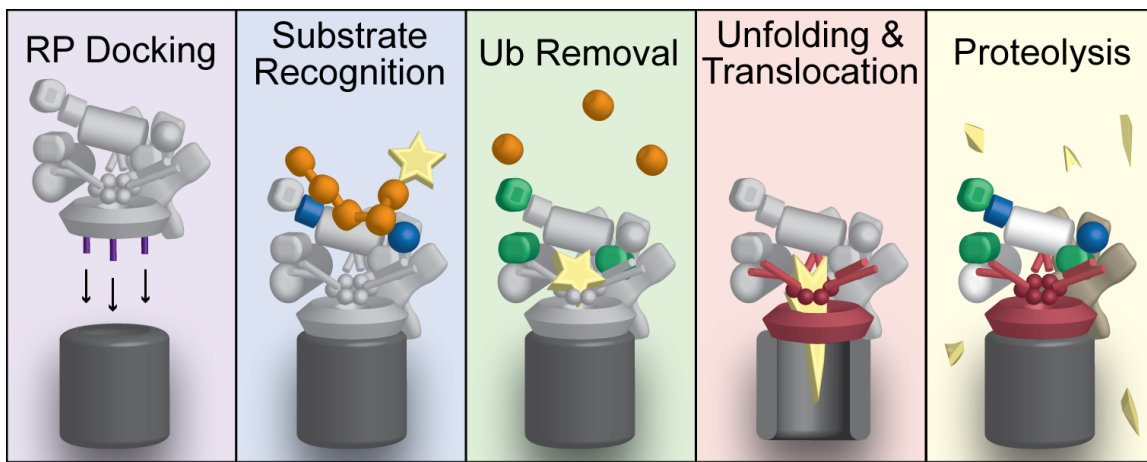
**Figure 2.** Pathway of 26S proteasome function

The RP activator caps the CP to form the 26S proteasome, which makes it competent for ubiquitin-mediated substrate degradation. The RP (light gray) templates onto the CP (dark gray) using C-terminal HbYX motifs (purple) that dock into pockets between the CP's $\alpha$ ring subunits. Substrates (yellow) may then be recognized by ubiquitin receptor proteins (blue) that bind to the ubiquitin moieties (orange) covalently attached to the substrate. Ubiquitin is then removed and recycled by deubiquitinating enzymes (green) in a function that is coupled to substrate and nucleotide binding by the ATPase ring (red). ATP hydrolysis produces conformational changes in the ATPases, which aids in the unfolding and translocation of the substrate into the CP where it is proteolyzed into short peptides.
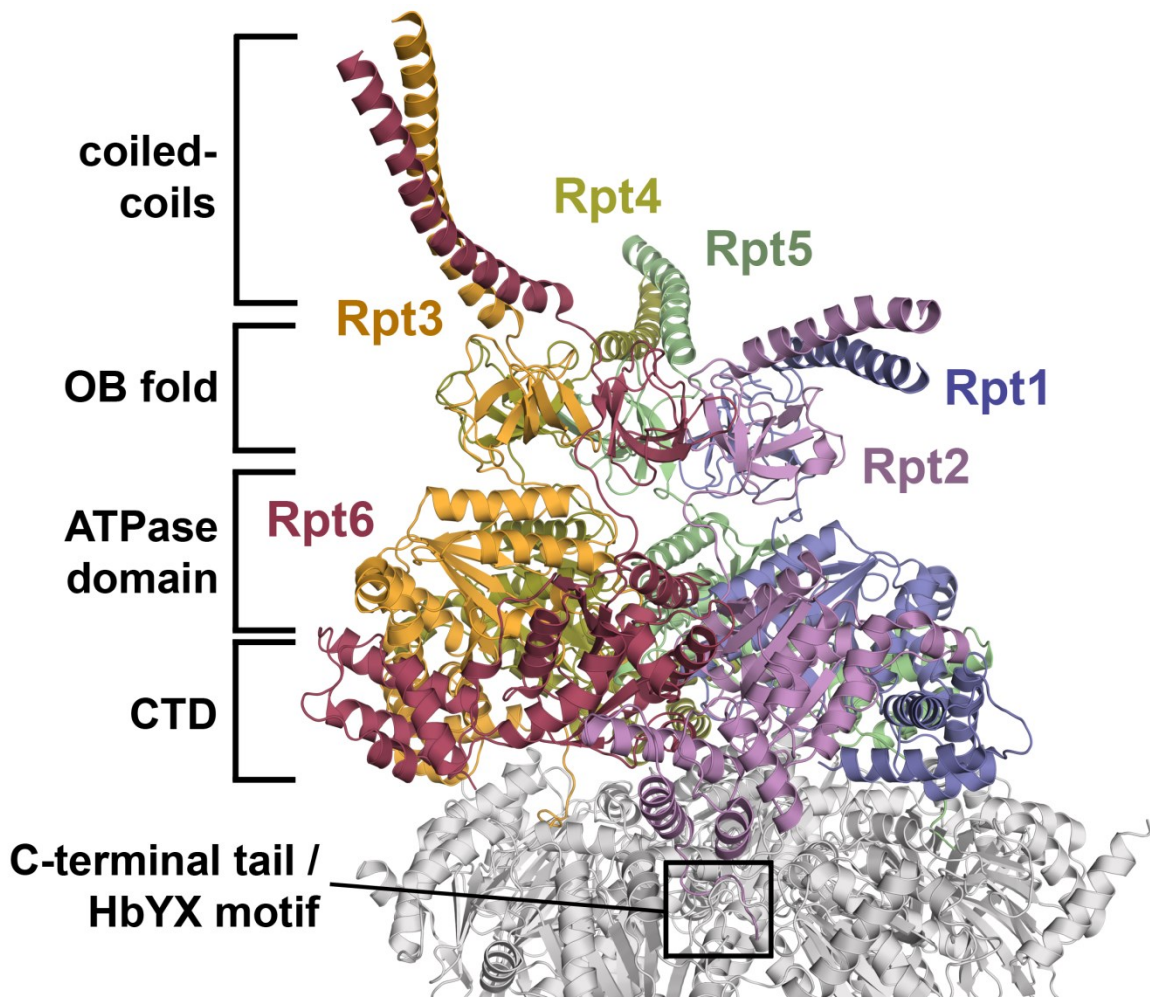
**Figure 3.** Arrangement of the Rpt ATPases

Model of the Rpt ATPases bound to the CP (light gray), determined by homology modeling from structures of PAN. Each subunit contains a coiled-coil (CC), OB fold, ATPase, and C-terminal domain (CTD). Rpt2, Rpt3, and Rpt5 have a C-terminal HbYX motif docked into the CP. The ATPases were fit in a 1-2-6-3-4-5 arrangement into a cryo-EM reconstruction (PDB entry 4B4T), and form an asymmetric 'lock washer'-like ring that is offset from the CP's axial pore.

Crystallographic structures of the ATP-independent Blm10[43] and 11S activators[42,60,61] complexed with CP illustrate their mechanism of gate opening. The 11S binds the CP as a heptamer and uses its C-termini to dock into the same CP pockets used by HbYX motifs[61]. The 11S does not contain the HbYX motif, and relies on the binding of activator loops adjacent to this pocket for gate opening[62]. This interaction initiates a conformational change in critical N-terminal gating residues Y8, D9, P17, and Y26 and opens the pore[63]. The 11S appears to perform ATP-independent proteolysis of short or intrinsically unfolded peptides to produce immune response factors such as MHC class I peptides[64,65].

Yeast Blm10 caps the CP $\alpha$ rings as a single 246 kDa protein, surrounding the entrance pore and with its C-terminal HbYX motif docked into the $\alpha5\alpha6$ pocket[43]. Its binding causes the gating residues to become disordered, partially opening the pore[43] and thus providing a mechanism for its proposed role in facilitating degradation of unfolded proteins[66]. Blm10 has been implicated in DNA repair[34], mitochondrial maintenance[43], as well as CP assembly and maturation[67], and can be found in mixed Blm10-CP-RP proteasomes[34].

## Composition of the RP

The RP can be biochemically divided into lid and base sub-assemblies[68]. The base comprises the six Rpt proteins, Regulatory Particle non-ATPase (Rpn) proteins Rpn1/2 (S2/S1 in humans), and ubiquitin receptors Rpn10 (S5a)[69] and Rpn13[70,71]. The lid contains Rpn8, Rpn15 (DSS1 or Sem1), deubiquitinating

enzyme (DUB) Rpn11 (Poh1)[72,73], as well as PCI-domain proteins Rpn3/5/6/7/9 with poorly understood functions and Rpn12, which has been implicated in late-stage assembly of the RP[74,75] (Figure 4). The base and lid are laterally adjacent relative to the CP pore in EM-based models with the PCI C-terminal regions in the formation of a hexameric shield-like structure lying opposite from the translocation pore[44] (Figure 4). PCI lid subunits contact ATPases (Rpn5/6/7) and the CP (Rpn5/6) in addition to Rpn11 and Rpn2[44,76]; thus the base and lid form extensive contacts.

Rpn1 and Rpn2 are ~100-110 kDa and structurally similar[77]; the crystal structure of Rpn2 forms a toroidal conformation of two concentric $\alpha$-helical PC repeats[78], which is consistent with the fold produced by EM analysis of Rpn1[78]. Their positioning in the RP has been controversial[77,79]. EM models place Rpn1 along the perimeter of the Rpt ring and in contact with the Rpt1/2 dimer[44,53] while Rpn2 extends from the N-terminal region of Rpt3/6, across Rpn8/11 and to the periphery of the lid[44,45,53]. The electron density from Rpn1 in EM reconstructions is weak, suggesting that its location may be dynamic[44]. Rpn1 binds ubiquitin receptor UBL-UBA proteins Dsk2 and Rad23[80–82] as well as the DUB Ubp6[83], and Rpn2 uniquely binds ubiquitin receptor Rpn13[84–86].
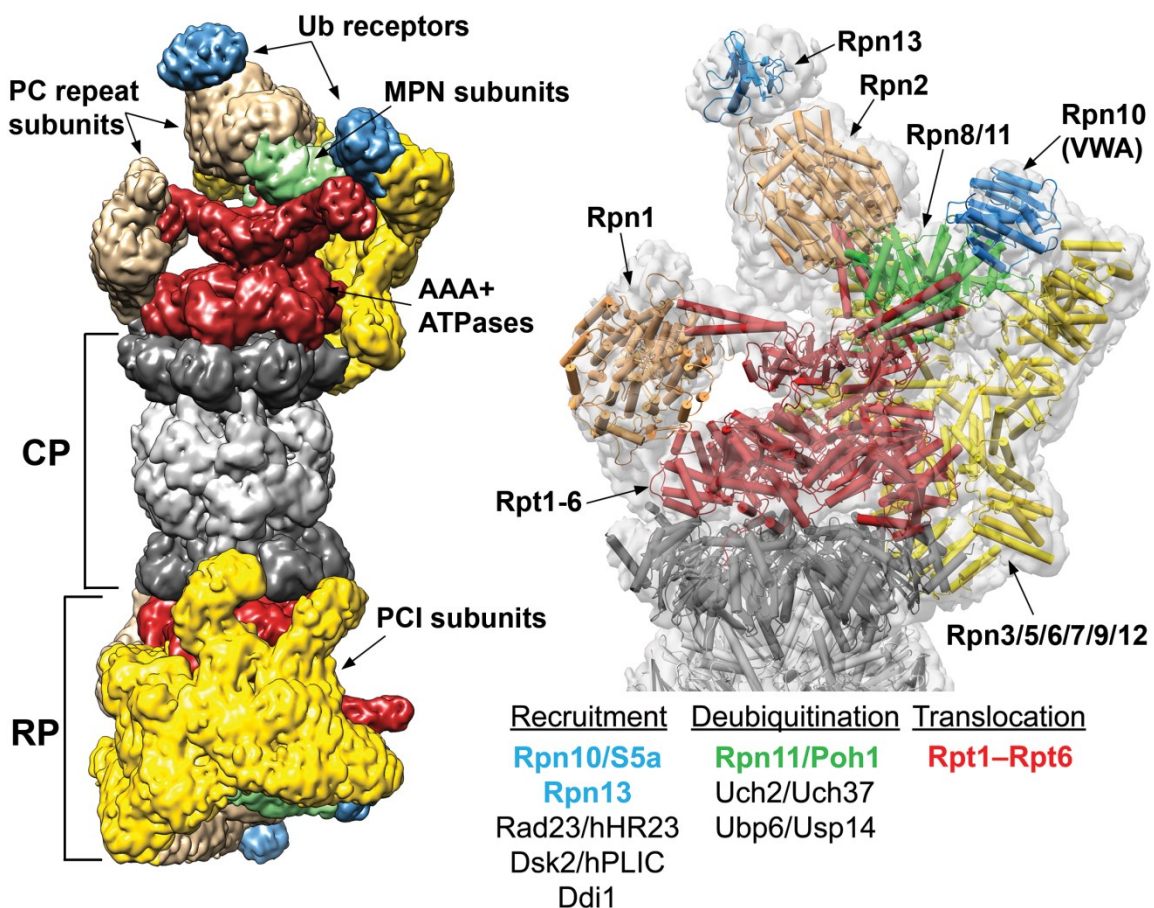
**Figure 4.** Electron microscopy models of the RP

Structure of the *S. cerevisiae* 26S proteasome by cryoEM (EMDB entry 2165)[54], illustrating the CP (gray) bound to two RP caps. Each RP is composed of the Rpt ATPases (red), ubiquitin receptors Rpn10 and Rpn13 (blue), MPN domain proteins Rpn8 and Rpn11 (green), PC repeat proteins Rpn1 and Rpn2 (beige), and PCI domain proteins (yellow). The subunits that perform ubiquitin recruitment, deubiquitination, and substrate translocation are indicated below and for those present in the model, are colored accordingly.

## Substrate recruitment

The RP has a diverse arsenal of ubiquitin receptors for substrate recognition. These include Rpn10 and Rpn13, which have dedicated binding sites in the RP, and UBL-UBA proteins, which appear to shuttle ubiquitinated cargo to proteasome through multiple overlapping docking sites.

## Ubiquitin receptors in the RP

Rpn10 (S5a) was the first discovered RP ubiquitin receptor[69], and contains an N-terminal von Willebrand factor type A (VWA) domain that docks it into the RP and one or two ubiquitin interacting motifs (UIMs), depending on species. Human Rpn10's two UIMs are composed of single helices connected by flexible regions that allow it to adapt to bind diverse ubiquitin chains[87,88] (Figure 5). This multivalency affords hRpn10 an 8-fold greater affinity for K48-linked diubiquitin compared to monoubiquitin[88]. A second receptor, Rpn13, contains an N-terminal pleckstrin-like receptor for ubiquitin (Pru) domain that interacts with ubiquitin through a surface formed by three loops[70,71] (Figure 5). Rpn13 gains additional affinity upon binding to ubiquitin moieties engaged in a G76-K48 isopeptide bond, giving it a 3-fold greater affinity for K48-linked diubiquitin over monoubiquitin[71]. Most ubiquitin-binding elements recognize a common surface that includes a hydrophobic pocket formed by L8, I44, and V70[13]. Rpn13's Pru and Rpn10's UIMs also bind to this surface[70,87]; however, Rpn13 engages in additional hydrogen bonds with ubiquitin's H68[70].

In contrast to Rpn10, Rpn13 uses its ubiquitin-binding domain to dock into the RP, and does so through Rpn2[85,89]. With the exception of *S. cerevisiae*, Rpn13 contains a 9-helix C-terminal domain that recruits DUB enzyme Uch37 to proteasome[85,89,90] and activates it[89,90]. The two structural domains of Rpn13 are connected by a flexible, low complexity linker, but interact when free of the RP, resulting in reduced affinity for ubiquitin[91]. The interdomain interaction is along a similar surface to where Rpn2 binds, and docking to Rpn2 dissociates Rpn13's interdomain interaction and activates it for ubiquitin binding[91].

The functional roles of the two receptors are not fully redundant, despite both binding ubiquitinated substrates. Knockout of Rpn10 or its UIMs is embryonic lethal in mice[92], and Rpn13 mice knockouts demonstrate growth defects and reduced litter size[93]; thus loss of one receptor cannot be fully rescued by the other. One possible explanation is the existence of receptor-specific substrates, which have been reported for both Rpn13[94,95] and Rpn10[96]. In addition, Rpn10 was found to bind the DUB Rpn11 and proposed to be important for proteasome integrity[97].
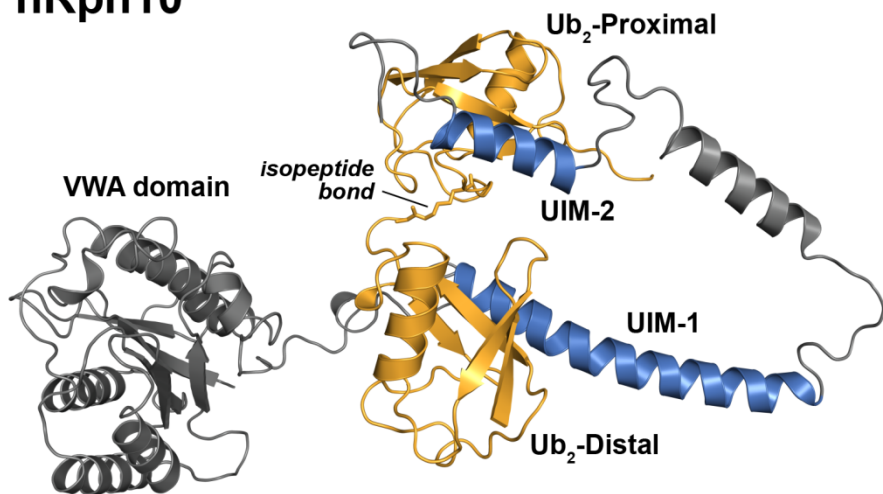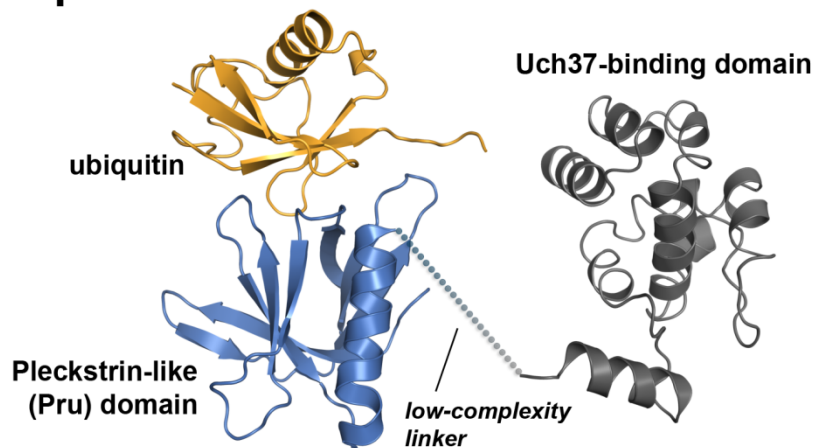
**Figure 5.** Structure of hRpn10 and hRpn13 bound to ubiquitin

Structures of human proteasome ubiquitin receptors hRpn10 (S5a) and hRpn13. hRpn10's UIMs (blue) are bound to ubiquitin moieties (orange) of K48-linked diubiquitin (PDB entry 2DKE). Its VWA domain was modeled separately (based on PDB entry 2X5N) to create full-length human Rpn10. hRpn13 Pru domain (blue) is bound to monoubiquitin (orange; PDB entry 2Z59). A low-complexity linker adjoins hRpn13's Pru domain with its C-terminal Uch37-binding domain (PDB entry 2KQZ).

Rpn10 and Rpn13 may not simply work as independent ubiquitin-sensing components, but rather coordinately bind ubiquitin chains on the same substrate. Both receptors bind simultaneously to K48-linked diubiquitin[88] and in this ternary complex, Rpn13 binds to the ubiquitin with its K48 involved in an isopeptide bond (proximal), while hRpn10's two UIMs interact dynamically with the other moiety (distal). In longer chains, it is likely that both UIMs interact cooperatively with different ubiquitins. EM models place Rpn10's VWA domain above the translocation pore and adjacent to Rpn11 whereas Rpn13's Pru domain lies ~90 Å away in a flag-like position at the distal end of the RP[44,45] (Figure 4). Ubiquitin chains that span this distance may enable dual binding of Rpn13 and Rpn10. It is not yet clear whether substrate binding alters the configuration of the ubiquitin receptors and DUBs to facilitate their coordinated activities.

Cross-linking studies have also implicated proteasome subunits Rpt5[98], Rpt1[99], and Rpn1[99] in binding ubiquitin chains, and the recruitment of ubiquitin chains to the proteasome by Rpn13 or Rpn10 may enable additional interactions through avidity effects[100]. Rpt1/5 and Rpn1 would provide additional docking sites for the ubiquitin chain near the CP, according to EM structures (Figure 4). Additional ubiquitin receptors have been demonstrated to exist in the RP as deletion of Rpn10's and Rpn13's ubiquitin-binding capacity does not eliminate RP binding of ubiquitinated proteins[71,91].

## UBL-UBA ubiquitin receptors that interact with the RP

UBL-UBA proteins appear to contribute an additional layer of regulation to degradation by the UPS. They contain a ubiquitin-like domain (UBL) named for its homology to ubiquitin, and ubiquitin-associating domains (UBA), which bind ubiquitin[101,102]. There are three UBL-UBA proteins in yeast, Rad23, Dsk2 and Ddi1, which have multiple orthologs in higher eukaryotes. UBL-UBA proteins have diverse ubiquitin chain specificities[103]. hHR23a's (human Rad23) C-terminal UBA domain prefers K48-linked chains[104] and inserts between neighboring ubiquitin moieties[105], whereas the hPLIC1/ubiquilin-1 (human Dsk2) UBA domain binds with significantly higher affinity to monoubiquitin than does hHR23 and does not exhibit notable preference for K48- versus K63-linked ubiquitin chains[106].

Rad23 and Dsk2 UBL domains bind Rpn10[107,108], Rpn13[71], and Rpn1[82], and proteomics studies from human cells identify hPLIC1 and hHR23B associated with RP[109]. Furthermore, hHR23B is reported to stimulate proteasome binding of K48-linked chains[18], and is essential for viability in over 90% of mice[110]. Like Rpn13, hHR23a's ubiquitin-binding domains engages in interdomain interactions, in this case with its UBL domain[111]. This interaction may convey selectivity for higher affinity ubiquitin interactions, as hHR23a's affinity for ubiquitin is increased when its UBL domain is deleted[112]. Depending on their protein levels, UBL-UBA proteins can facilitate or inhibit the degradation of ubiquitinated substrates[113], suggesting a complex role with the UPS. hHR23 proteins have long flexible linker regions connecting their functional domains[111], but their non-complex amino acid

composition protects these proteins from proteolysis by proteasome[114]. UBL-UBA proteins share redundant functions[115–118] and can bind each other[119], but they also have distinct roles, such as for Rad23 in DNA repair[120] and Dsk2 in neuropathology[121].

## Substrate processing

The axial channel of the CP is ~13 Å when open[21], a sufficiently narrow space to prevent the passage of the majority of ubiquitinated substrates in their native form. Moreover, ubiquitin forms a very stable structure with a melting temperature in excess of 80 °C[122], and turnover of stably folded proteins proceeds slowly due to the high energy requirement for their thermodynamic destabilization[123]. Thus, DUB removal and recycling of ubiquitin is coordinated with substrate unfolding and translocation into the CP for proteolysis.

## Deubiquitination

The RP lid metalloenzyme Rpn11 (Poh1) is critical for degradation-coupled substrate deubiquitination[72,73,124], and its activity in mature proteasomes requires ATP hydrolysis[72,73]. It is placed above the ATPases and near the translocation pore by EM[44,45,54] (Figure 4). Cross-linking studies on *Schizosaccharomyces pombe* co-localize the Rpn11 C-terminal domain with the N-terminal end of Rpt3[52], potentially linking its activity to this ATPase. ATP hydrolysis by the Rpt proteins may initiate a "commitment step"[125], whereby an unstructured end of the substrate is bound

tightly through conformational changes in the Rpts that position it in an orientation to allow deubiquitination[52]. Consistent with this model, Rpn11 preferentially hydrolyzes isopeptide linkages at the ubiquitin proximal to the substrate, thus cleaving the ubiquitin chain as a whole[72].

Rpn11 and Rpn8 both contain N-terminal MPN domains and these two proteins interact in the RP[44,45]. The MPN domain in Rpn11 coordinates a zinc ion and catalyzes deubiquitination[72,73], whereas Rpn8 lacks a zinc-binding motif and is unlikely to perform DUB activity[124]. Overexpressed Rpn8 can partially rescue phenotypes of Rpn11 C-terminal domain mutation[126], suggesting that it may aid Rpn11 through a non-catalytic role. The exact function of Rpn8 and its link to Rpn11 is not known.

Although removal of ubiquitin is an important step in RP processing, it is antagonistic for degradation if it occurs prematurely. If the chain is shortened or eliminated prior to substrate commitment, the target protein may escape. The RP houses two additional DUBs responsible for shortening ubiquitin chains. Ubp6 (Usp14)[83,127] and Uch2 (Uch37)[128] cleave short polymers from ubiquitin chains, which may delay proteolysis[129]. Curiously, Ubp6 appears to maintain inhibitory effects on substrate turnover even in catalytically inactive mutants[129], suggesting that it may assume non-catalytic roles in proteasome regulation. Studies have linked Ubp6 to RP assembly[130] and channel opening[131].

Uch37 (also known as UCHL5) binds to the C-terminal domain of Rpn13, which activates it and brings it in proximity to RP-bound substrates[85,89,90]. It is

reported to selectively remove single ubiquitin moieties from the distal end of chains, and it therefore may be responsible for processing poorly ubiquitinated or unproductively bound substrates[128]. That Uch37 binds and is activated by Rpn13 raises the potential for its selective activity on substrates docked via Rpn13.

## Unfolding and translocation

Substrate interaction with the Rpt proteins is thought to initiate through intrinsically unfolded regions[132], and occur through a stepwise process that couples ATP hydrolysis with unfolding. PAN[133] and the bacterial AAA ATPases HslU[134], ClpA[135,136], and ClpX[137,138] contain aromatic residue–hydrophobic residue (Ar-$\phi$) loops in their ATPase domain that undergo a conformational switch in response to ATP hydrolysis, thus coupling chemical energy to mechanical force. A comparison of 26S EM structures with hydrolyzable versus non-hydrolyzable ATP demonstrates conformational mobility of the Rpts[55], consistent with this model (Figure 6). Mutation of the Ar-$\phi$ sequence in yeast RP ATPases results in accumulation of ubiquitinated protein conjugates[133], and as in the bacterial ATPases, these loops are flexible[52]. ATP binding and hydrolysis has been proposed to proceed stepwise or "wobble" around the Rpt ring, based on a study that found ATP to bind optimally to two PAN subunits at a time and a maximum of four PAN subunits[59]. Mutations in these loops for single Rpt proteins provide a range of phenotypes that vary depending on the particular Rpt affected[139], suggesting their functional asymmetry. The requirement for the C-terminal HbYX

motif also differs according to the Rpt protein with Rpt2/5 HbYX sufficient for gate opening[41,140] and Rpt3 HbYX essential for RP assembly[141].

Structures of the CTD fragments of PAN[51,142], Rpt1[143,144], Rpt3[145], and Rpt6[146] each contain a similar 4-helix bundle adjoined by nonstructured loop regions. Electron density was not observed for the C-terminal region containing their HbYX, and the corresponding Rpt6 tail was directly observed to be randomly coiled and flexible by NMR[146]. Isolated yeast Rpt6 CTD exhibits helix-coil transitions that influence its interaction with assembly chaperone Rpn14, and conformational exchange was similarly observed in yeast Rpt4 and Rpt5 CTDs[146]. Rpt6 may play an important role in nucleating formation of the RP base[58,147], a process which its CTD dynamics may facilitate[146]. Upon lid attachment, the yeast Rpt-CP interface appears to be reconfigured such that a specific Rpt6 interaction with the $\alpha2\alpha3$ pocket is broken to accommodate stable binding of Rpt2/3/5 in mature proteasomes[58].
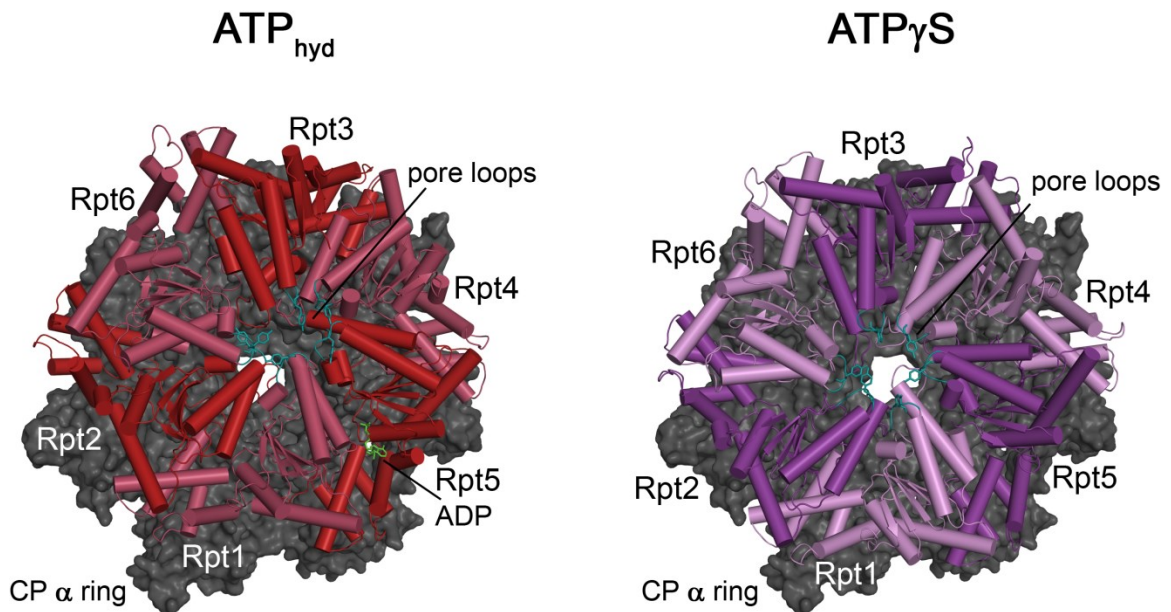
**Figure 6.** Model of the Rpt unfoldase pore

View of the Rpt ring illustrating the translocation pore relative to the CP (gray), with hydrolyzable ATP (red; adapted from PDB entry 4B4T) or non-hydrolyzable ATPγS (purple; adapted from PDB entry 4BGR) and the CC and OB regions omitted for clarity. The pore loops that contain the Ar-ϕ motif are highlighted (teal). A modeled ADP molecule (green) is shown bound to Rpt5 of the EM reconstruction generated with hydrolyzable ATP; its placement is based on that observed in PAN (PDB entry 3H4M).

An NMR study demonstrated CP from *Thermoplasma acidophilum* to exhibit high conformational variability, rapidly interconverting between multiple conformers that differ along contiguous regions that connect activator binding sites to the catalytic site[148]. Binding of the 11S and mutation of residues that contact activators shifts the relative population of these conformers and results in changes in substrate hydrolysis[148]. Similarly, the cleavage preference of human CP varies depending on the 11S variant present[149]; humans have REGα, REGβ, and REGγ 11S activators. Thus, an allosteric pathway appears to span the ~60Å distance between the activator-binding and catalytic regions of the CP and this allostery provides a mechanism by which activators influence product formation.

## 26S holoenzyme assembly

A major emphasis of recent studies has centered on the process by which the CP is capped by the RP, known as proteasome assembly. The timing and regulation of assembly has the potential to provide insights into the turnover of substrates under various physiological times or conditions.

The main stabilizing force of the assembled 26S proteasome is the interaction between the Rpt ATPase ring and the α ring, as described previously. Even with the dynamics of the ATPases, they are believed to form a specific Rpt1-Rpt2-Rpt6-Rpt3-Rpt4-Rpt5 arrangement on the basis of cross-linking and interaction data[56]. This suggests that despite the sequence and structural similarity among Rpt proteins, they carry important features that limit interchangeability and

thus require specific interactions for correct assembly and function. Unlike the unfolding and translocation functionality of the Rpts that are heavily dependent upon the ATPase domain, the assembly and docking functionality is facilitated by their C-terminal domain (CTD; Figure 3).

Although the Rpt ring comprises most of the interface, other proteins may form interactions with the CP. The lid component Rpn6 has been implicated to function as a molecular clamp that makes contacts with the lid, Rpt6, and the CP[76], potentially stabilizing the assembled structure. However, association of the lid complex is believed to be the final element of proteasome assembly[74], and Rpn6 has not been implicated as a contributor of base formation.

## Chaperone-mediated base assembly

In 2009, several research groups simultaneously identified four proteins that led to a rapid expansion in understanding proteasome assembly in eukaryotes. These proteins, Hsm3/S5b, Nas6/gankyrin, Nas2/p27, and Rpn14/PAAF1, had been previously identified in yeast as transient proteasome interacting proteins, but with little known functional roles. Now those roles have been identified – specific interaction with the CTD of Rpt subunits and the regulation of their docking to the CP[147,150–154]. Since they are not thought to be stable subunits and are critical for producing the proper structure of the 26S proteasome, they are collectively recognized as chaperone proteins. Each chaperone preferentially interacts with one Rpt subunit, forming Rpt1-Hsm3, Rpt3-Nas6, Rpt5-Nas2, and Rpt6-Rpn14

complexes[150–154]. No chaperones are yet known to preferentially interact with Rpt2 or Rpt4.

Based on their high-resolution structures, the chaperones are structurally distinct; Rpn14 forms a WD40 domain with a unique N-terminal region[155], Nas6 is composed of seven ankyrin repeats[145], Nas2 is predicted to be a PDZ domain[151], and Hsm3 contains eleven HEAT repeats[143,144]. The binding modes between ATPase and chaperone are known for three of these. X-ray structures were solved for the Rpt1-Hsm3[143,144] and Rpt3-Nas6[145] complexes, and the Rpt6-Rpn14 structure was simulated using NMR and mutagenesis data[146]. Despite the very different chaperone structures, they each bind along a similar surface on their Rpt CTD[146], likely a function of convergent evolution as they all interact on the remaining cytosol-exposed CTD surface.

The chaperone's functions are highlighted through their association with specific dimeric Rpt:Rpt complexes (Figure 7). These three complexes include Rpt1:Rpt2 , Rpt3:Rpt6, and Rpt4:Rpt5 interactions[150–153,156], and each of these subassemblies have at least one associated chaperone protein. Although no unique chaperones have been identified for Rpt2 and Rpt4, Hsm3 may additionally contact Rpt2[144], and Rpt4 may interact with Rpn14[150]. The modules that include the heterodimeric Rpt interaction and their chaperones are functional precursors of the RP base[150–153], and are known as base precursors or pre-assembly complexes. It is possible that other lid or base components may interact with these modules, but more information is needed to determine their role as a physiological

intermediate. It has been suggested that one such protein is Rpn1 that may be a component of the Hsm3:Rpt1:Rpt2 module[151–153]. This is supported by a study in which the DUB Ubp6 facilitates base assembly through a mechanism where is clears ubiquitinated substrates from binding to Rpn1, presumably while part of this pre-assembly complex[130].
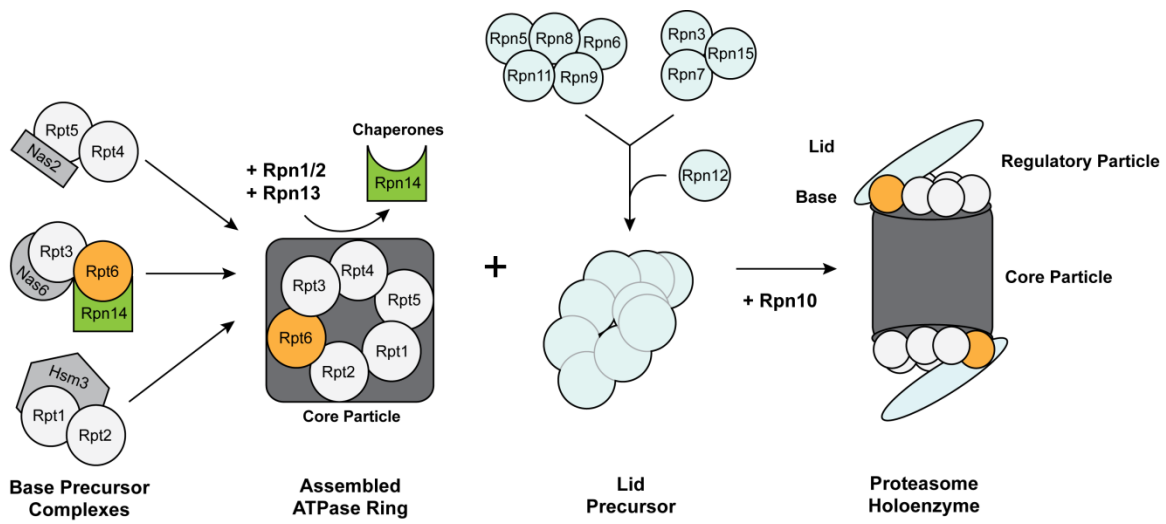
**Figure 7.** Templated assembly pathway of the RP

Rpt proteins form heterodimeric pre-assembly complexes (left) with chaperone proteins (green for Rpn14) containing intrinsic specificity for a unique Rpt C-terminal domain (orange for Rpt6). These base precursors are templated onto the CP (dark gray) to form the ATPase ring in a specific 1-2-6-3-4-5 arrangement. The chaperone proteins are released to form the assembled RP base. It is unclear precisely when base components Rpn1, Rpn2, and Rpn13 are added during this process. Lid precursors Rpn5/6/8/9/11 form a stable complex that attaches to the complex of Rpn3/7/15. Addition of Rpn12 (along with Rpn10) is then required for stable attachment of this lid precursor (light blue) to the RP base-CP complex in order to form the mature 26S proteasome holoenzyme.

There is some controversy as to exactly how the RP base is formed during assembly. One potential mechanism is that the base precursors may combine to form a complete Rpt ring which is subsequently lowered onto the CP, forming all necessary contacts at once. Indeed, free RP is found in yeast[157], and *in vitro* experiments using purified RP have shown their competency at docking with the CP[158]. However, this model provides little mechanism for producing the proper Rpt orientation or for chaperone displacement upon formation of the ring. Although RP may assemble independently, it is possible that is only a *post facto* explanation for the assembly of components that were originated by another mechanism.

Recent evidence has suggested an alternative model whereby assembly is templated on the CP and proceeds by stepwise addition of pre-assembly complexes. Initially, it was found that assembly deficient mutations of the CP lead to assembly deficiencies in the RP as well, suggesting that the CP is an RP assembly factor[159]. Data also suggested that single-residue truncations in the C-termini of Rpt4 and Rpt6 cause assembly defects and incomplete chaperone displacement from the holoenzyme[147]. Linking the region of the Rpts responsible for CP interaction to assembly defects would suggest a requirement for CP interaction. One complication of this model is the mechanism of chaperone displacement. In models of the Rpt-chaperone complexes of Rpt1[144] and Rpt3[150] oriented to the CP, their respective chaperones appear to sterically occlude the C-terminal tail that would be required for CP templating. However, if base assembly is a stepwise process, previously docked Rpts may aid in the assembly of other

components. Research described in this dissertation indicates that the *S. cerevisiae* Rpn14:Rpt6 interaction shows a similar steric orientation that prevents simultaneous interaction of Rpn14 and CP with Rpt6[146], but unlike Rpt1 and Rpt3, it appears that the C-terminal tail is not occluded from CP interaction. In fact, the CTD of Rpt6 is highly dynamic, and interaction with the CP may trigger a conformational change to an intrinsically unfolded structure that loses affinity for Rpn14, displacing it from the CP:Rpt6 complex[146]. In this manner, Rpt6 would be a good candidate for the nucleation of base assembly, which had been suggested previously[147]. Although yeast Rpt4 and Rpt5 CTDs contain similar intrinsic dynamics to Rpt6[146], it is unknown whether this mode of chaperone displacement is conserved with other Rpts or in mammalian proteasomes.

## Lid assembly and proteasome maturation

Attachment of the lid to the RP is expected to occur after assembly of the base, but only a few studies have yet emerged to indicate how this occurs. Similar to the base, lid is thought to be assembled in a multistep mechanism on the basis of mutagenic complex disruption phenotypes[74,75]. One module is expected to contain Rpn5/6/8/9/11 subunits that later recruit a module of Rpn3/7/15[74,75] (Figure 7). Independent from base, these proteins combine to form a lid precursor lacking in Rpn12[74,75]. Stable incorporation of lid precursor onto the proteasome occurs only upon binding of Rpn12, which uses a highly conserved C-terminal peptide[74] to form interactions that bind the lid to the base. This appears to be facilitated

through an interaction with Rpn10[160], and is required for incorporation of Rpn10 at the base-lid interface[161]. Attachment of the lid to Rpn12 may even drive conformational changes important for proteasome maturation[74]. EM data have shown that the specific subunits used for the contacts that comprise the Rpt-CP interface are adjusted between base formation and holoenzyme formation, suggesting a reconfiguration of the Rpt ring takes place during maturation[58]. It is possible that Rpn12 is the driving contributor to this effect, but to date this is speculative. Nonetheless, the function of Rpn12 appears to be a key regulation point for lid attachment and completion of 26S assembly[74].

## Proteasome in action

Decades of concerted effort have yielded snapshots of the CP docked with various activators. These snapshots reveal shared mechanistic features and highlight an important role for protein dynamics at the proteasome. In addition to the act of activator binding, dynamics are propagated at the proteasome by transient associations, ATP binding and hydrolysis, and DUB activity, as discussed in this review. Other factors may also drive proteolysis and motion, including post-translational modifications of proteasome subunits[162–164] and substrate interactions[165,166]. Recent studies have also identified the involvement of multiple chaperones in RP nucleation and base assembly that interact with the CTD of specific Rpt subunits, as reviewed[167,168]. Attachment of the lid complex may drive conformational changes that alter the Rpt-CP interaction profile and promote

31

holoenzyme maturation[58,74]. The timing and regulation of base assembly and lid attachment has the potential to regulate substrate turnover in response to specific physiological conditions. This area holds promise for the development of therapeutics that specifically target the activation of proteasomes, the use of different activator types, or the formation of heterogeneous doubly-capped CP, which may alter degradation rate or substrate preference.

Recent advances in cryoEM have provided structures of RP-CP holoenzymes at subnanometer resolution, allowing more accurate models of the RP's topology as it recognizes and processes substrates (Figure 8). One of these studies found differences between the two RP caps[54], in agreement with its dynamic nature. The transient nature of proteasome interacting proteins, altered conformations upon ATP binding and hydrolysis, and functional subunit redundancies may produce many independently functioning "minor" states that represent a part of the dynamic portrait of the 26S proteasome in action.
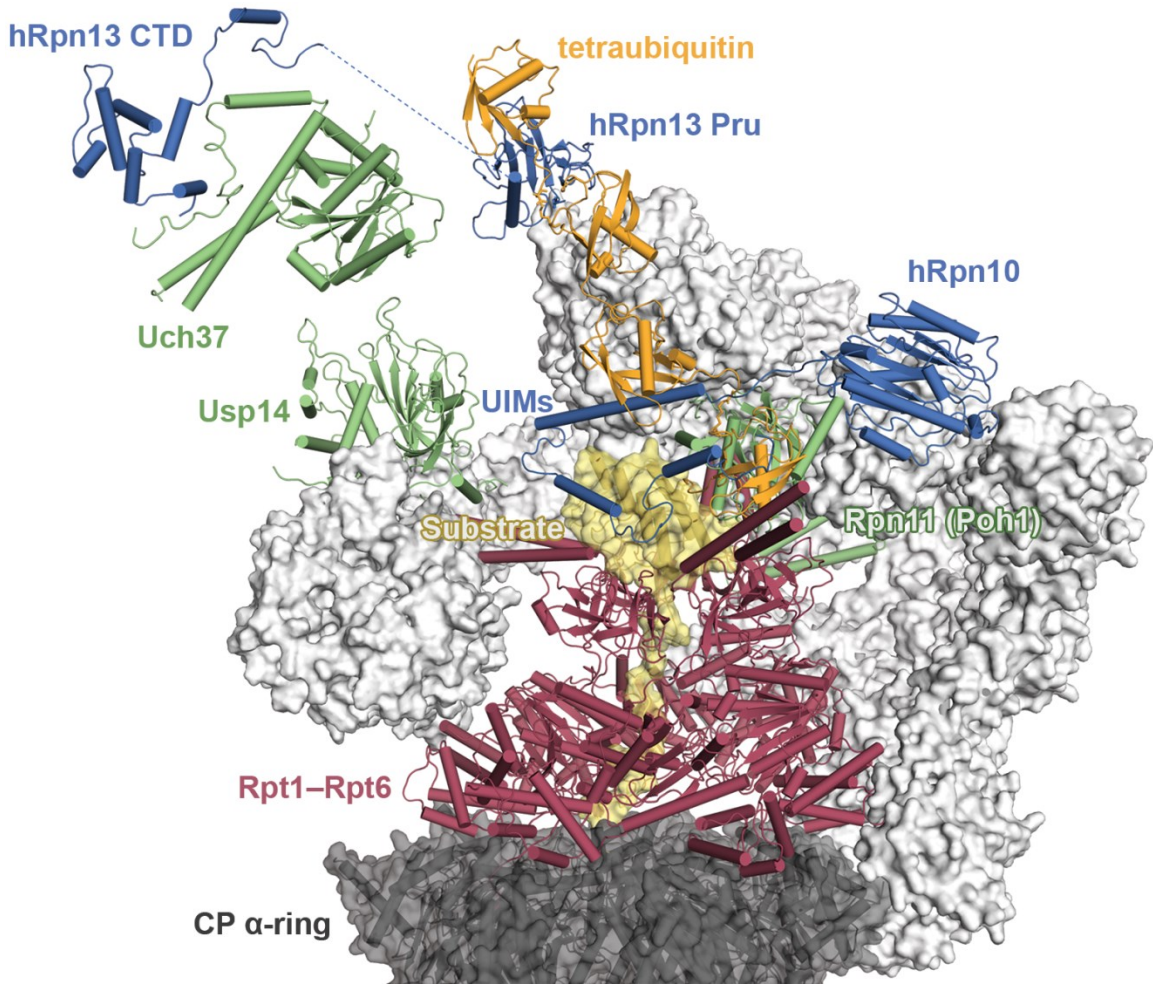
**Figure 8.** Modeling the RP as it processes substrate

Model structure of the human RP (adapted from PDB entry 4B4T) as it recognizes and processes a ubiquitinated substrate. A K48-linked tetraubiquitin chain (orange) connected to a substrate (yellow) is bound simultaneously by ubiquitin receptors hRpn13 and hRpn10 (blue). The ATPase ring (red) is bound to a non-structured end of the substrate, committing it to degradation. The ubiquitin-substrate isopeptide bond is placed adjacent to Rpn11 (Poh1; green) for hydrolysis as the substrate is unfolded and translocated into the CP (dark gray). hRpn13's C-terminal domain is bound to Uch37 (green; adapted from PDB entry 3IHR), which along with Ubp6 (Usp14; green; PDB entry 2AYN) deconjugates chains. The remaining RP subunits are displayed with a light gray surface.

The roles of certain RP components and their conformation may be related to properties of the substrate and ubiquitin chain. As its UIMs are essential[92], Rpn10-mediated substrate recognition may be critical for localizing the proximal ubiquitin near Rpn11, which in turn places the substrate at the mouth of the ATPase ring. It is not known exactly how the proteasome locks on to substrate, although the Rpt OB folds are positioned at the most distal end of the substrate's path (Figures 3 and 8). These folds are defined by their ability to form versatile interactions[169] and those of the Rpts are viable candidates for this. The presence of other subunits may be necessary only under certain conditions; for example, Rpn13 may be required for degrading certain substrates or to orient substrates with extended ubiquitin chains. K48-linked chains require a minimum of four ubiquitins to interact with both receptors in the current model (Figure 8), and it seems likely chain length would affect the catalytic roles of Uch37 and Ubp6, although the specifics are unclear. It is not yet known what factors influence RP composition under various contexts.

Other questions are inspired by structural models of the RP-CP proteasome. The doubly capped $RP_2$-CP contains an intrinsic rotation between the two RP assemblies due to the subunit-level asymmetry of the eukaryotic CP (Figure 4). The 11S is a homoheptamer and the homohexameric PAN binds to the symmetric archaeal CP, but the unique Rpts interact with partial specificity for unique CP pockets[58,170]. It is not known what this RP orientation may mean for substrate proteolysis. Similarly, little is known of the functional role of the PCI

hexameric shield (Figure 4), and it is hard to envision its conservation if serving solely as a scaffold. Each proteasome structure solved is a snapshot of the process that occurs during proteolysis, and the ability to integrate structure, dynamics, and function may hold the key to fully understand its molecular mechanisms.

# Chapter 1

## Conformational Dynamics of the
## Rpt6 C-terminal Domain*

### Introduction

The major process for selective protein degradation in eukaryotes is through the ubiquitin-proteasome pathway, in which substrate ubiquitination signals for proteolysis by the 26S proteasome[1]. Dysfunctions of this pathway as well as its hijacking by pathogens are associated with numerous human diseases[4], making it a major pharmaceutical target. Proteasome inhibitor bortezomib is used to treat multiple myeloma, relapsed mantle cell lymphoma, and acute allograft rejection, while more recently developed inhibitors are in clinical trials, as reviewed[171].

Substrate proteolysis occurs within the 20S proteasome core particle (CP), which is capped at either or both ends with a 19S regulatory particle (RP) that recognizes ubiquitinated substrates and prepares them for translocation into the CP[2,172]. The RP is a multiprotein complex that contains several subunits with known function, including ubiquitin receptors Rpn10/S5a[69] and Rpn13[70,71]; deubiquitinating enzymes Rpn11[72,73,124], Ubp6/Usp14[83], and Uch37/UCHL5[128]; and a heterohexameric ring of six AAA+ ATPase proteins (Rpt1-Rpt6) that abuts

---

the $\alpha$-subunit ring of the CP and opens its channel for substrate entry[41,173]. The RP can be divided into a lid and base, which includes Rpt1-6, two large scaffolding proteins, Rpn1 and Rpn2, and the ubiquitin receptors, Rpn10 and Rpn13.

The best RP structural characterization has been provided by cryo-electron microscopy studies at 7.4 Å for *S. cerevisiae*[54] and 8.4 Å for *S. pombe*[44,52]. The topological arrangement of RP subunits and of the RP-CP interface was modeled into the 3-dimensional reconstructions by incorporating intersubunit crosslinking approaches, including a study that revealed an Rpt1-Rpt2-Rpt6-Rpt3-Rpt4-Rpt5 arrangement[56], and crystallographic structures of RP subunit orthologs, especially the archaeal AAA-ATPase regulator PAN[51,142].

Crystal structures of PA26 (11S activator) complexed with archaeal[42] or *S. cerevisiae*[61] CP demonstrate C-terminal extensions docking into CP $\alpha\alpha$ subunit interfaces to form a salt bridge deep within the cavity[42]. This interaction was also observed in an archaeal CP:PAN complex[57]. Like PAN, Rpt2, Rpt3, and Rpt5 terminate in a conserved hydrophobic-tyrosine-any amino acid (HbYX) motif, and C-terminal peptides of PAN, Rpt2 and Rpt5 that preserve this motif are sufficient for CP gate opening[41]. Rpt6 has an HbYX variant in which tyrosine is replaced by phenylalanine in yeast and tryptophan in humans. A recent study found that synthetic Rpt6 C-terminal peptides bind with high specificity to the $\alpha2\alpha3$ pocket whereas the other Rpts are more promiscuous[58]. This finding implicates Rpt6 as having a unique role in templating RP onto CP during assembly and since Rpt6's tail is not docked into an $\alpha$ pocket in mature proteasome, also suggests that the

Rpt:CP interface is reconfigured upon lid addition[58]. Modification of the C-terminal end of Rpt4 and Rpt6 causes a biosynthetic proteasome assembly defect[147] and Rpt6's C-terminal tail is critical for base-CP complex formation[58].

Three Rpt heterodimeric RP assembly intermediates (Rpt1:Rpt2, Rpt3:Rpt6, and Rpt4:Rpt5) have been identified[147,150–153,156], along with four chaperone-like proteins that interact transiently with C-terminal domains of Rpt proteins. These chaperone:Rpt complexes include Nas2 (p27):Rpt5, Nas6 (p28 or gankyrin):Rpt3, Hsm3 (S5b):Rpt1, and Rpn14 (PAAF1):Rpt6[147,150–154]. Knockdown of the chaperones causes RP assembly defects in HEK293T cells[152] and in yeast[150,151,153,154].

X-ray crystallography has demonstrated significant structural diversity among Rpn14, Nas6 and Hsm3. Rpn14 forms a WD40 motif with a unique N-terminal domain[155] whereas Nas6 and Hsm3 contain a 7-fold ankyrin repeat[145] and eleven HEAT repeats, respectively[143,144]. The Nas6 and Hsm3 structures were solved complexed with their Rpt binding partner (Rpt3 and Rpt1 respectively), which use the same side of a 4-helix bundle to bind their chaperone[143,145]. Hsm3 was recently found to contact the ATPase domain of Rpt2 as well and may thus act as a scaffold that bridges Rpt2 to Rpt1[144].

Passage of substrates from RP to CP is expected to require protein dynamics and multiple methods suggest that Rpt proteins govern motion at the RP-CP interface. A 3D variance map calculated from electron microscopy data for *Schizosaccharomyces pombe* 26S proteasome revealed the region surrounding

the Rpt proteins to exhibit significantly higher conformational variation than the lid and CP[52]. Crosslinking studies have demonstrated asymmetry at the RP-CP interface in yeast, as on one side, Rpt2, Rpt6 and Rpt3 contact $\alpha$4, $\alpha$3 and $\alpha$2, respectively, while at the other side, Rpt4, Rpt5, and Rpt1 interact dynamically with multiple $\alpha$ subunits[170]. Furthermore, the AAA domains of Rpt proteins may undergo ATP-induced conformational changes[55,174]. NMR experiments recently demonstrated that the CP interconverts between multiple conformations in solution, and that this distribution is shifted to accommodate PA26 or an inhibitor[148].

In this study, NMR spectroscopy is used to investigate the structure and dynamics of the Rpt6 C-terminal domain (Rpt6-C) and its interaction with assembly chaperone Rpn14 (see Table 2 for experimental abbreviations). These data demonstrate that Rpt6-C undergoes conformational exchange that is abrogated by alanine substitution of two glycines located within its two most C-terminal $\alpha$-helices. The exchange region is centered among Rpt6's expected CP-facing, ATP-binding and Rpn14-binding surfaces, and these data present evidence for a model in which Rpt6-C dynamics plays a role in its interaction with Rpn14 and proteasome assembly.

**Table 2.** Experimental abbreviations

| Abbreviation | Description |
|---|---|
| AU | Analytical Ultracentrifugation |
| BMRB | Biological Magnetic Resonance Bank |
| CD | Circular Dichroism |
| CSI | Chemical Shift Index |
| EM | Electron Microscopy |
| EMDB | Electron Microscopy Data Bank |
| EXSY | ZZ-Exchange Spectroscopy |
| hetNOE | Heteronuclear Nuclear Overhauser Effect |
| HMQC | Heteronuclear Multiple Quantum Coherence |
| HSQC | Heteronuclear Single Quantum Coherence |
| NMR | Nuclear Magnetic Resonance |
| PDB | Protein Data Bank |
| PRE | Paramagnetic Relaxation Enhancement |
| $R_N(N_X)$ | Transverse (T2) relaxation |
| $R_N(N_Z)$ | Longitudinal (T1) relaxation |
| *rpt6AA* | Chromosomal $G^{360,387}A$ mutant |
| Rpt6-C | Rpt6 C-terminal domain (P318-K405) |
| TROSY | Transverse Relaxation Optimized Spectroscopy |

## Rpt6's C-terminal domain exchanges reversibly between two conformational states

In an effort to structurally characterize Rpt6 and its interaction with Rpn14, $^1H$, $^{15}N$ Heteronuclear Single Quantum Coherence (HSQC) experiments were acquired on $^{15}N$-labeled *Saccharomyces cerevisiae* Rpt6-C (Figure 9A), which spans P318-K405. A protein with one conformational state displays in the resulting spectrum one backbone amide signal for each amino acid except proline. Rpt6-C however displayed a greater than expected number of NMR signals, indicating conformational heterogeneity. Its six glycines produced eleven signals for example (Figure 9B). Therefore, Rpt6-C protein samples were generated in which lysine, alanine, leucine, or valine were selectively $^{15}N$-labeled. These samples also displayed greater than expected numbers of NMR signals in HSQC spectra (Figure 9B and 10A). This heterogeneity was observed even at low protein concentrations (Figure 10B for a spectrum at 40 $\mu$M).

By using deuteration and state-of-the-art triple resonance and exchange experiments, 32 Rpt6-C amino acids (36% of the protein sequence) were assigned two sets of NMR signals (Figure 9C for A385-K388). A subset of these had sufficient signal-to-noise to demonstrate two C$\alpha$ signals of unequal intensity in the HNCA and HNCOCA experiments with the weaker signal of each set corresponding to the stronger one of the other; this effect is illustrated for V386 and K388 (Figure 9C). To assess whether the two observable Rpt6-C states undergo dynamic exchange in solution, $^1H$, $^{15}N$ ZZ-exchange spectroscopy

(EXSY) experiments were acquired[175]. Variable mixing times were used to determine an optimal value of 80 ms (Figure 10C) at which EXSY crosspeaks were observed for all 30 Rpt6-C amino acids identified to have two sets of amide signals (Figure 9D and 9E). EXSY crosspeaks were also observed for M350 and F382 (Figure 9D), which appeared to have second amide signals that overlap with Y368 and K392, respectively. Altogether, these findings indicate that Rpt6-C undergoes dynamic conformational exchange between two states.

Structures of human Rpt6-C are available (PDB entries 2KRK and 3KW6) and demonstrate it to form the expected 4-helix bundle present in *S. cerevisiae* Rpt1 and Rpt3 C-terminal domains[143,145]. The calculated chemical shift assignments (see Appendix; BMRB entry 18885) and CS-ROSETTA[176] were used to generate a structure of the Rpt6-C state with the most complete and dispersed set of assignments. The resulting structure contained a 4-helix bundle (Figure 9F) that matches the structure predicted by homology modeling alone via Rosetta[177] (Figure 10D). This structure has a backbone root-mean-square deviation of 1.07 Å and 1.10 Å to the hRpt6-C NMR and x-ray structures, respectively. The location of the amino acids found to undergo reversible chemical exchange were mapped onto the model structure to reveal that the majority forms a surface at the interface of helices α3 and α4 (Figure 9F). V346 and K349 in α2 lie adjacent to α3 and also undergo exchange, whereas no amino acid from α1 was found to undergo chemical exchange. N336, R339, G340, I341, H376, and T378 also undergo

exchange and these amino acids are in the inter-helical loops bridging $\alpha 1$ to $\alpha 2$ and $\alpha 3$ to $\alpha 4$ (Figure 9F).

**Figure 9.** Rpt6-C exhibits reversible exchange

**(A)** Sequence alignment for the C-terminal domain of Rpt1-Rpt6 from *S. cerevisiae* and for human Rpt6. Amino acid positions that identical in at least five sequences are indicated (dark gray). Glycines in scRpt6-C are marked (^), and two of these, G360 and G387, located in helices $\alpha 3$ and $\alpha 4$ respectively are highlighted in yellow. All other glycines located within helices are highlighted in orange.

**(B)** $^1$H, $^{15}$N HSQC spectra demonstrating two sets of signals for Rpt6-C glycines (left) and lysines (right). One set of amide signals for K388 and K392 is degenerate and was resolved in triple resonance experiments.

**(C)** HNCA (black) and HNCOCA (red) spectra for Rpt6-C A385-K388 demonstrating their two sets of NMR signals (left, right). The two amide signals for V386 and K388 each exhibit both sets of C$\alpha$ signals (cyan boxes).

**(D)** $^1$H, $^{15}$N HSQC (black) and $^1$H, $^{15}$N EXSY (red) spectra for Rpt6-C. Dashed lines trace amide-exchange peak correlations to a central non-dispersed region. The signal in the right panel indicated by an asterisk is from an arginine side chain that has been folded into the spectral window.

**(E)** Enlarged regions of the spectrum in (D) to demonstrate amide and exchange signals for G387.

**(F)** CS-Rosetta structure and sequence of Rpt6-C highlighting its amino acids that undergo chemical exchange (blue).

**Figure 9.** *(see legend on previous page)*
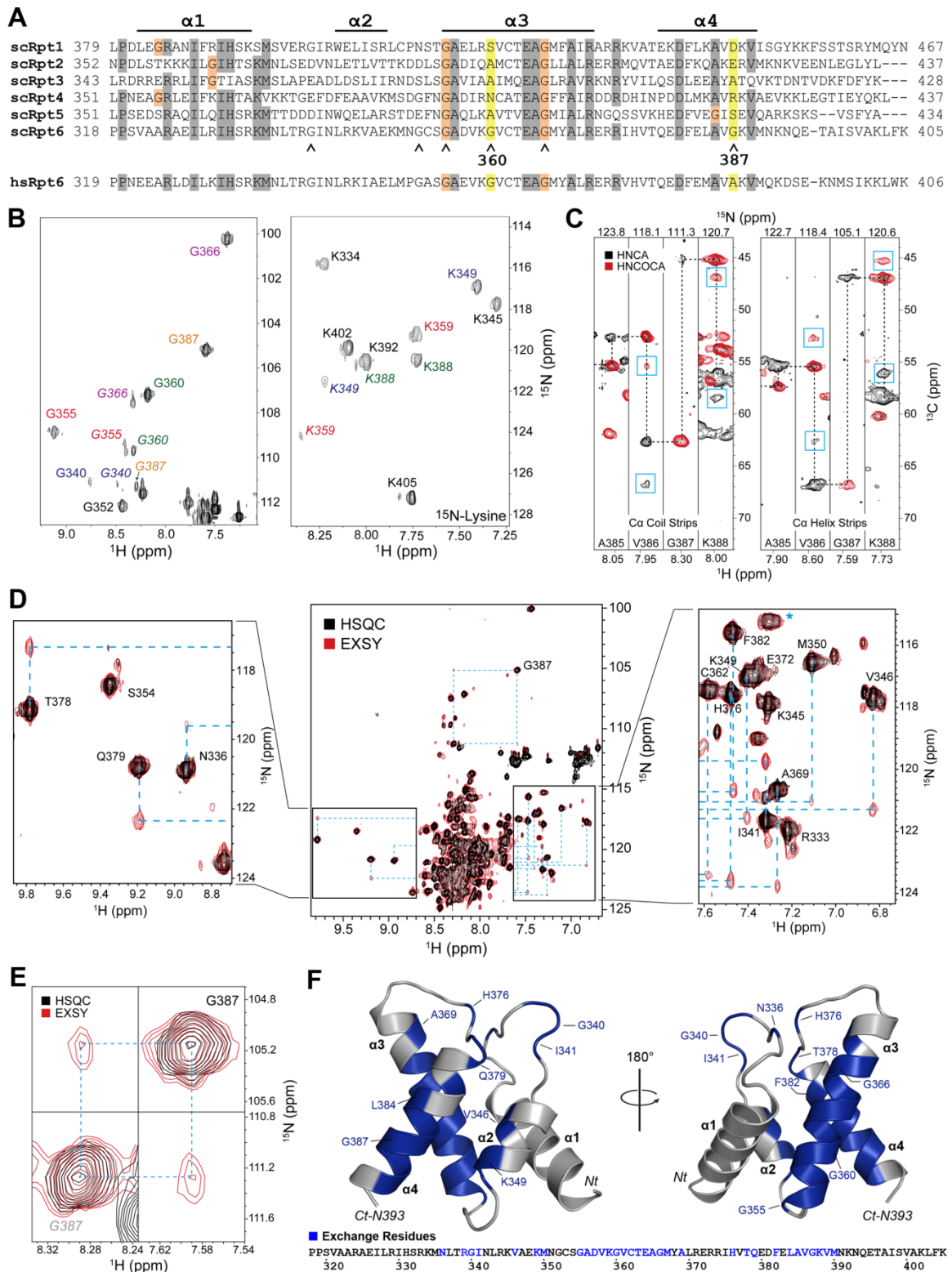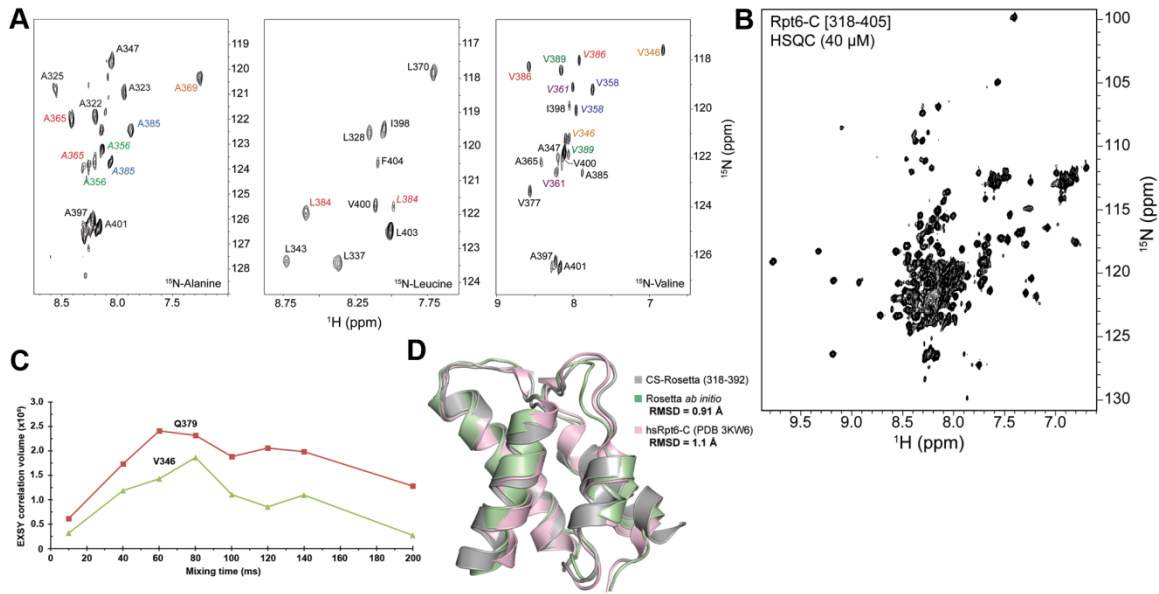
**Figure 10.** NMR assignment validation

**(A)** $^1$H, $^{15}$N HSQC spectra acquired on Rpt6-C with alanine (left), leucine (center), or valine (right) selectively $^{15}$N-labeled.

**(B)** $^1$H, $^{15}$N HSQC spectrum of Rpt6-C at 40 μM concentration.

**(C)** ZZ-Exchange build-up curve for V346 and Q379.

**(D)** Aligned CS-Rosetta (gray) and *ab initio* Rosetta (green) Rpt6-C structures with hsRpt6-C (pink) determined by x-ray crystallography (PDB entry 3KW6); these have an RMSD of 0.91 Å and 1.1 Å to the CS-ROSETTA structure, respectively. The flexible C-terminal residues (393-405) are omitted.

## Rpt6-C exchanges between a 4-helix bundle and a partially unfolded state that exhibits increased dynamics

To determine the structural distinction between the two Rpt6-C states, assigned C$\alpha$ and carbonyl chemical shift values were used to perform Chemical Shift Index (CSI) analyses[178], which is an established means to identify secondary structural elements. CSI analyses on the set of NMR signals used for the CS-ROSETTA 4-helix bundle structure (Figure 9F) yielded the expected secondary structure arrangement with all four predicted helices demonstrating negative C$\alpha$ (Figure 11A, black) and carbonyl (Figure 12A, black) CSI values. The second set of signals, by contrast, demonstrated random coil values in regions predicted to be $\alpha$-helical (Figures 11A and 12A, blue). This finding suggests that the reversible exchange exhibited by Rpt6-C is principally characterized by a helix-coil transition. CS-ROSETTA was used to generate model structures for this state based on the chemical shift assignments (see Appendix). The resulting structures were diverse in their tertiary fold, and among the ten lowest energy structures, that which most closely matches the 4-helix bundle was selected for demonstration (Figure 11B as compared to Figure 9F). The lack of convergence among the top ten lowest energy structures suggests structural heterogeneity for this second Rpt6-C structural state, which is henceforth referred to as partially unfolded.
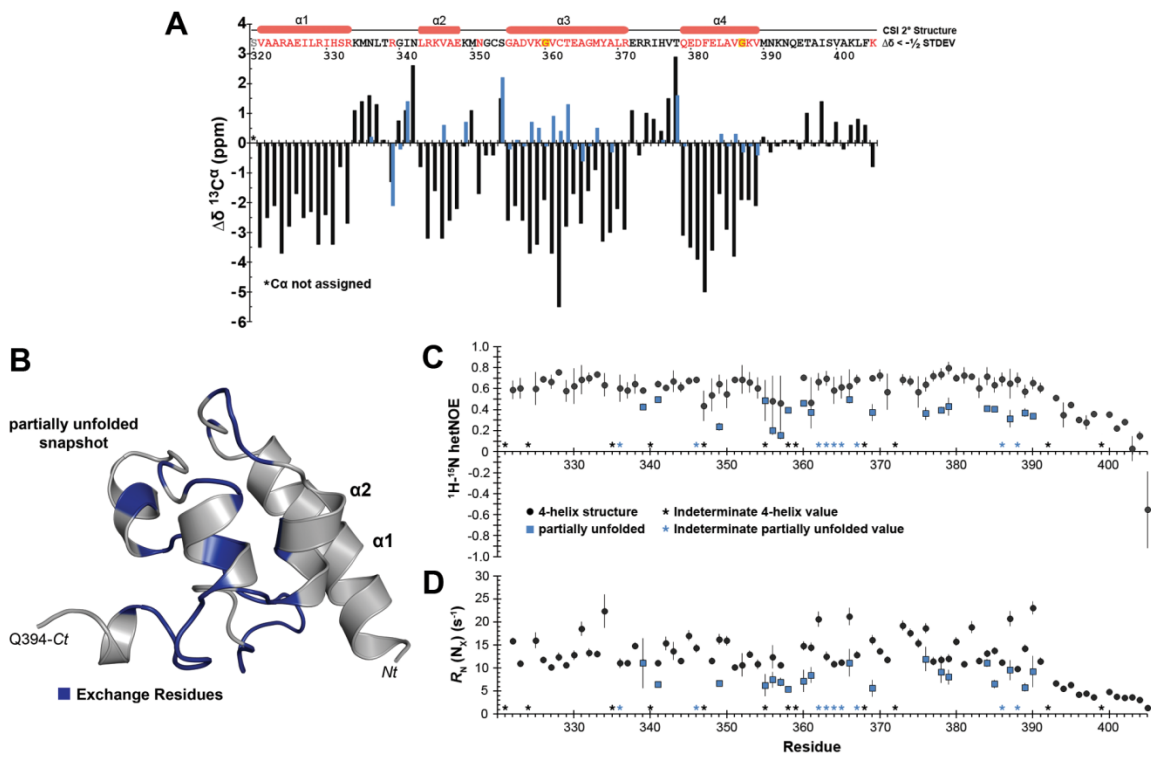
**Figure 11.** Rpt6-C transitions between a structurally intact and partially unfolded state that exhibits increased dynamics

**(A)** CSI analysis for Rpt6-C Cα atoms with the amino acid sequence and predicted secondary structure displayed. For amino acids with two states, the less dispersed one is shown in blue.

**(B)** CS-Rosetta snapshot of a possible configuration of Rpt6-C's partially unfolded state highlighting residues with two amide signals in blue. The C-terminal tail spanning 395-405 is omitted.

**(C and D)** Plots of **(C)** hetNOE ratios and **(D)** $R_N(N_X)$ rates for the structurally intact (black circle) and partially unfolded (blue square) state. Positions are indicated (*) where peak overlap prevented reliable integration.
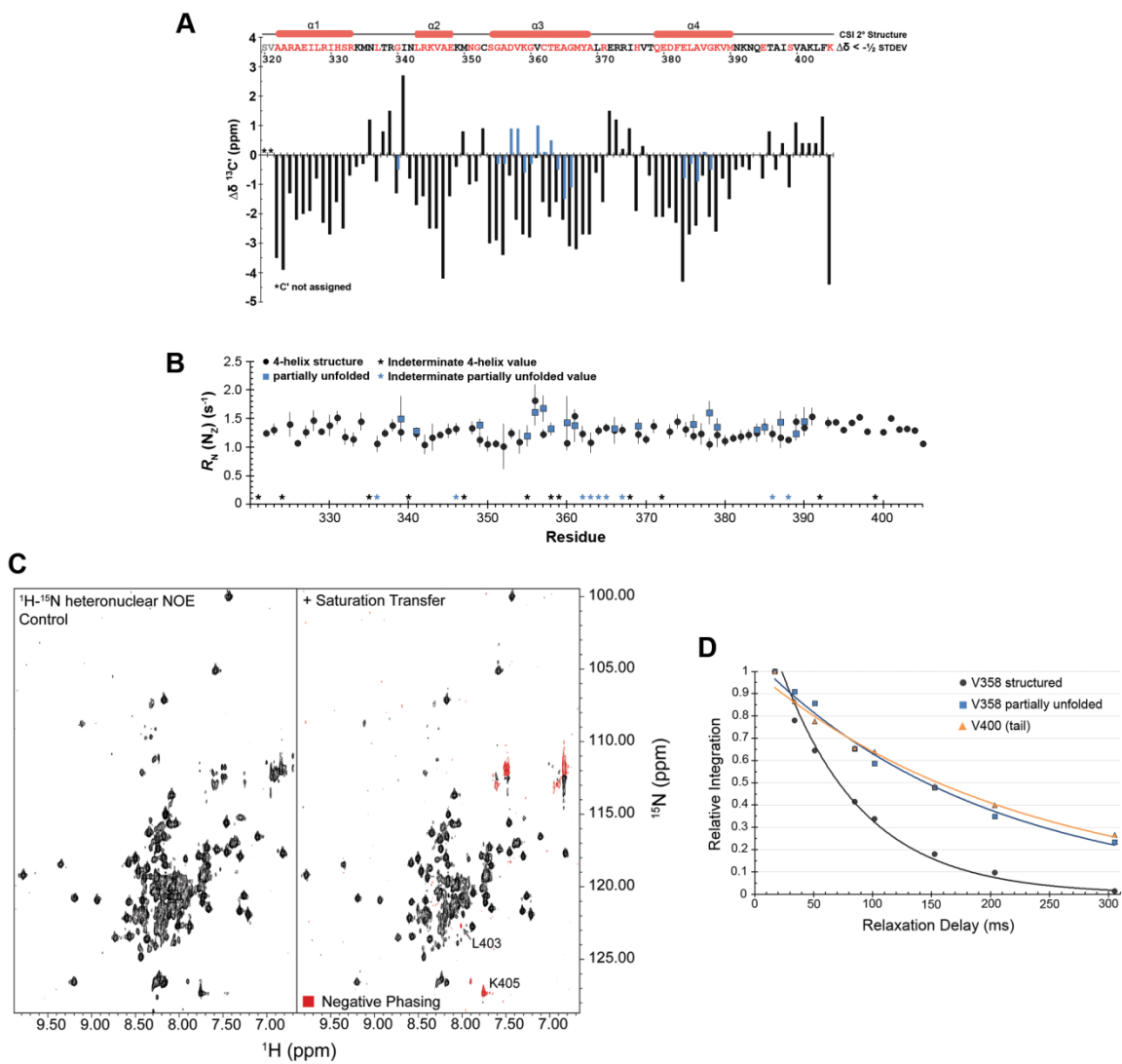
**Figure 12.** Amide dynamics of Rpt6-C

**(A)** Chemical shift index plotted for Rpt6-C backbone carbonyl carbons with coloring and labeling identical to Figure 11A.

**(B)** Amide $R_N(N_Z)$ data for Rpt6-C's 4-helix bundle (black circles) and partially unfolded state (blue squares). Peaks that cannot be unambiguously integrated are indicated (*).

**(C)** $^1$H-$^{15}$N heteronuclear NOE spectra containing a four second saturation transfer period (right) and without saturation transfer (left). L403 and K405 exhibit negative phases (red), indicating their flexibility.

**(D)** Amide $R_N(N_X)$ data for amino acids from the 4-helix bundle (V358, black), partially unfolded state (V358, blue), and C-terminal tail (V400, orange). Integrations for each resonance are normalized relative to their 10 ms delay value.

48

The internal dynamics of the two Rpt6-C structural states were probed on the picosecond to millisecond time scale by using $^1$H-$^{15}$N heteronuclear NOE (hetNOE), transverse relaxation ($R_N(N_X)$), and longitudinal relaxation ($R_N(N_Z)$) (Figure 12B) experiments. Rpt6-C's C-terminal tail and its partially unfolded state exhibited significantly smaller hetNOE (Figures 11C and 12C) and $R_N(N_X)$ (Figure 11D and 12D) values. These data demonstrate that as expected, Rpt6-C's partially unfolded state and its C-terminal tail are more dynamic than its 4-helix bundle. The program relax[179,180] was used to calculate a rotational correlation time of 8.5 ns for Rpt6's 4-helix bundle, which is typical for a monomeric protein of this size.

## Rpt6 glycines facilitate its helix-coil exchange and decrease its melting temperature

Rpt6 sequence analysis revealed glycines within helices α3 and α4 (Figure 9A) at the heart of the exchanging region (Figure 9F). G355 and G366 are conserved among all *S. cerevisiae* and human Rpt proteins. G360 is present in *S. cerevisiae* and human Rpt6 whereas G387 is unique to *S. cerevisiae* Rpt6 (Figures 9A and 13A). Glycine is second only to proline as the most energetically destabilizing amino acid for helix formation; alanine, by contrast, is the most stabilizing for helices[181]. G360 and G387 were replaced with alanine and acquired $^1$H, $^{15}$N HSQC and EXSY experiments on the resulting protein. All of the assigned amide signals for the partially unfolded state were lost (Figure 13B), as shown for the glycines in Figure 14A, as were all EXSY exchange peaks (Figure 13C).

Moreover, the sedimentation coefficient of Rpt6-C increased from 1.213 ±0.003S to 1.284 ±0.002S upon alanine substitution of G360 and G387 (Figure 14B)**. The sedimentation coefficient is directly proportional to molecular weight and inversely proportional to the frictional coefficient. As the two proteins have a negligible molecular weight difference, this increase reflects a decreased frictional coefficient for Rpt6-C $G^{360,387}A$, which is consistent with it having a more compact structure as averaged over time. Altogether, these results demonstrate that the observed Rpt6-C chemical exchange relies on the presence of two glycines within helices $\alpha3$ and $\alpha4$, and that their substitution to alanine stabilizes the Rpt6-C 4-helix bundle.

It was hypothesized that Rpt6-C's exchange to a partially unfolded and dynamic structural state would reflect a lower melting temperature, which would therefore be increased for Rpt6-C $G^{360,387}A$. Circular dichroism (CD) was used to evaluate secondary structure content across a temperature range spanning 5 °C to 80°C. Rpt6-C and its G-to-A variants converted from a predominantly helical CD spectrum to one characteristic of a random coil across this temperature range (Figure 13D). Molar ellipticity was plotted at 222 nm (Figure 14C) or 208 nm (Figure 13E) to find that the Rpt6-C melting temperature increased from 36 °C to 40 °C and 43 °C when G387 and G360 were substituted with alanine respectively, and to 50 °C when both glycines were substituted. Using these spectra, ~20% and ~33% of Rpt6-C was estimated to be in the partially unfolded state at 25 °C and

---

** AU experiments were performed by Jeffrey W. Lary and James L. Cole, as described[146]

30 °C, respectively, which is within the physiological range for *S. cerevisiae* growth. Additional alanine substitution of G366 resulted in only a 2 °C increase in melting temperature over Rpt6-C G$^{360,387}$A (Figures 13E and 13F) and its $^{1}$H, $^{15}$N HSQC spectrum resembled that of Rpt6-C G$^{360,387}$A (Figure 13G as compared to 13B). Similarly, the melting temperature of Rpt6-C G366A increased by only 1 °C relative to wild-type Rpt6-C (Figure 13F), suggesting G366 does not play a role in destabilizing Rpt6-C structural integrity. Rather, G366 enables M335 and V377 side chains to pack into the protein core, thus facilitating the $\alpha$1-$\alpha$2 and $\alpha$3-$\alpha$4 loop configuration. This steric arrangement is conserved in structures of Rpt1-C (PDB entry 2DZN), Rpt3-C (PDB entry 4A3V), and PAN (PDB entry 3H4M).

**Figure 13.** Thermal stability and folding of Rpt6-C mutants

**(A)** Sequence alignment for the C-terminal domain of human Rpt1-Rpt6. Amino acid positions that are identical (dark gray) in at least five sequences are indicated. The positions of *S. cerevisiae* Rpt6 G360 and G387 are highlighted (yellow), and additional glycines located within helices are indicated (orange). G360 is conserved in humans and G387 is an alanine.
**(B)** Overlaid $^{1}$H, $^{15}$N HSQC spectra comparing Rpt6-C wild-type (black) to Rpt6-C G$^{360,387}$A (red).
**(C)** A $^{1}$H, $^{15}$N HSQC spectrum (black) overlaid with a $^{1}$H, $^{15}$N EXSY spectrum for Rpt6-C G$^{360,387}$A demonstrating the absence of EXSY exchange peaks.
**(D)** Complete wavelength spectra of circular dichroism thermal arrays from 5°C to 80°C for Rpt6-C and its G-to-A variants, as indicated.
**(E)** Comparison of molar ellipticity at 208 nm, arrayed by temperature, for Rpt6-C and with G-to-A amino acids substitutions as in Figure 14C.
**(F)** Comparison of molar ellipticity at 222 nm, arrayed by temperature, for Rpt6-C and with G-to-A amino acids substitutions, highlighting the effect of G366A.
**(G)** $^{1}$H, $^{15}$N HSQC spectrum of Rpt6-C wild-type (black) overlaid with that for Rpt6-C G$^{360,366,387}$A.

*(see image on next page)*

51

Figure 13. *(see legend on previous page)*
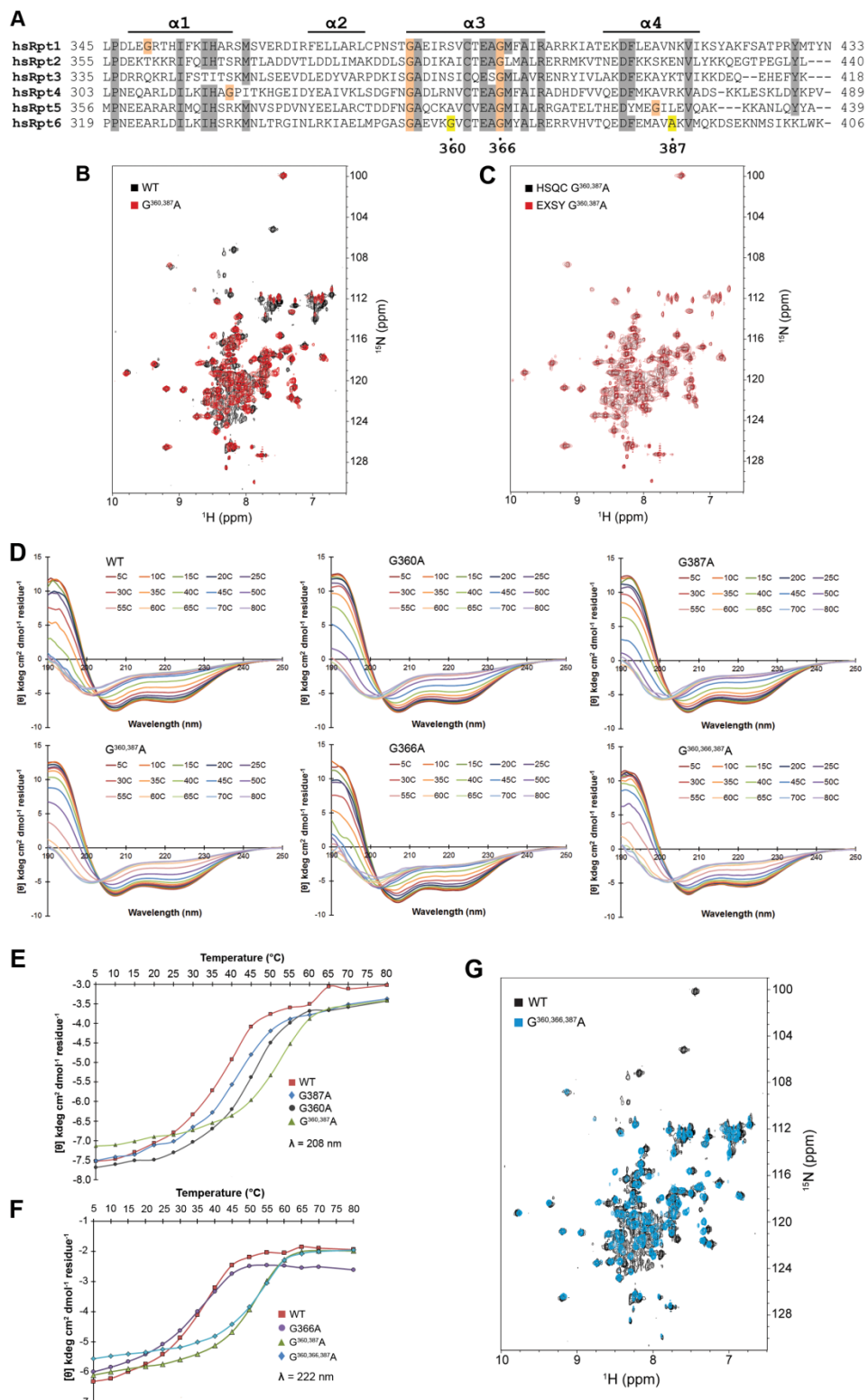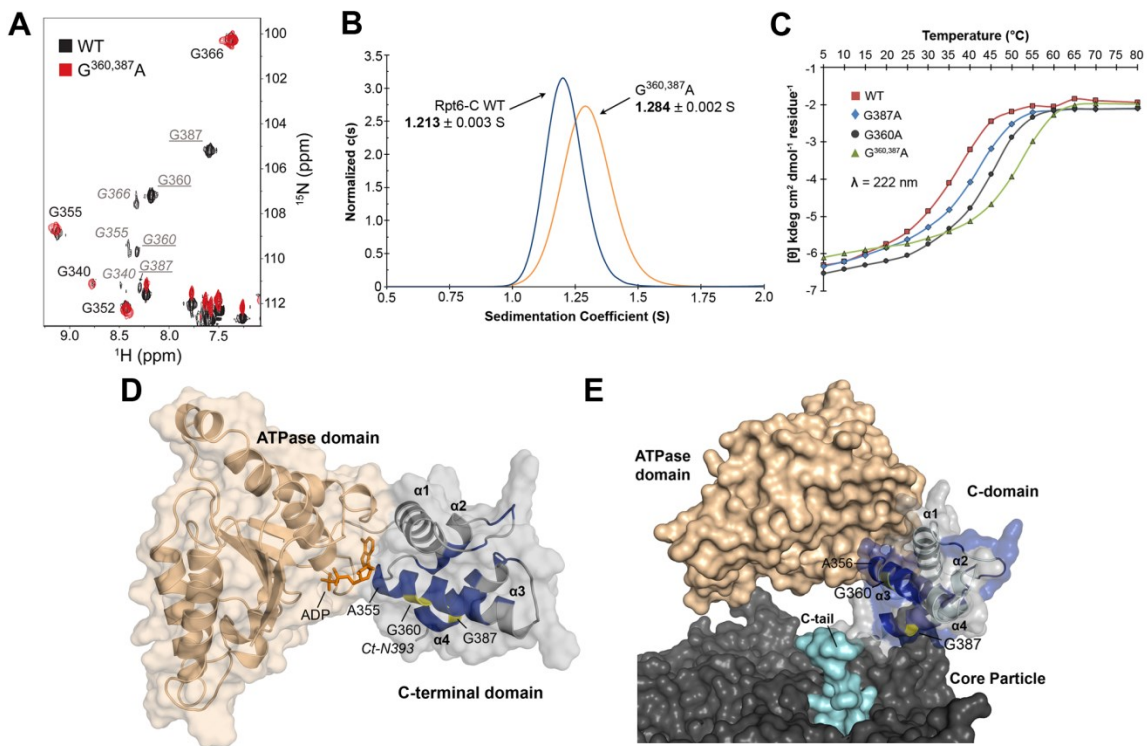
**Figure 14.** Rpt6-C chemical exchange relies on two glycines in $\alpha3$ and $\alpha4$

**(A)** Overlaid $^1$H, $^{15}$N HSQC spectra of Rpt6-C (black) and Rpt6-C G$^{360,387}$A (red). NMR signals unique to Rpt6-C are labeled in gray with G360 and G387 underlined. Signals from Rpt6-C's partially unfolded state are italicized.

**(B)** Sedimentation velocity analysis for Rpt6-C (blue) and Rpt6-C G$^{360,387}$A (orange).

**(C)** Thermal denaturation experiment by CD plotting molar ellipticity [$\theta$] versus temperature at 222 nm for Rpt6-C wild-type (red), G387A (blue), G360A (black) and G$^{360,387}$A (green).

**(D)** Rpt6's N-terminal ATP-binding domain (beige) and putative nucleotide-binding site (ADP, orange) abuts the surface undergoing helix-coil transitions (dark blue with G360 and G387 in yellow), which is also proximal to Rpt6's C-terminal extension.

**(E)** Surface rendition of a model structure containing Rpt6 showing its C-terminal extension (cyan) docked with CP (dark gray). Amino acids in exchange (blue, yellow) bridge the interface between the ATPase domain and CP.

To determine whether Rpt6-C conformational exchange influences its interaction with Rpt6's N-terminal ATPase domain (spanning 136-317, NTD), purification of full-length *S. cerevisiae* Rpt6 protein was attempted from *E. coli*, but it precipitated during purification. Therefore, the structure of PAN subcomplex II from *Methanocaldococcus jannaschii*[51,133] was used to create a homology model of full length Rpt6 using Prime (Schrödinger, Inc.; Figure 14D). Rpt6-C's α1 lies at the interface with Rpt6's NTD and this helix does not contain any amino acids that undergo chemical exchange (Figure 9F). Interestingly, the exchange surface formed by amino acids in helices α3 and α4 is predicted to be exposed in the full length protein, but is interpolated between the Rpt6 ATP-binding pocket (Figure 14D) and the expected location of the CP interaction surface (Figure 14E). The remaining loop amino acids in conformational exchange form a peripheral ridge that may lie distal to these expected interaction surfaces.

## Summary

These experiments establish a helix-coil conformational exchange on the millisecond time scale for the *S. cerevisiae* Rpt6 C-terminal domain. The domain is thermally stabilized to the native helical form by mutation of glycines 360 and 387 to alanine, implicating these residues in nucleating the exchange. Circular dichroism data suggests that each of these two residues contributes to thermodynamic destabilization independently. A strictly conserved glycine in helix α3 (G366) did not stabilize the 4-helix state independently, nor in complement to

G360 and G387 alanine mutants. NMR relaxation experiments confirmed that the partially unfolded state is more dynamic than the 4-helix bundle, and suggested a rotational correlation time of 8.5 ns. This value is similar to other monomeric proteins of this size, and the NMR spectral properties are not concentration-dependent, providing additional evidence that the exchange is due to sequence-related energy effects and not multimerization.

Computational models of these two states based on NMR chemical shift data suggest a 4-helix bundle for one state, similar to the AAA structures of PAN, Rpt1, Rpt3, and human Rpt6. In addition, the simulation for the partially unfolded state chemical shifts did not converge to a single structure, which is consistent with its dynamic nature. The exchange interface lies between the NTD and the expected CP docking site, and it is possible that these dynamics play a role in facilitating dynamics of the Rpt ring as a whole.

The human ortholog of Rpt6 contains a genetic variant in which the residue at the position of yeast G387 is natively an alanine. This implies that the human protein may be intrinsically more resistant to thermal denaturation effects, which is suggested by the structures of the human CTD that imply a uniform 4-helix bundle. It is possible that this difference has evolved to adapt for the endothermic environment of humans, but it does not solely exclude the existence of exchange in human Rpt6, which may potentially still occur at higher temperatures, in certain solvent conditions, or upon specific binding interactions or post-translational modifications.

# Chapter 2

## Implications of Rpt6-C Exchange for Rpn14 Binding and Proteasome Base Assembly*

### Assembly chaperone Rpn14 binds strongly and preferentially to Rpt6-C's 4-helix bundle

In an effort to characterize Rpt6-C interaction with Rpn14, $^{1}$H, $^{15}$N HSQC and $^{1}$H, $^{15}$N Transverse Relaxation Optimized Spectroscopy (TROSY)-HSQC experiments were acquired on $^{15}$N labeled Rpt6-C in the presence of unlabeled *S. cerevisiae* Rpn14. A subset of Rpt6-C signals is significantly shifted by Rpn14 (Figure 15A), which bound to Rpt6-C in the slow exchange regime on the NMR time scale such that Rpt6-C signals from its unbound state disappear as its Rpn14-bound state signals emerge. NMR signals from Rpn14-bound Rpt6-C are attenuated due to the large molecular weight of the complex, and many emergent peaks are dispersed, suggesting that they belong to amides with structural integrity in the complex (Figure 15A, marked with asterisks). The $K_d$ for the Rpt6-C:Rpn14 interaction was measured by sedimentation velocity. The data obtained at three Rpt6:Rpn14 ratios fit well to a 1:1 binding model but the affinity was too strong for

---

a precise measurement by these methods.  Global analysis indicates a best-fit $K_d$ of 0.25 nM with an upper 95% confidence limit of 13 nM (Figure 16).

With Rpn14 present, both states of 23 of the Rpt6-C signals that undergo conformational exchange were resolved. Among these, only G340, G355, A356, T378, and V386 were notably affected by the presence of Rpn14 (Figures 15A-C). In all cases, the helical state of these amino acids was shifted to another location in the Rpt6-C spectrum acquired with equimolar quantities of Rpn14, as exemplified for A356 (Figure 15B) and V386 (Figure 15C). By contrast, the partially unfolded state signal is present at the same location in the spectrum (Figures 15A-C). This finding suggests that Rpn14 binds selectively to the structurally intact state of Rpt6.

Rpt6-C reversibly exchanges between its two conformational states (Figures 9D and 9E) and therefore, Rpn14 binding to Rpt6-C's 4-helix bundle should lead to a reduced population of its partially unfolded state. This effect is manifested throughout the Rpn14 titration, as increasing quantity of Rpn14 leads to reduced signal intensity from Rpt6-C's partially unfolded state, as exemplified for V386 (Figure 15C, in which all spectra are plotted at an equivalent threshold). It is important to note that Rpn14 aggregates during this titration and the molar ratio reported here is based on protein added and that the effective Rpn14 available for Rpt6-C binding may be reduced.
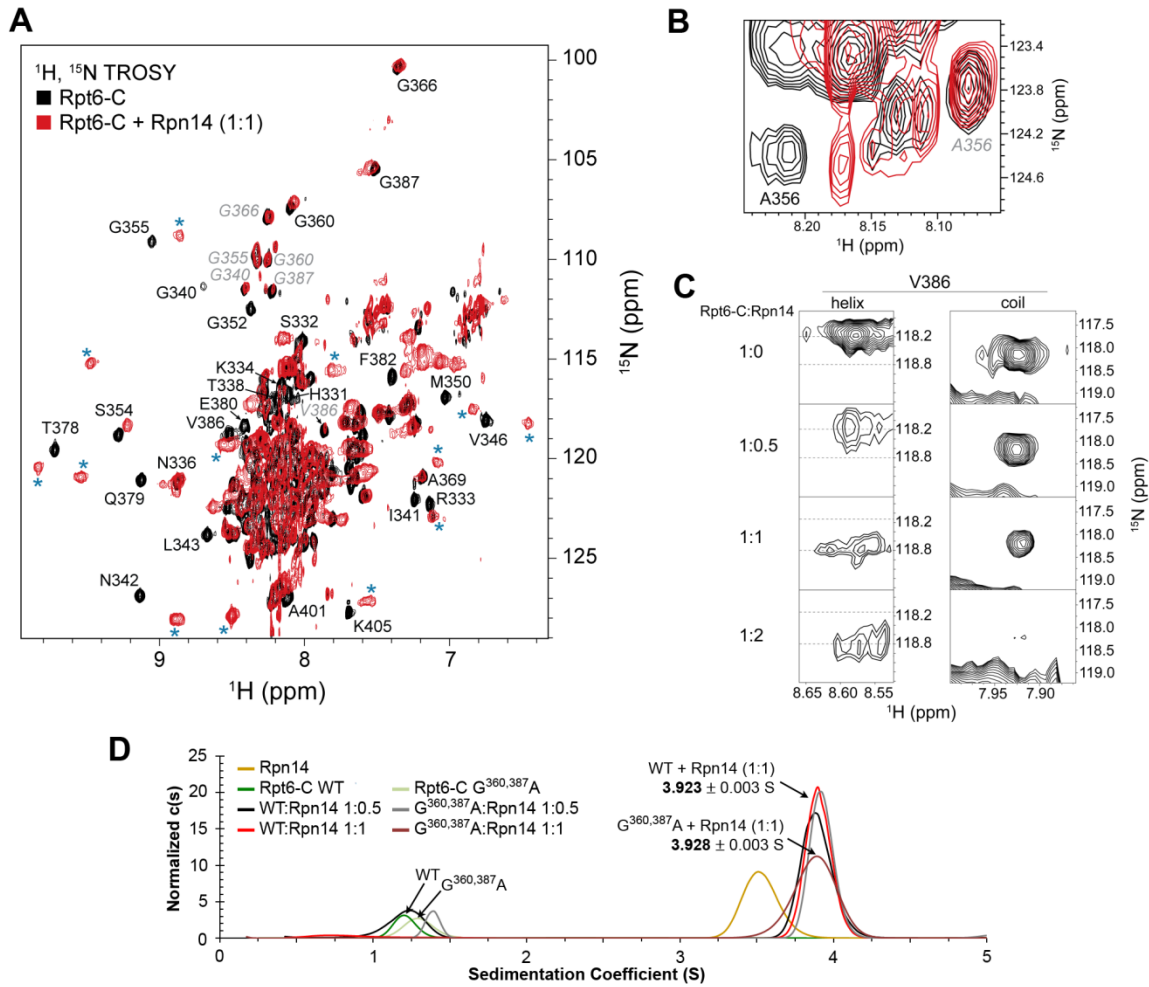
**Figure 15.** Rpn14 binds preferentially to Rpt6-C's structurally intact state

(**A**) $^1$H, $^{15}$N TROSY-HSQC spectra of $^{15}$N Rpt6-C (black) and with equimolar unlabeled *S. cerevisiae* Rpn14 (red). Gray, italicized labels indicate signals from the partially unfolded state. NMR signals that appear upon Rpn14 addition are indicated (cyan asterisks).

(**B**) Enlarged region of Figure 4A showing the two states of A356.

(**C**) Enlarged $^1$H, $^{15}$N HSQC spectra of V386's amide signals for Rpt6-C and with incrementally increased quantities of Rpn14, as labeled.

(**D**) Sedimentation velocity analysis of Rpt6-C and Rpt6-C G$^{360,387}$A, free and complexed with Rpn14, as indicated.

The binding of Rpn14 to Rpt6-C's 4-helix bundle suggested that this interaction should not be diminished in Rpt6-C G[360,387]A, unless G360 and G387 are within the Rpn14-binding surface. Analytical ultracentrifugation was used to test whether Rpt6-C G[360,387]A affinity for Rpn14 is reduced**. As in the case of wild-type Rpt6-C, this analysis revealed high affinity binding, with a $K_d$ of 0.01 nM and an upper 95% confidence limit of 20 nM (data not shown). The confidence limits are broad relative to $K_d$ due to the high concentrations required for detection in the experiment; however, it is clear that high affinity binding is preserved upon introducing the alanine substitutions.

Whereas the sedimentation coefficients of Rpt6-C and Rpt6-C G[360,387]A are significantly different (Figure 14B), that of their Rpn14-bound states (Figure 15D) differ by only 0.005S (Figure 15D). Hydrodynamic models[182,183] suggest that if Rpt6-C were to remain partially unfolded, the sedimentation coefficient of the Rpt6-C:Rpn14 complex would be 0.06S smaller than that of the Rpt6-C G[360,387]A:Rpn14 complex. This finding is consistent with the NMR evidence that Rpt6-C is folded when bound to Rpn14 (Figures 15A-C).

---

** AU experiments were performed by Jeffrey W. Lary and James L. Cole, as described[146]
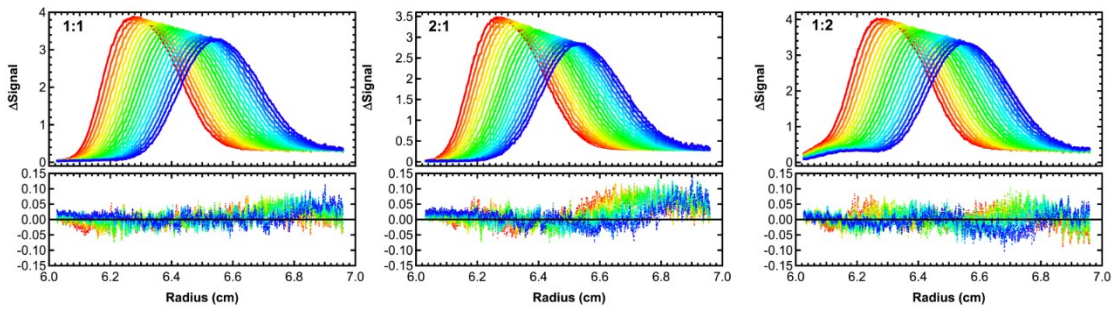
**Figure 16.** Global analysis of sedimentation velocity difference curves

Three samples were prepared at 25 μM Rpn14 and mixing ratios of Rpt6-C to Rpn14 of 1:1, 2:1 and 1:2. The sedimentation velocity scans were subtracted in pairs to remove time-invariant noise and the three data channels were globally fit to a 1:1 binding model using SEDANAL. The top panels show the data (points) and fit (solid lines) and the bottom panels show the residuals (points). For clarity, only every 3rd difference scan is shown. A good fit was obtained with low systematic deviations in the residuals with an RMS deviation of 0.021 fringes. The best-fit $K_d$ is 0.25 nM; however, the 95% confidence limits of 0-13 nM indicate that the binding affinity is too strong to be measured precisely under these conditions. The rotor speed was 50,000 RPM with a temperature of 20°C and interference optics and scan interval of one minute.

## The N-terminal ends of $\alpha2$ and $\alpha4$, and the $\alpha1$-$\alpha2$ and $\alpha3$-$\alpha4$ loops are involved in Rpn14-binding

The slow exchange binding regime of the Rpt6-C:Rpn14 interaction prevents the tracking of Rpt6-C signals from their free to their Rpn14-bound state (Figure 15A). The Rpn14 bound-state peaks exhibited significant signal attenuation due to the increased size of this 57 kDa complex, and attempts to increase sample concentration above 0.3 mM resulted in precipitation. In an effort to identify the Rpt6-C amino acids that participate in Rpn14 binding, Rpt6-C amide chemical shift changes caused by Rpn14 addition were examined for each amino acid (Figure 17A). Fourteen amino acids were excluded from this analysis, including those suffering from severe spectral crowding and those with an unknown free-state assignment (Figure 17A, asterisks). Rpt6-C produced 24 signals that were identified as shifted to a location in the spectrum that is remote from their free state upon Rpn14 addition (Figure 17A, ^). Their Rpn14-bound state signals were unable to be unambiguously assigned; however it can be concluded that they are significantly shifted. These amino acids most affected by Rpn14 propagate through the Rpt6-C structure and are included within the $\alpha1$-$\alpha2$ and $\alpha2$-$\alpha3$ loops, the N-terminal ends of $\alpha2$ and $\alpha4$, and the C-terminal end of $\alpha1$ (Figure 17B).
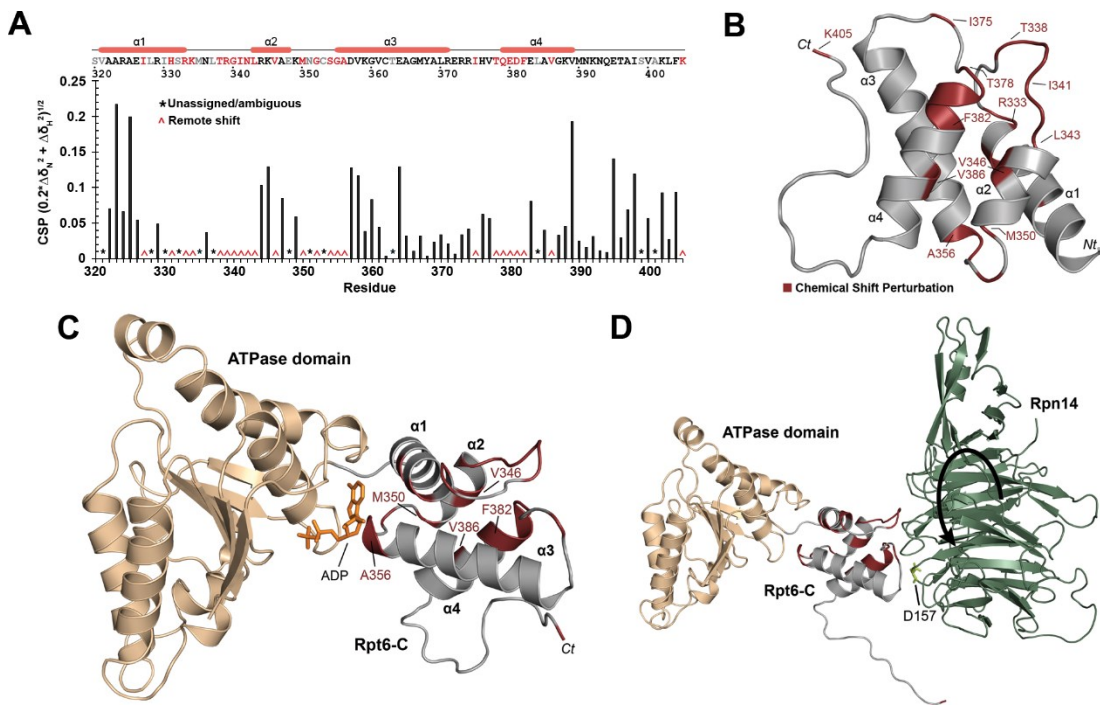
**Figure 17.** Rpt6-C binds Rpn14 through a surface undergoing conformational exchange and formed by the N-terminal ends of α2 and α4 and the α1-α2 and α3-α4 loops

(**A**) Quantification of Rpn14's effect on Rpt6-C amide signals, as displayed in Figure 15A. Signals that unambiguously shift to a remote location upon Rpn14 addition are indicated with ^ and red lettering, whereas those without assignment in the free state or with ambiguous shifted state values are marked with *. Rpt6-C's partially unfolded state is omitted from this analysis.
(**B**) Rpt6-C structure highlighting amino acids that shift significantly upon Rpn14 addition (red) and (**C**) with the modeled ATPase domain (beige) from Figure 14D and ADP (orange) included.
(**D**) Model structure of Rpt6 complexed with Rpn14 (green). The lowest energy TreeDock structure of the most occupied orientation (Figure 18C) is displayed with an arrow symbolizing Rpn14's rotation about D157 in other structural models. The orientation of the Rpt6-C C-terminal tail in (B), (C), and (D) represents a snapshot as it is randomly coiled and flexible (Figure 11).

Four buried hydrophobic amino acids (V346, M350, F382, and V386 (Figure 15C)) as well as G355 (Figure 15A) and A356 (Figure 15B) at the N-terminal end of $\alpha$3 are shifted upon Rpn14 addition (Figure 17A); these amino acids demonstrate two conformational states in free Rpt6-C (Figure 9F). V346, M350, F382, and V386 within Rpt6-C's hydrophobic core are not exposed for Rpn14 interaction and G355 and A356 abut the putative nucleotide-binding pocket in full length Rpt6 (Figure 17C). Since Rpn14 appears to bind to Rpt6-C's 4-helix bundle (Figure 15), these inaccessible amino acids may be shifting upon Rpn14 addition due to stabilization of Rpt6-C's structurally intact state rather than their direct interaction with Rpn14. Significant shifting for Rpt6-C's C-terminal amino acid, K405, was also observed. A truncated Rpt6-C protein construct, Rpt6-C (P318-N393), in which its C-terminal tail spanning Q394-K405, is missing binds Rpn14 in the same manner as wild-type Rpt6-C (Figure 18A). This finding suggests that Rpt6's C-terminus is not necessary for its binding to Rpn14. Nonetheless, the C-terminal tail shifting upon Rpn14 addition suggests that it may be reconfigured as a consequence of Rpt6 binding to Rpn14 or form additional contacts with Rpn14 that are not required for the Rpt6:Rpn14 interaction.
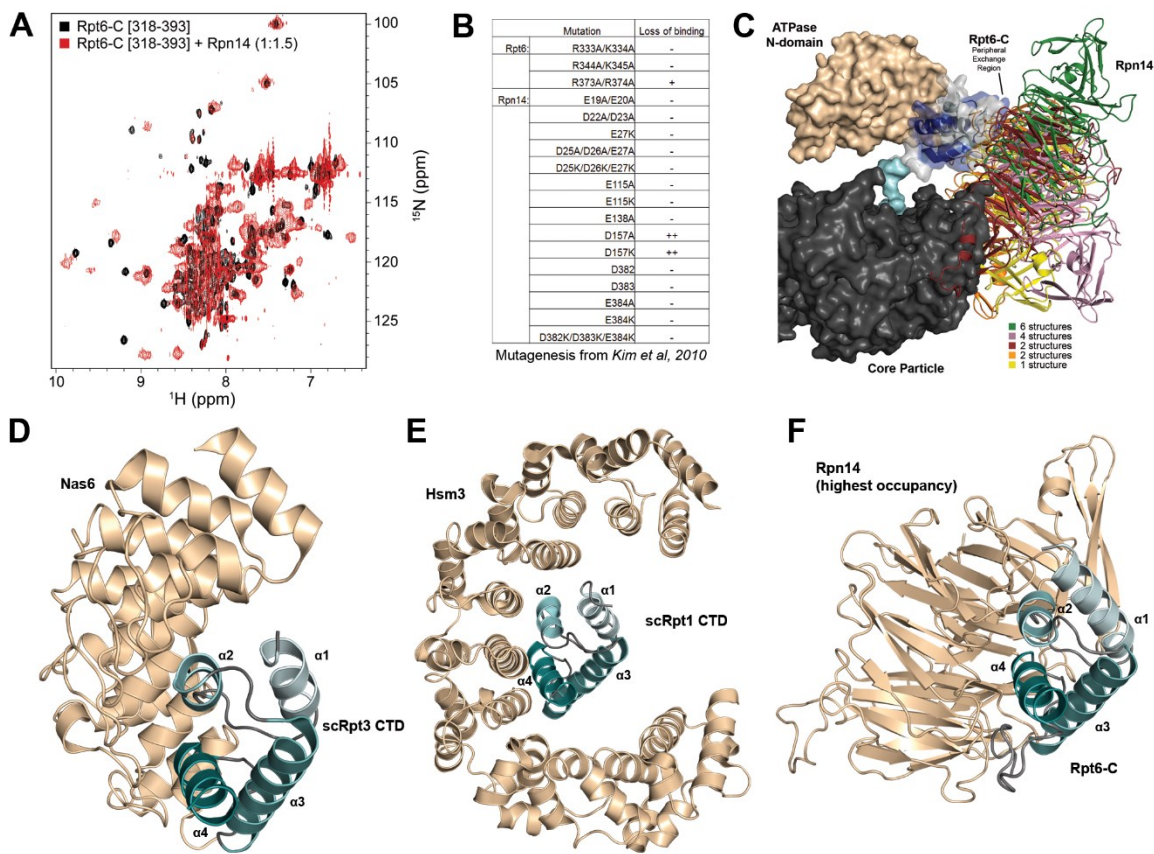
**Figure 18.** Modeling of the Rpt6-Rpn14 interaction at the proteasome

 (A) ^{1}H, ^{15}N HSQC spectra of ^{15}N-labeled Rpt6-C [318-393] construct lacking its C-terminal tail in the free (black) and Rpn14 (1:1.5) bound state (red).

(B) Table of published mutagenesis data[155] used in modeling the Rpt6:Rpn14 interface.

(C) Display of all sampled orientations of the Rpn14:Rpt6-C interface within the twenty lowest-energy simulated structures. Rpn14 rotates about D157, but in all structures binds to Rpt6-C's peripheral exchange region. Rpn14 structures either clash or directly abut the CP (dark gray) in the assembled CP-RP interface.

(D-F) Structural comparison of **(D)** Rpt3-Nas6 (PDB entry 2DZN), **(E)** Rpt1-Hsm3 (PDB entry 3VLF), and **(F)** the lowest-energy and the most occupied cluster for Rpt6-C:Rpn14, as determined by TreeDock.

The NMR data (Figure 17A) was combined with previously published mutagenesis data (Figure 18B) to generate structural models of the Rpt6-C:Rpn14 protein complex by using TreeDock[184].** Complexes were excluded that yielded steric clashes with the expected location of Rpt6's NTD and that were not affected by Rpn14 D157A and D157K amino acid substitution or alanine substitution of Rpt6 R373 and R374 (Figure 18B)[155]. In the remaining model structures, Rpn14 is placed at an Rpt6-C surface formed by the N-terminal ends of $\alpha2$ and $\alpha4$, and the $\alpha1$-$\alpha2$ and $\alpha3$-$\alpha4$ loops (Figure 18C). It is noteworthy that the peripheral edge of Rpt6-C formed by loops $\alpha1$-$\alpha2$ and $\alpha3$-$\alpha4$, which was found to undergo chemical exchange (Figure 14E), contributes to Rpn14 binding (Figure 17D).

## Quantitative validation of chemical shift perturbation mapping

Although the binding interface of Rpt6-C with Rpn14 is similar to that of Rpt1 and Rpt3 CTDs with their respective chaperones (Figure 18D-F), the assessment of chemical shift perturbations (Figure 17A) used for TreeDock simulation relies on the qualitative measurement of remotely shifted versus proximally shifted. In order to cross-validate this result, spectra of the free and complexed Rpt6-C protein were subjected to a quantitative analysis using the integrative volume of the chemical shift region surrounding the peak of the Rpt6-C unbound spectrum. This identical chemical shift region was then integrated in

---

** TreeDock simulations were performed by Amr Fahmy, as described[146]

the spectrum of Rpt6-C with equimolar amounts of Rpn14. By comparing the signal intensity of the two regions as represented by their volume, it was then possible to observe the reduction in intensity of the signal that was due to Rpn14 by using the equation:

$$CSP_{RA} = 1 - \frac{I_{bound}}{I_{free}}$$

where $CSP_{RA}$ is the measure of chemical shift perturbation due to relative attenuation of signal from addition of the binding partner, and $I$ is the volume recorded over a chemical shift boundary in the bound or free spectrum, as indicated. Only peaks that can be fully resolved as independent of other signals in the free spectrum can be discretely integrated. Any peaks that appreciably overlap must be omitted from the analysis.

Signal loss as measured by relative attenuation may be caused by several factors. Most significantly, peaks that are shifted due to protein binding will not produce signal within the initial peak boundary in the complex spectrum, thus will give a low bound/free ratio and ultimately a high RA value. In addition, all peaks that are not fully flexible in the complex will demonstrate an increase in their rotational correlation time, causing their NMR signal to broaden in the complex. Although dependent upon protein flexibility, highly ordered proteins or domains will theoretically demonstrate a similar and consistent drop in signal from this

effect, altering the baseline of a RA plot. Finally, addition of binding partner will dilute the labeled protein, although in a highly variable amount depending on the concentration of the added protein. With all other sample and acquisition parameters equal, dilution of the sample will decrease the intensity of the observed protein for all peaks as compared to that of the unbound spectrum. By adding the binding partner in high concentration and small volumes, this effect can be minimized

This $CSP_{RA}$ value was tracked across the Rpt6-C sequence and assessed for the most attenuated signal (Figure 19). The baseline was intrinsically high, with an average RA of 0.78. This is likely due to the proportionally significant volume of Rpn14 sample added due to its aggregation propensity at high concentrations, as indicated previously. In addition, the Rpt6-C construct signal has an effective molecular weight of 11.2 kDa, which is increased to ~60 kDa in the complex, leading to a significant amount of broadening. However using a threshold of one-half standard deviation above the average (0.95) highlights only those peaks that are nearly fully attenuated. Those residues identified by this analysis (Figure 19) were identical to those identified by standard analysis (Figure 17A) after exclusion of regions confirmed by mutagenesis to not be involved in binding (Figure 18B). Thus, the binding interface used for TreeDock simulation is supported by quantitative analysis of the chemical shift perturbation spectra.
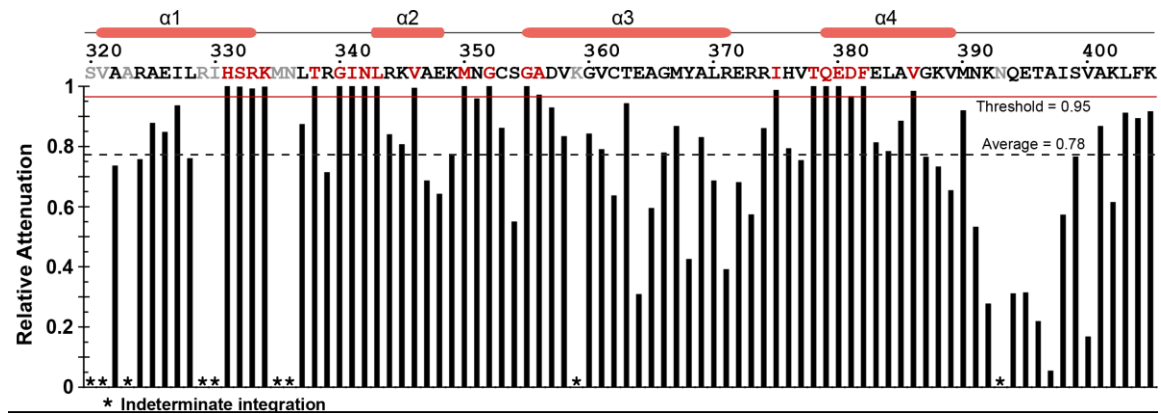
**Figure 19.** Quantitative integration-based analysis of Rpn14 perturbation

Chemical shift perturbation analysis of Rpt6-C by comparing relative attenuation values of free and Rpn14-bound values of each residue. Significantly perturbed residues were identifies by choosing values one-half standard deviation above the average (red and dashed lines, respectively). Residues identified by this method form a similar binding surface to that of the qualitative method (Figure 17A) that was used for TreeDock simulation (Figure 17D).

68

## Rpt6 G$^{360,387}$A reduces Rpn14 association with proteasome base in *S. cerevisiae* and disrupts holoenzyme formation in vitro

To test the functional significance of restricting Rpt6-C to the 4-helix bundle *in vivo*, *S. cerevisiae* was mutated such that G360 and G387 of *RPT6* contained alanine on its chromosomal locus; this mutant strain is referred to as *rpt6AA*\*\*. The interaction of endogenous Rpn14 with proteasome complexes purified from wild-type or *rpt6AA* mutants was examined. Strikingly, the level of Rpn14 was significantly decreased in proteasome complexes from the *rpt6AA* mutant (Figure 20A, lane 1 and 2). The proteasome regulatory particle can be divided into base and lid sub-complexes. The base includes the Rpt1-6, Rpn1, Rpn2, Rpn13 and Rpn10. Purified base isolated via high-salt wash (1 M NaCl) similarly showed a decrease in Rpn14 level for the *rpt6AA* mutant (Figure 20A, lane 3 and 4).

Since RP chaperones including Rpn14 have been proposed to temporally order RP assembly through interactions with specific Rpt subunits, the status of proteasome assembly in the *rpt6AA* mutant was examined. Together with the mature proteasome holoenzymes (RP$_2$-CP, RP-CP), major assembly intermediates (RP and base) were readily detected in both wild-type and *rpt6AA* mutants (Figure 20B). However, Rpn14, which specifically associates with RP and base (Figure 20B; wild-type)[147,150], was nearly absent from either assembly intermediate in the *rpt6AA* mutant (Figure 20B). These results were confirmed by using 2-dimensional native PAGE followed by SDS-PAGE (Figure 20C). Moreover,

---

\*\* Yeast experiments were performed by Soyeon Park and Daniel Finley, as described[146]

immunoblotting the 2D gel for Rpn1 revealed additional species in *rpt6AA* proteasomes, which migrate between $RP_2$-CP and RP-CP (Figure 20C). These species may result from enhanced Ecm29 or Blm10 recruitment to RP-CP, which is charateristically observed in assembly-deficient proteasome mutants[185].

It was tested whether Rpn14 reduction on *rpt6AA* base stems from its decreased cellular abundance. Immunoblotting of whole cell extracts demonstrated slightly less Rpn14 in *rpt6AA* compared to wild-type cells (Figure 20D) and this might in part contribute to the near absence of Rpn14 on *rpt6AA* base (Figure 20B and 20C). However, *RPN14* deletion (*rpn14Δ*) abolishes the presence of base in yeast[153], suggesting that it is essential for either its accumulation or formation *in vivo* and is functional in the *rpt6AA* strain.
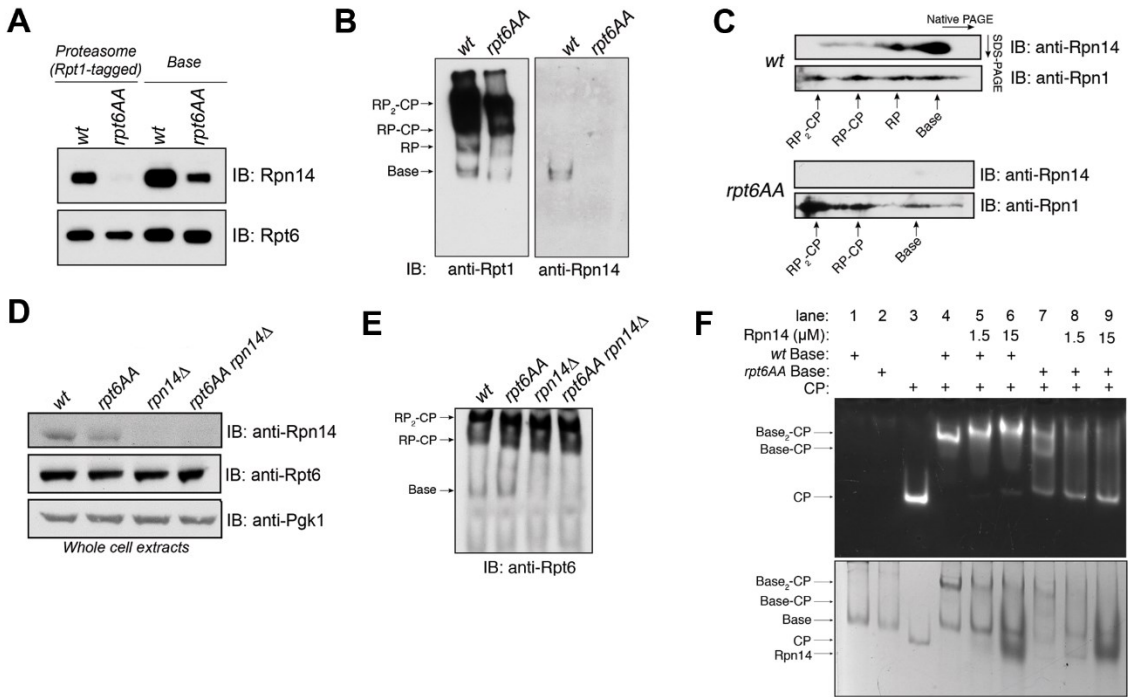
**Figure 20.** Rpt6 G[360,387]A disrupts proteasome assembly

(**A**) SDS-PAGE and immunoblotting of affinity purified proA-TeV-Rpt1-containing species from *wt* (lane 1 and 3) or *rpt6AA* (lane 2 and 4) strains. Base was isolated by 1 M NaCl washes and elution with TeV protease (lanes 3 and 4).

(**B**) Native PAGE and immunoblotting following affinity purification with proA-TeV-Rpt1.

(**C**) 2-dimensional, native SDS-PAGE and immunoblotting following affinity purification with proA-TeV-Rpt1.

(**D**) SDS-PAGE and immunoblotting with whole-cell extracts.

(**E**) 3.5% native PAGE followed by immunoblotting for Rpt6.

(**F**) Purified base (150 nM) and CP (70 nM) were incubated in the presence or absence of recombinant Rpn14 for 15 min at 30°C. The reactions were then resolved on 3.5% native gels and subjected to in-gel peptidase assay in the presence of 0.02% SDS. The gel was subsequently stained with Coomassie blue.

To better understand the effect of Rpn14 and its interaction with Rpt6 during assembly, the formation of base between *rpt6AA* and *rpn14* null mutants was compared via 3.5% and 5% native gel assays using whole cell extracts (Figure 19E). As expected[151,153], base was scarcely present in *rpn14Δ*. In *rpt6AA* however, base appeared at a level comparable to wild-type (Figure 20E). The *rpt6AA rpn14Δ* double mutant mimicked *rpn14Δ*, demonstrating strongly diminished levels of base (Figure 20E). This finding suggests that despite its reduced levels on *rpt6AA* base (Figure 20B and 20C), Rpn14 is still actively contributing to base formation in this mutant.

The effect of Rpt6 $G^{360,387}A$ on base-CP assembly in the presence of excess Rpn14 was therefore tested *in vitro* by native PAGE with either Coomassie blue staining or an in-gel peptidase assay. For this experiment, CP and base purified from *wt* or *rpt6AA* strains were incubated with or without recombinant Rpn14 (Figure 20F). Whereas *wt* base readily integrated into base-CP complexes (Figure 20F, lane 4), *rpt6AA* base demonstrated poor complex formation (Figure 20F, lane 7). The addition of excess Rpn14 resulted in a reduction of base-CP species with wild-type Rpt6, consistent with the current model that RP chaperones, such as Rpn14, compete with CP for Rpt binding during assembly[147,150]. Importantly, Rpn14 was more potent in reducing the formation of base-CP complexes in the presence of *rpt6AA* base (Figure 20F, lanes 8-9). These findings indicate that the intrinsic helix-coil transition of Rpt6 may provide a critical control for proper binding and release of Rpn14 during proteasome assembly.

## Rpt4 and Rpt5 also exhibit structural heterogeneity and loss of Rpt6 conformational exchange enhances Rpn14 requirement during proteasome stress

To assess the impact of *rpt6AA* on substrate degradation by proteasome, canavanine-induced stress response sensitivity was assayed. *rpn14Δ* and *rpt6AA* single mutants demonstrated modest canavanine sensitivity at 37 °C; however, this growth defect was significantly increased in the *rpn14Δ rpt6AA* double mutant (Figure 21A). This finding indicates that *rpt6AA* does not simply mimic *rpn14Δ*. Nonetheless, assembled proteasome is observed in *rpn14Δ rpt6AA* (Figure 20E). It is possible that in contrast to *in vitro* CP-base assembly (Figure 20F), structural heterogeneity is not important for RP-CP assembly. Alternatively, structural heterogeneity may be enabled through other Rpt proteins (Figure 9A). To test whether other Rpt proteins exhibit conformational exchange, $^{1}$H, $^{15}$N HSQC and EXSY experiments were acquired on *S. cerevisiae* Rpt4 (Figure 21B) and Rpt5 (Figure 21C). Both proteins demonstrated millisecond-scale conformational exchange in the EXSY experiments (Figures 21B and 21C, red). Similar to Rpt6 (Figure 9D), correlations were observed between dispersed and non-dispersed signals, suggesting that Rpt4 and Rpt5 may also exhibit helix-coil transitions. Thus, conformational exchange may be a general phenomenon of proteasome *S. cerevisiae* Rpt proteins to facilitate RP-CP assembly (Figure 21D). Future experiments are needed to evaluate this hypothesis.
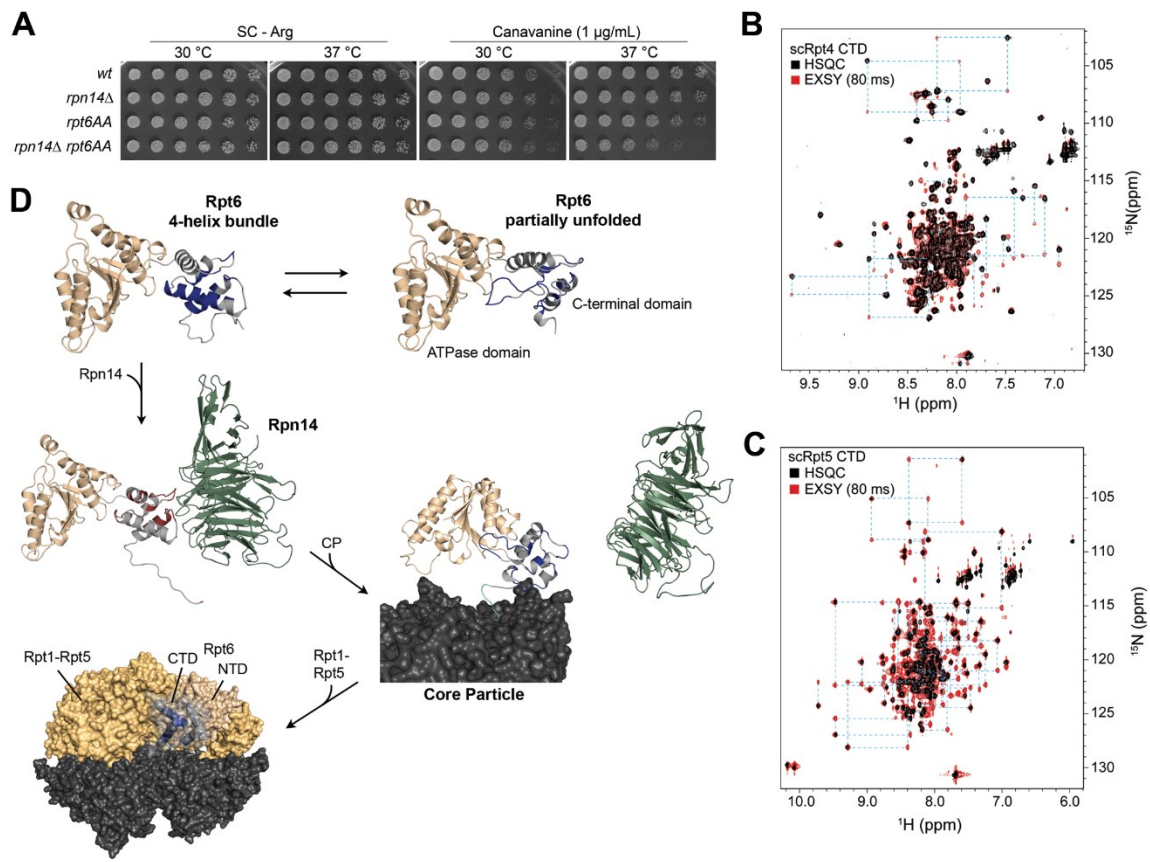
**Figure 21.** Rpt4-C and Rpt5-C exhibit conformational exchange

**(A)** Growth phenotypes of *rpt6AA*. Cells were spotted in 4-fold dilutions on synthetic medium lacking arginine (SC-Arg) or containing canavanine at 1 μg/mL and were grown at 30°C or 37°C for 2-3 days.

**(B)** Overlay of HSQC (black) and EXSY (red) experiments of Rpt4-C and

**(C)** Rpt5-C showing millisecond conformational exchange between two states. Cyan boxes highlight dispersed exchange correlations.

**(D)** Model of exchange-facilitated base formation as templated on the CP. Rpn14 (green) is displaced upon initiation of a conformational switch that causes Rpt6-C transition from a 4-helix bundle to a partially unfolded state. The transient Rpt6-CP structure may then nucleate addition of other Rpt proteins [58,147], ultimately forming the assembled RP, as previously modeled by EM [54].

74

## Summary and Discussion

These data demonstrate that the two most C-terminal helices of *S. cerevisiae* 26S proteasome ATPase Rpt6 undergoes helix-coil transitions. Alanine substitution of G360 and G387, located within these helices, restricts Rpt6's C-terminal domain to its structurally intact 4-helix bundle and increases its melting temperature. It is noteworthy that exchange in the $\alpha1$-$\alpha2$ and $\alpha3$-$\alpha4$ loop region is abrogated in Rpt6 $G^{360,387}A$, as this finding demonstrates that the $\alpha3$ and $\alpha4$ helix-coil transitions are propagated to this more peripheral Rpn14-binding region.

Rpt6 $G^{360,387}A$ affinity for Rpn14 is not decreased compared to wild-type Rpt6 and is in the low nM range, as assessed by analytical ultracentrifugation. This affinity is surprisingly high, but specific to Rpt6-C's 4-helix bundle state. It is possible that Rpt6-C conformational exchange could play a role in Rpn14 binding and release during proteasome assembly. Interestingly, base from *rpt6AA* exhibited reduced Rpn14, suggesting that Rpt6-C conformational heterogeneity may also help accommodate Rpn14 on base.

Rpt1-C, Rpt3-C and Rpt6-C use a similar surface to bind their molecular chaperones (Figure 18D-F), which may have evolved to position the chaperones proximal to the CP. Chaperone clashes with CP are suggested by the Rpt1:Hsm3[144] and Rpt3:Nas6[150] structural complexes. Steric clashes are also predicted between Rpn14 and the CP when Rpt6's C-terminal HbYX-like motif is docked into the CP $\alpha$-ring pockets (Figure 18C). These structural models provide support for the hypothesis that chaperones and CP compete for Rpt binding during

assembly[147,150]. Structural transitions could fine tune this competition to enable effective interconversion between Rpt:chaperone and Rpt:CP complexes. In particular, steric clashes between Rpn14 and CP may favor Rpt6 exchange to its partially unfolded state and in turn promote Rpn14 expulsion.

*In vitro* base-CP complex formation was inefficient with Rpt6 G$^{360,387}$A, perhaps because base isolated from *rpt6AA* has significantly reduced levels of Rpn14. Nonetheless, addition of recombinant Rpn14 exacerbated the base-CP assembly defect, most likely because its interaction with base cannot be fine tuned by Rpt6-C dynamics. Assembly defects were also apparent for *rpt6AA in vivo*. Proteasome species were observed in *rpt6AA* extracts that migrate between RP$_2$-CP and RP-CP by native gel; these are not present in wild-type cells and are hallmarks of assembly defects[185]. *rpt6AA* exhibited hypersensitivity to canavanine when introduced into an *rpn14* null, suggesting Rpt6-C dynamics also plays an Rpn14-independent role. Altogether, these results suggest that Rpt6-C dynamics facilitate proteasome assembly in yeast. It is possible that structural heterogeneity in other Rpt proteins also contributes to proteasome assembly, as Rpt4 and Rpt5 were found to undergo conformational exchange. Future experiments are needed to evalute the effect of losing conformational exchange in these Rpt proteins.

# Chapter 3

## Insights into Multireceptor Substrate Recruitment: Avidity-coordinated Dynamics of S5a and Rpn13[†]

### Introduction

Ubiquitin conjugation plays a key regulatory role in a wide array of biological processes. In its most established role, ubiquitination targets proteins for degradation by the 26S proteasome[186], a process important for controlling the lifespan of regulatory proteins, removing misfolded proteins, producing immunocompetent peptides[187], and regulating cell cycle progression[188,189].

The 26S proteasome contains a 20S catalytic core particle (CP) capped at either or both ends by 19S regulatory particles (RPs), which prepare substrates for hydrolysis in the CP. RP ubiquitin receptors S5a/Rpn10[69] and Rpn13[71] capture substrates by recognizing their covalently attached ubiquitin chains, which are removed and disassembled by three deubiquitinating enzymes Rpn11[73], Ubp6/Usp14[83] and Uch37/UCHL5[128]. These actions of the RP's ubiquitin processing enzymes are complemented with that of six ATPases that unfold protein substrates to allow their passage into the CP for degradation.

Ubiquitin receptors play an integral role in substrate capture and apparently contribute to ubiquitin chain deconjugation, as Rpn13 binds and activates deubiquitinating enzyme Uch37[85,89,90]. S5a and Rpn13 may receive ubiquitinated proteins from extra-proteasomal receptors, including the hHR23 and hPLIC proteins, which bind to them with ubiquitin-like (UBL) domains[71,107,108] and to ubiquitin with ubiquitin-associated (UBA) domains[101,102,190]. UBL-UBA proteins can also dock substrates into the proteasome by binding to Rpn1 (S2)[82], a protein that may also bind S5a[191]. S5a is also abundant free of the proteasome, where it has been demonstrated in budding yeast to prevent the hPLIC homolog Dsk2 from binding to proteasome and inhibiting substrate degradation[192]. Although not essential in budding yeast[193], S5a is essential in mice[92] and *D. melanogaster*[194].

Unique roles for the ubiquitin receptors associated with proteasome degradation are suggested by their diverse ubiquitin binding properties. hHR23a is sandwiched between the ubiquitin subunits of K48-linked diubiquitin[105], effectively sequesters subunits of polyubiquitin up through octaubiquitin[195], and protects ubiquitin chains from deubiquitination[104,113]. By contrast, Rpn13 binds preferentially to the proximal subunit of K48-linked diubiquitin leaving the distal one available for other interactions[70], presumably including that of Uch37, which may facilitate its distal end[128] deubiquitinating activity[85,89,90].

Although S5a was the first proteasome ubiquitin receptor discovered[69], its structure complexed with polyubiquitin has not yet been solved. Like Rpn13, the yeast Rpn10 protein is significantly truncated compared to its human S5a

homologue[88]. Whereas mammalian Rpn13 gains a deubiquitinating enzyme binding domain (that of Uch37), the extension in mammalian S5a affords a second UIM that binds ubiquitin more strongly than the conserved one[87]. In previous work, the structure of S5a (196–306) was solved alone and complexed with monoubiquitin to reveal that its UIMs act independently[87].

NMR spectroscopy and analytical ultracentrifugation were previously used to solve the S5a (196–306):K48-linked diubiquitin structure[88]. In contrast to S5a's binding of monoubiquitin, its two UIMs bind a common diubiquitin molecule rather than recruit two diubiquitins simultaneously. Moreover, it exhibits subunit specificity and binding determinants that make its interaction with ubiquitin chains unique from that of Rpn13 or hHR23a. This chapter provides evidence that S5a and Rpn13 bind K48-linked diubiquitin simultaneously with subunit specificity. This information provides a model of how the proteasome recognizes polyubiquitinated substrates in light of multiple ubiquitin receptors.

## S5a binds the distal subunit of K48-linked diubiquitin while Rpn13 binds the proximal subunit

Rpn13's ubiquitin-binding domain binds to K48-linked diubiquitin with an affinity of 90 nM[71]. Therefore, it was tested whether Rpn13 precludes S5a from binding to K48-linked diubiquitin. Equimolar quantities of K48-linked diubiquitin and Rpn13 (1–150) were added to $^{13}$C labeled S5a (196–306). A $^1$H,$^{13}$C HMQC experiment revealed S5a UIM1 and UIM2 resonances that shift upon addition of

K48-linked diubiquitin (Figure 22A, green) to appear at similar positions when Rpn13 was added with diubiquitin (Figure 22A, blue). Hence, Rpn13 does not preclude S5a from binding to K48-linked diubiquitin. To test whether Rpn13 and S5a bind diubiquitin simultaneously, equimolar quantities of unlabeled K48-linked diubiquitin and S5a were added to $^{15}$N-labeled Rpn13. Rpn13 amino acids that are close to the isopeptide bond linkage when bound to the proximal subunit shift in a different manner when bound to K48-linked polyubiquitin versus monoubiquitin[70]. These Rpn13 resonances were found to shift to their proximal-bound state when S5a (196–306) is present (Figure 22B). Therefore, it was hypothesized that Rpn13 binds to the proximal subunit while S5a binds to the distal subunit.

**Figure 22**. Ubiquitin Receptors Rpn13 and S5a Bind K48-Linked Diubiquitin Simultaneously

**(A)** $^1$H, $^{13}$C HMQC experiments recorded on $^{13}$C-labeled S5a (196–306) alone (black) or with equimolar K48-linked diubiquitin (green) or K48-linked diubiquitin and Rpn13 (1–150) (blue) reveal P276 (left) and V222 (right) to interact with diubiquitin when Rpn13 is present.

**(B)** $^1$H, $^{15}$N HSQC experiments on $^{15}$N-labeled Rpn13 (1–150) alone (black) and with monoubiquitin (orange), K48-linked diubiquitin (red), or K48-linked diubiquitin and S5a (196–306) (blue) reveal L73 to shift to its diubiquitin-bound state when S5a is present.

**(C and D)** K48-linked diubiquitin with its proximal **(C)** or distal **(D)** subunit $^{15}$N labeled alone (black) or with Rpn13 (1–150) (red), S5a (196–306) (green), or both of these receptors (blue) indicates shifting that mimics Rpn13 binding to the proximal subunit, but S5a binding to the distal one, as shown for F45 and Q62 of the proximal subunit and I44 and I61 of the distal subunit. Additional data is provided in Figure 23.

**(E)** Model illustrating Rpn13 bound to K48-linked diubiquitin's proximal subunit and S5a's UIMs interacting dynamically with the distal one.

*(see image on next page)*

**Figure 22.** *(see legend on previous page)*
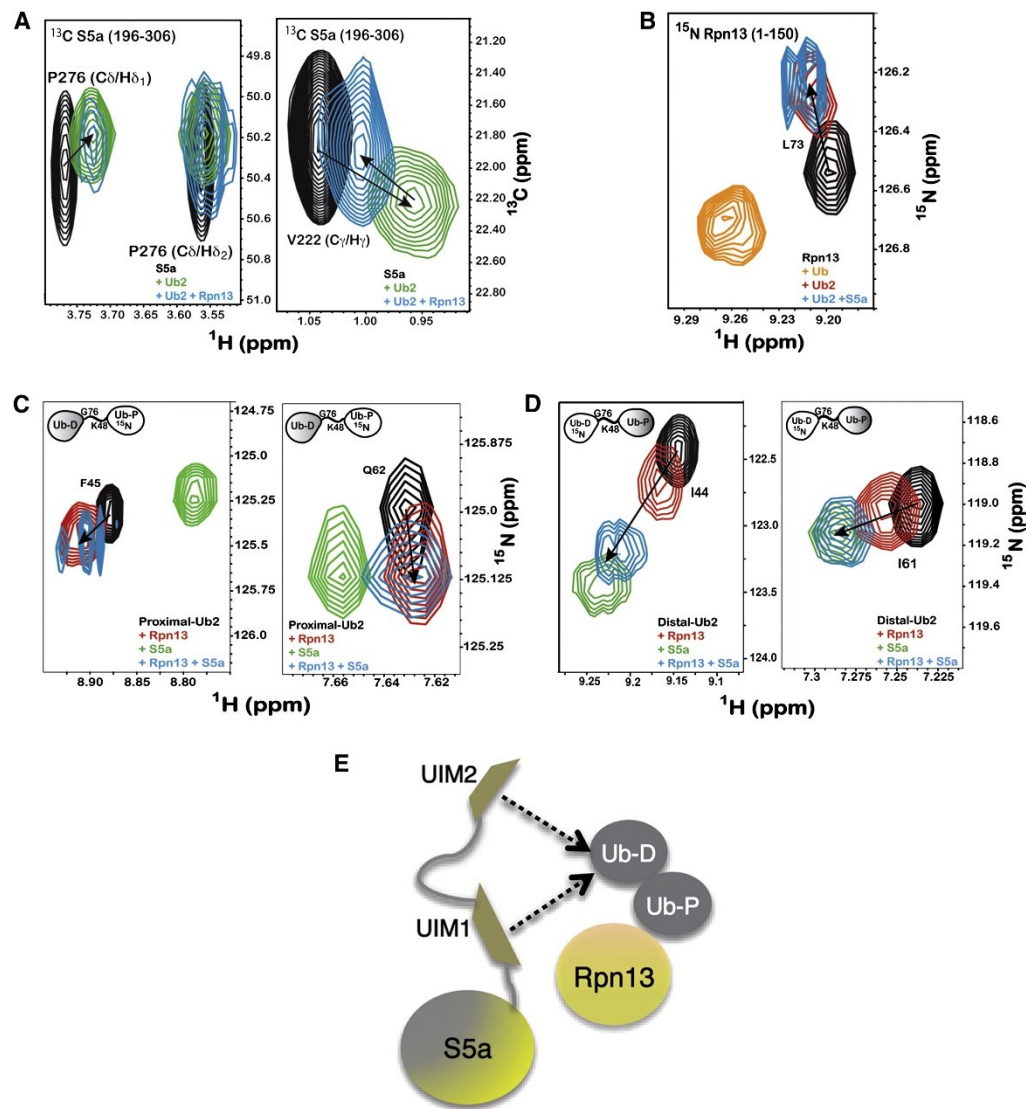
To test more directly which receptor binds K48-linked diubiquitin's proximal subunit, S5a (196–306) and Rpn13 (1–150) or just one of these proteins were added to equimolar quantities of K48-linked diubiquitin with its proximal subunit $^{15}$N labeled. The observed chemical shift changes with both receptors present were similar to those caused by only Rpn13 addition, as demonstrated for F45 and Q62 (Figures 22C and Figure 23). In contrast, the addition of equimolar quantities of S5a (196–306) and Rpn13 (1–150) to K48-linked diubiquitin with its distal subunit $^{15}$N labeled revealed the larger chemical shift changes characteristic of S5a (196–306) interaction, as illustrated for I44 and I61 in Figure 22D. Altogether, these data indicate that S5a binds predominately to the diubiquitin distal subunit while the stronger binding Rpn13 maintains its position at the proximal subunit.

Although UIM2 has the stronger affinity for K48-linked diubiquitin, $^{13}$C resonances from both UIM motifs shift upon addition of K48-linked diubiquitin when Rpn13 is present (Figure 22A, blue). Rpn13, however, either mitigates the chemical shift perturbations, as shown in Figure 22A for V222, or causes attenuation, as shown in Figure 22A for P276. These differences suggest that UIM1 and UIM2 compete for K48-linked diubiquitin's distal subunit when Rpn13 occupies the proximal one (Figure 22E). Dynamic binding behavior was also evident in spectra recorded on the proximal subunit, although to a lesser extent. The observed spectral changes with both receptors present largely mimic those caused by only Rpn13; however, additional attenuations are observed for A46 and H68 (Figure 23).
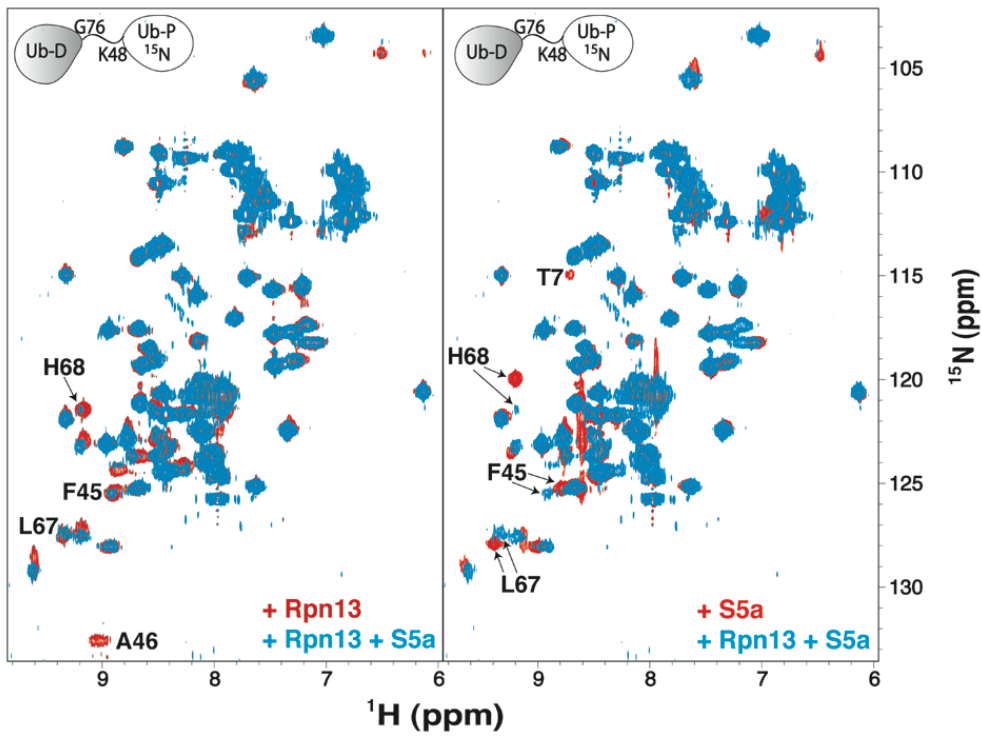
**Figure 23.** Diubiquitin's proximal subunit binds predominately to Rpn13

$^1$H, $^{15}$N HSQC spectra of K48-linked diubiquitin with its proximal subunit $^{15}$N labeled in the presence of equimolar Rpn13 (left, red), S5a (right, red), or both of these ubiquitin receptors (blue). Selected ubiquitin resonances are labeled, including T7, F45, L67, and H68, which shift in a manner that reflects Rpn13 binding. Attenuation of A46 and H68 in the presence of Rpn13 and S5a suggests that, although a large fraction of the proximal subunit is bound to Rpn13, some minor exchange most likely occurs.

The model presented in Figure 22E was tested directly by labeling either the UIM1 or UIM2 region of S5a with the paramagnetic spin label S-(2,2,5,5-tetramethyl-2,5-dihydro-1H-pyrrol-3-yl)methyl methanesulfonothioate (MTSL)**. MTSL causes distance-dependent attenuation with effects apparent up to distances of ~20 Å by paramagnetic relaxation enhancement (PRE). It forms a disulfide bond with cysteine residues and, since S5a (196–306) contains no cysteines, it was straightforward to produce protein samples with either UIM1 or UIM2 labeled. UIM1 and UIM2 labeling was performed by substituting Q227 and A298 with cysteine, respectively. These two residues were chosen based on the NMR structure[88]. They do not contact diubiquitin directly and their mutation is therefore not expected to disrupt S5a:diubiquitin interaction; however, they are close enough for MTSL-induced attenuation of diubiquitin atoms (model structures are provided for the major conformation in Figure 24A).

Samples were produced in which either diubiquitin's proximal or distal subunit is $^{15}$N labeled and mixed these at 1:1 molar ratio with S5a (196–306) samples with either Q227C or A298C MTSL labeled. The amide resonance of Q62 from diubiquitin's proximal subunit was partially attenuated by UIM1 spin labeling, but obliterated by UIM2 spin labeling (Figure 24B, middle panel compared to left). Q62 is not attenuated upon S5a (196–306) addition when S5a is not spin labeled (Figure 25). Moreover, D21 and A28, which are over 20 Å away from each of S5a's MTSL labels, are not greatly attenuated, whereas D58, which is ~15 Å away, is

***

** MTSL experiments were performed by Leah Randles, as described[88]

slightly attenuated (Figure 24B). This finding is consistent with the presence of two S5a:diubiquitin conformations, with the predominant species having UIM2 bound to the proximal subunit and the minor species with it bound to the distal one. Consistent with this model, UIM1 spin labeling resulted in partial attenuation of Q62 from the proximal subunit, but obliterated this residue's amide resonance from the distal subunit (Figure 24B, middle panel compared to left). Similarly, D58 is slightly affected by the induced paramagnetic relaxation effects from S5a MTSL labeling whereas the more remote D21 and A28 are not affected. Altogether, these data are consistent with the NOE-derived S5a:diubiquitin structures[88]. Confident that this approach is effective, the effect of having hRpn13 (1–150) present was tested.

**Figure 24.** *(see legend on next page)*
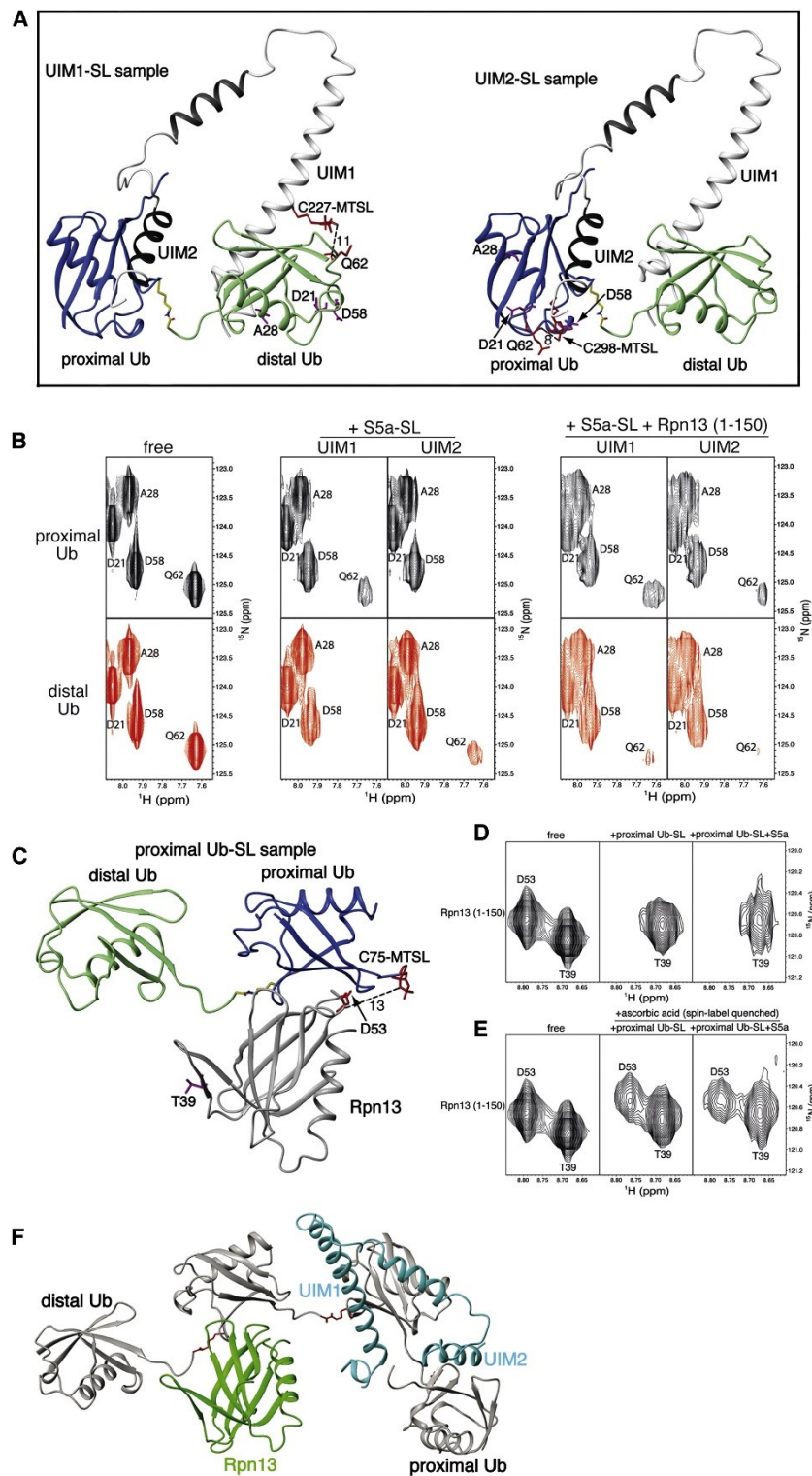
**Figure 24.** MTSL labeling demonstrates hRpn13's preference for K48-linked diubiquitin's proximal subunit as S5a's two UIMs bind the distal subunit

**(A)** Ribbon representation of the major S5a (196–306):K48-linked diubiquitin structure displaying MTSL covalently attached to C227 (left) or C298 (right). Each of these cysteines was introduced for UIM1 or UIM2 spin labeling by MTSL. Q62 is also displayed as well as approximate distances in angstroms between its backbone amide proton atom and MTSL's single-electron center (oxygen atom). It is worth noting that MTSL and the cysteine side chain atoms are flexible such that the distances shown are only approximations. D21, A28, and D58 are also displayed and highlighted in purple, as they are used for comparison.

**(B)** Expanded view of $^1$H, $^{15}$N HSQC spectra for the proximal (top panels) or distal (bottom panels) subunit of K48-linked diubiquitin alone (left panel), with added MTSL labeled C227 (UIM1), or C298 (UIM2) only (middle panel), or with hRpn13 (1–150) in addition (right panel), as labeled. S5a-SL refers to MTSL-labeled S5a (196–306).

**(C)** Ribbon representation of Rpn13:K48-linked diubiquitin structure displaying MTSL covalently attached to C75 of the proximal ubiquitin. D53 of hRpn13 is displayed as well as the approximate distance in angstroms between its backbone amide proton atom and MTSL's single-electron center (oxygen atom). T39 is displayed and highlighted in purple, as it is used for comparison.

**(D)** Expanded view of $^1$H, $^{15}$N HSQC spectra for the hRpn13 (1–150) alone (left panel) with MTSL-labeled K48-linked diubiquitin only (middle panel) or with S5a (196–306) in addition (right panel), as labeled. Proximal Ub-SL refers to K48 diubiquitin with its proximal subunit MTSL labeled.

**(E)** Expanded view of $^1$H, $^{15}$N HSQC spectra for the hRpn13 (1–150) alone (left panel) and with either spin label quenched K48-linked diubiquitin G75C only (middle panel) or with unlabeled S5a (196–306) in addition (right panel). All spectra of protein mixtures were acquired with all components at 0.3 mM.

**(F)** Model of one possible binding configuration for Rpn13 (1–150) (green) and S5a (196–306) (blue) simultaneously bound to K48-linked tetraubiquitin (gray with K48-G76 linker region in red). In a tetraubiquitin chain, a ubiquitin subunit is available to each ubiquitin-binding module and K48 and G76 of the interior subunits are both engaged in isopeptide bonds with neighboring units. It is worth noting that the highly dynamic nature of S5a binding to polyubiquitin ensures that other configurations are possible.
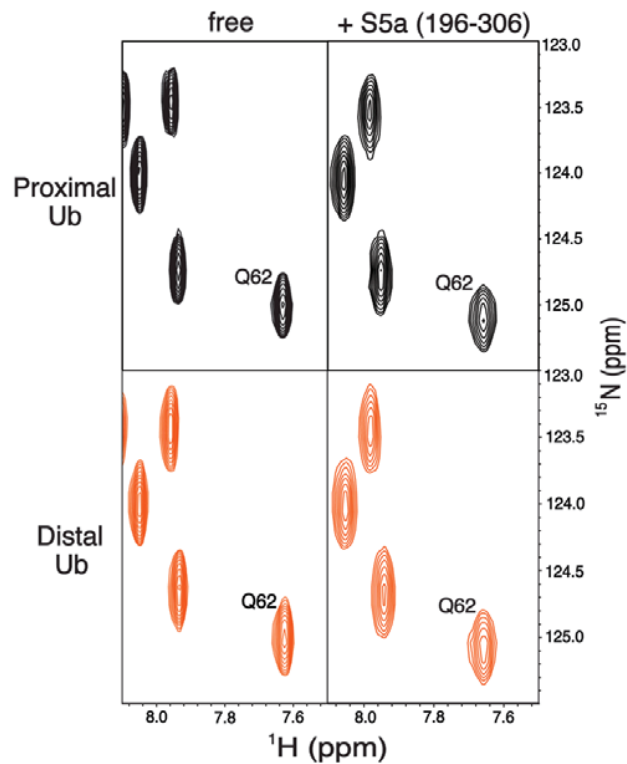
**Figure 25.** Q62 of diubiquitin's proximal and distal subunits is not attenuated upon addition of unlabeled S5a (196-306)

Expanded view of $^1$H, $^{15}$N HSQC spectra for the proximal (top panels) or distal (bottom panels) subunit of K48-linked diubiquitin alone (left panel), or with added unlabeled S5a (196-306) (right panel).

hRpn13 (1–150) and S5a (196–306) with either its UIM1 or UIM2 spin-labeled was added to diubiquitin with either its proximal or distal subunits $^{15}$N labeled. All three proteins were at 0.3 mM concentration. In this case, general resonance broadening is observed due to the larger size of the ternary complex. However, Q62 of the proximal subunit is only slightly more broadened than D21, A28, and D58 when either UIM1 or UIM2 is MTSL labeled (Figure 24B, right panel compared to left). In contrast, the NMR signal of this residue in the distal subunit is almost obliterated by UIM1 and UIM2 MTSL labeling. The greatly reduced attenuation of the proximal subunit's Q62 upon Rpn13 addition indicates that UIM2 is largely displaced from this subunit by Rpn13, as modeled in Figure 22E. That UIM2 spin labeling causes increased attenuation of Q62 from the distal subunit indicates that it now interacts with this ubiquitin moiety. The UIM2-distal ubiquitin interaction causes partial restoration of Q62 in the sample with UIM1 labeled and hRpn13 present (Figure 24B, right panel compared to left). Hence, UIM1 and UIM2 appear to compete for the distal subunit of diubiquitin when Rpn13 is present.

It was tested directly whether hRpn13 binds to the K48-linked diubiquitin proximal subunit when S5a (196–306) is present by substituting G75 of the proximal subunit with cysteine and then labeling it with MTSL. Proximal G75 is not in the immediate Rpn13 binding surface and therefore its mutation is not expected to disrupt binding; however, it is close enough to some residues to cause paramagnetic attenuation when labeled with MTSL (Figure 24C). Addition of proximal G75C MTSL diubiquitin to $^{15}$N-labeled hRpn13 (1–150) obliterates NMR

signals from Rpn13 residues that are close to the proximal subunit in the Rpn13 (1–150):K48-linked diubiquitin complex[71], as demonstrated for D53 in Figure 24D (middle). When this experiment is repeated with unlabeled S5a (196–306) present, the obliteration due to hRpn13 binding to the proximal subunit is preserved (Figure 24D, right panel). These experiments were also performed with all three proteins at 0.3 mM. Residues with distances to the MTSL label that are too far for paramagnetic relaxation enhancement effects do not exhibit such dramatic signal attenuation, as demonstrated for T39 in Figure 24D. Moreover, the D53 resonance reappears in the binary and ternary complexes after spin label quenching (Figure 24E). The quenching reaction was done by reducing the MTSL moiety with 5-fold molar excess ascorbic acid (Figure 24E). Therefore, the attenuation observed in Figure 24D is due to the distance-dependent paramagnetic relaxation enhancement induced by MTSL. These data indicates that Rpn13 predominately binds to the proximal subunit when S5a is present, as suggested by the chemical shift perturbation data and the results of spin labeling S5a.

Altogether, these data indicate that Rpn13 and S5a can bind to a common K48-linked polyubiquitin chain, even for diubiquitin, which has only two ubiquitin subunits. In longer chains, each ubiquitin-binding element can readily bind a ubiquitin subunit. The internal subunits of longer chains harbor the advantages of both the proximal and distal subunits of a diubiquitin chain, as K48 and G76 of these subunits are both engaged in isopeptide bonds with neighboring ubiquitin subunits. Internal ubiquitins therefore provide the additional contact of the linker

region preferred by S5a's UIM2 and Rpn13 as well as the increased rigidity of the C-terminal stretch of residues[196], which is preferred by UIM1. A model of Rpn13 and S5a's UIMs bound to internal and proximal subunits is provided in Figure 24F.

## Summary and Discussion

The coordinated binding of both S5a UIMs greatly enhances its affinity for K48-linked diubiquitin over monoubiquitin and that although the UIMs can be accommodated on either subunit, a preference exists for UIM1 on the distal subunit while UIM2 occupies the proximal one[88]. These data demonstrate that S5a and Rpn13 are able to bind a common diubiquitin chain and that as Rpn13 retains its preferred position at the proximal subunit, S5a binds the distal one. In a diubiquitin chain, the two UIMs compete for the distal subunit when Rpn13 is present; however, in a longer chain these two ubiquitin-binding elements would no doubt occupy separate subunits, as they do in Rpn13's absence[88]. In the absence of the proteasome, these data suggest that multiple binding configurations are available for Rpn13 and S5a binding to K48-linked tetraubiquitin, one of which is shown in Figure 24F.

It is not yet clear whether such coordinated binding occurs in the context of the proteasome; however, it is possible that Rpn13 and S5a bind chains simultaneously to orient substrates for optimal capture and deubiquitination. The distance across the proteasome's RP is similar to that spanned by an opened tetraubiquitin structure. Therefore, even if S5a and Rpn13 are not docked next to

each other, it is still conceivable for them to bind a common ubiquitin chain, as modeled in Figure 8. The proteasome appears to require most substrates to be conjugated to a chain of four or more ubiquitins[197]. This minimal chain length may be preferred to allow for the coordinated binding of ubiquitin receptors, which may, in turn, orient the chain in a manner conducive for the effective activity of deubiquitinating enzymes. For example, S5a- and Rpn13-coordinated binding may lead to the substrate end of the ubiquitin chain being proximal to Rpn11, which performs degradation-coupled deubiquitination[72,73,124], and the distal end of the chain near Uch37, which performs distal-end deubiquitination[128]. Future experiments are required to test this hypothetical model.

The experiments described here used K48-linked chains because of their established importance in triggering degradation by the proteasome. S5a can also bind to K63 linkages with no apparent reduction in affinity compared to K48-linked chains[87]. Rpn13's ubiquitin-binding domain has high affinity for even monoubiquitin[70], suggesting that it too can bind chains of varying linkage. Although K63-linked chains mediate nonproteasomal events, they can support degradation by the proteasome[198]. Thus, these data suggest that the outcome of K63-linked ubiquitination is not determined by the proteasome's ubiquitin receptors. Rather, as demonstrated here, S5a and Rpn13 are adaptive and collaborative in their binding to ubiquitin chains, which supports their primary job of enabling proteasomes to capture ubiquitinated proteins.

Although contacts were revealed between the UIMs and diubiquitin that were unique to the conjugated subunits, their overall binding mode is similar to that used to bind monoubiquitin. Moreover, the two UIMs share the same basic ubiquitin-binding scaffold. The key residues involved in binding to ubiquitin units are [216]LALAL[220] for UIM1 and [287]IAYAM[291] for UIM2, and, in both cases, residues N-terminal to these helical structures participate in binding ubiquitin[88]. UIM1 is conserved in *S. cerevisiae*, and it is possible that UIM2 evolved in higher eukaryotes by UIM1 duplication and optimization for ubiquitin binding, as UIM2 is the stronger binding partner for diubiquitin[88] and monoubiquitin[87]. S5a (196–306) affinity for diubiquitin was determined to be significantly higher than either UIM's affinity for monoubiquitin[87,88,199] and showed that S5a binds diubiquitin with 1:1 stoichiometry even when diubiquitin is 8-fold in excess. Thus, UIM2 is apparently not used to recruit in multiple substrates simultaneously, but rather to enhance affinity for each substrate.

Although not essential in budding yeast[193], S5a is required for murine embryonic development[92]. It is also essential in *Drosophila melanogaster*, in which its deletion results in larval-pupal polyphasic lethality and multiple mitotic defects, as well as accumulation of ubiquitinated proteins and defective 26S proteasome[194]. Therefore, in higher eukaryotes, Rpn13 and the UBL-UBA proteins cannot substitute for S5a.

A prior study on a related system demonstrated S5a-bound K48-linked tetraubiquitin can also bind to hHR23a, even though hHR23a precludes additional

UBL-UBA family members from binding a common ubiquitin chain[195]. In this ternary complex, UIM1 of S5a physically contacts the ubiquitin chain, as UIM2 binds to hHR23a's UBL domain. S5a therefore appears to be able to share ubiquitinated substrates with other ubiquitin receptors. Altogether, these data support a model in which S5a has evolved to bind polyubiquitinated substrates in a manner that takes advantage of other ubiquitin receptors.

# Summary and Future Directions

The 19S regulatory particle is a highly dynamic protein complex with secondary structure exchange, subunit and domain flexibility to adapt with various ubiquitin chain linkage types and lengths, and response to binding of other proteins or ATP. Despite concerted effort to characterize the full RP at high resolution, no such structure has been solved. The RP composition may fluctuate, such that transient proteins may be required under only certain contexts. The ATPase ring appears to shift upon nucleotide binding and hydrolysis[54,55], and the specific Rpt-CP contacts may change during the course of proteasome assembly[58]. In addition, chaperone proteins may bind only prior to holenzyme maturation. The research presented in this dissertation gives two examples of RP subunit dynamics influencing protein-protein interactions, and ultimately, their function.

The Rpt heterohexameric ring contains at least three discrete subunits that undergo conformational exchange in their C-terminal domain in *S. cerevisiae*, Rpt4, Rpt5, and Rpt6. In the case of Rpt6, this exchange is characterized by a helix-coil transition in the millisecond time scale. This produces two predominant species: a 4-helix bundle consistent with the AAA fold, and a partially unfolded state with increased dynamics. This exchange is nucleated independently at Rpt6 G360 and G387, and their substitution with alanine stabilizes the 4-helix state. Future studies will investigate the nature of conformational exchange in other Rpt proteins. Rpt4 and Rpt5 were shown to exchange on a similar time scale, but it is

not yet clear where the exchange interface is located or the structural and dynamic properties of each state. Although the exchange state in these two proteins is located in the non-dispersed region of NMR spectra similar to Rpt6, it is not firmly established that the exchange is primarily helix-coil transition or whether there are two or more discrete states. Similarly, the two nucleating glycines in Rpt6 are not present in Rpt4 or Rpt5, and thus, the structural initiation site of their exchange is unclear. Future studies will similarly investigate Rpt1, Rpt2, and Rpt3 for these properties.

The implications of Rpt6-C exchange were investigated in light of its interaction with proteasome assembly chaperone Rpn14. NMR and AU data suggest that Rpn14 binds selectively to the 4-helix bundle and with a tight dissociation constant of 0.25 nM. In *S. cerevisiae* with the *rpt6AA* chromosomal mutation, proteasome assembly is inefficient. Rpn14 is retained at the proteasome, suggesting that Rpt6 dynamics are required for proper RP assembly and may suggest inefficient expulsion of Rpn14 after Rpt6 docking. This gives evidence for a model in which Rpt exchange serves as a mechanism for chaperone release. Since Rpt6 is believed to assemble as part of the early nucleation of the base[58,147], it is possible that Rpt6 could be unique in this mechanism of chaperone release. Nonetheless, *rpt6AA* contains only slight sensitivity to canavanine, suggesting that other Rpts may partially rescue this phenotype *in vivo*. Rpt4 and Rpt5 exchange, and there remains a possibility that Rpt1, Rpt2, and Rpt3 exchange. In this regards, RP base assembly may be a highly coordinated process. Although Rpt2

and Rpt4 are not known to bind chaperone proteins, dynamics may play a role in chaperone interactions of their heterodimeric partner in the base pre-assembly complexes. Future studies will investigate the effects of Rpt exchange on chaperone binding and how the Rpts coordinate their dynamics and interactions to facilitate base assembly and chaperone release.

A second example of RP dynamics concerns conformational flexibility of components that adapt to ubiquitin chains on various substrates. Upon 26S maturation, the RP recognizes these substrate targets through the use of ubiquitin receptor proteins. Two intrinsic ubiquitin receptors are known, Rpn13 and Rpn10 (known as S5a in humans). The two receptors were found to interact simultaneously to diubiquitin and with subunit specificity. S5a contains two UIM motifs that are connected by flexible linkers that adapt to the configuration of ubiquitin chains. In this regard, the two ubiquitin receptors may function coordinately or possibly cooperatively to recognize and orient substrates prior to processing by other subunits. Both proteins have receptor-specific substrates, and future studies will focus on the determinants for receptor binding to specific types of substrates and chains. In addition, studies will likely search for a mechanism of substrate orienting such that the proximal isopeptide bond is placed in proximity to Rpn11, and whether this process is dependent upon either or both receptors, additional DUBs, or perhaps the ATPases. Additionally, future work will look into the possibility of other subunits containing intrinsic ubiquitin receptor activity and whether these proteins work coordinately with Rpn10 and Rpn13.

Structural study of the RP is still in relatively early stages, and even less is known about the dynamics of individual subunits and their coordinated motions as a requisite of their function. Although this dissertation focused on the ATPases and ubiquitin receptors, critical dynamics are certain to extend to other subunits and functions, such as DUBs or PCI proteins. As the RP is highly dynamic, there are likely multiple minor configurations to each cap during the processes of RP assembly and proteolysis. NMR is well suited to study this, but advances in the effective resolution of EM single particle analysis may be able to highlight certain regions with high configurational variability, which may then attract more scrutiny by other techniques. A true mechanism for the RP will likely involve the integration of many techniques under many chemical environments that each hope to capture small snapshots of the process.

# Materials and Methods

## Protein Expression and Purification

S. cerevisiae Rpt6-C [P318-K405], Rpt5-C [L351-A434][200], Rpt4-C [L351-L437], Rpn14, and their variants were expressed from pRSF-duet1 (Rpt) and pGEX-6p (Rpn14) vectors in *E. coli* fused with N-terminal polyhistidine (for Rpts) or glutathione S-transferase followed by a PreScission protease cut site (for Rpn14), as described[150]. Affinity chromatography using Talon resin (Clontech) was followed with size-exclusion chromatography by FPLC. Buffer 1 (20 mM NaPO$_4$, 60 mM NaCl, 14 mM β-mercaptoethanol, at pH 6.8) was used unless otherwise indicated. Selectively labeled samples were produced by growing cells in minimal media supplemented with 200 mg/L unlabeled tryptophan, 150 mg/L of $^{15}$N labeled amino acid of interest, and 150 mg/L of unlabeled amino acid for the remaining 18 types.

His-tagged S5a (196-306) and GST-tagged hRpn13 (1-150) were similarly expressed in *E. coli* and purified by using a combination of affinity chromatography and size exclusion chromatography on an FPLC system. hRpn13 (1-150) was cleaved from its GST-tag during elution from glutathione S-sepharose resin by using PreScission protease (GE healthcare). Amide atoms were exchanged into D2O as needed by using lyophilization.

## Synthesis of K48-linked diubiquitin

K48-linked diubiquitin were produced as previously described[201]. Recombinant monoubiquitin was purified in which either an aspartic acid is added to the chain (Ub-D77) or the lysine at position 48 was mutated to an arginine (Ub-K48R). Using these two monoubiquitin samples, K48-linked diubiquitin could be synthesized. Ub-D77 and Ub-K48R that were selectively labeled or unlabeled were incubated with 0.1 $\mu$M UBE1 (E1, Boston Biochem), 25 $\mu$M UBE2K (E2), 2 mM ATP, and 1/5 total volume PBDM8 buffer at 37 °C for ~12 hours. The diubiquitin formed was subsequently purified by using a monoQ column, followed by monoS ion-exchange columns (GE Healthcare). A similar procedure was used to produce K48-linked diubiquitin mutant with its proximal subunit MTSL labeled. In this case, however, a ubiquitin truncated mutant (Ub-G75C) with the C-terminal G75 substituted with cysteine was used.


## NMR Spectroscopy

NMR experiments were conducted at 25 °C on 800, 850, or 900 MHz spectrometers equipped with cryogenically cooled probes. $^1$H, $^{15}$N HSQC, $^1$H, $^{15}$N ZZ-Exchange, $^1$H-$^{15}$N heteronuclear NOE, $R_N(N_z)$, and $R_N(N_X)$ experiments were acquired on $^{15}$N-labeled Rpt6-C at 40-400 $\mu$M. $^1$H, $^{15}$N, $^{13}$C HNCA, HNCOCA, HNCO, HNCACO, and HNCACB spectra were acquired on $^{15}$N, $^{13}$C and 50% $^2$H-labeled Rpt6-C at 300-500 $\mu$M. $^1$H, $^{15}$N, TROSY-HSQC experiments were conducted on $^{15}$N, 90% $^2$H samples at 200 $\mu$M. All spectra were acquired in 10%

$D_2O$ and 0.1% $NaN_3$. $R_N(N_X)$ and $R_N(N_Z)$ data were collected in parallel with a pseudo-3D experiment and a repeated data point for error calculation. $^1H$-$^{15}N$ heteronuclear NOE data were acquired with a 4 s saturation transfer or control period. Relaxation data fitting and model-free analysis were performed by using the program relax[179,180]. The global rotational correlation time was estimated from the average of local $\tau_m$ values derived from the Lipari-Szabo method[202].

## Spin Labeling Experiments

Based on the S5a (196–306):K48-linked diubiquitin complex structure of the major species[88], two S5a (196–306) mutants were designed for MTSL labeling, namely Q227C and A298C. These two residues are not directly involved in binding diubiquitin, so their mutation was not expected to disrupt binding. They were also chosen because they are close enough to K48-linked diubiquitin amide atoms to cause distance-dependent attenuations. After being treated with the spin labeling reagent (MTSL), a single electron (carried by oxygen atom) containing moiety will be attached to the sulfur atom of cysteine residue in S5a mutants. The strong magnetic field of the NMR instrument causes the single electron carried by oxygen atom to accelerate the relaxation of residues within ~20 Å.

## Protein Structure Calculation and Modeling

Hydrodynamic modeling was performed by estimating free Rpt6-C, Rpt6-C $G^{360,387}A$ and Rpn14 as spheres with radii corresponding to their experimentally-determined Stokes' radii and molecular weights corresponding to their amino acid composition. The Rpt6-C:Rpn14 and Rpt6-C $G^{360,387}A$:Rpn14 complexes were then modeled as two adjacent (touching) beads, and the two complexes were compared using the program HYDRO++[182,183].

The Rpt6-C structures for each of the two states were calculated with CS-ROSETTA version 3.1[176] and HN, N, carbonyl, C$\alpha$, and C$\beta$ chemical shift assignments. TreeDock[184] was used to model the Rpt6-C:Rpn14 protein complex. Rpn14's D157 and Rpt6-C amino acids identified to be most affected by Rpn14 addition (Figure 17A) were paired in all possible arrangements and placed at optimal van der Waals distance. Rpt6-C was fixed while Rpn14 was translated and rotated at 0.7 Å increments about the anchored atoms. All non-clashing orientations that satisfied the chemical shift perturbation data were saved. The program Octopus[203] was used to simulate the mutation experiments (Figure 18B).

Full-length Rpt6 was modeled with Prime (Schrödinger, Inc.) using the CS-Rosetta structure and the AAA-ATPase subunit of the *M. janaschii* Proteasome Activating Nucleotidase (PDB entry 3H4M). To generate a structure with Rpt6's C-terminal HbYX-like motif docked into the CP, the Rpt6 structure was aligned 6-fold to the AAA-ATPase structure from HslU (PDB entry 1DO0)[204] with the modeled Rpt6-C:Rpn14 structure replacing one of the Rpt C-terminal domains. The

resulting ATPase:Rpn14 complex was lowered onto the CP α-ring (PDB entry 3H4P) with Rpt6's C-terminal twelve residues oriented based on the PA26/PAN fusion protein (PDB entry 3IPM)[57].

## Analytical Ultracentrifugation

Sedimentation velocity analysis was conducted at 20 °C and 50,000 RPM using interference optics with a Beckman-Coulter XL-I analytical ultracentrifuge. Double sector synthetic boundary cells equipped with sapphire windows were used to match the sample and reference menisci. The rotor was equilibrated under vacuum at 20 °C and after a period of 1 hr., the rotor was accelerated to 50,000 RPM. Interference scans were acquired at 60 second intervals. Rpt6-C, Rpt6-C $G^{360,387}A$ and Rpn14 were each analyzed in Buffer 2 (20 mM NaPO$_4$, 130 mM NaCl, 14 mM β-mercaptoethanol, at pH 6.8) at three concentrations spanning a ~10-fold range with Rpt6-C at 17-130 μM, Rpt6-C $G^{360,387}A$ at 17-160 μM, and Rpn14 at 4-33 μM. The complexes were analyzed at 20-25 μM Rpn14 and 0.5, 1 and 2 equivalents of Rpt6-C or the $G^{360,387}A$ variant. The c(s) sedimentation coefficient distribution plots were obtained using SEDFIT[205]. Sedimentation coefficients and dissociation constants were obtained by global analysis using SEDANAL[206].

## Thermal Denaturation

CD was conducted on a JASCO J-815 spectrophotometer between 190 and 250 nm and with Rpt6-C in Buffer 1 diluted 20-fold with $H_2O$ for a protein concentration of 10 $\mu$M. The temperature was raised in 5 °C increments with 12 minutes of equilibration before acquisition.

## Purification of proteasome base and CP

Protein A resin was used to purify Rpt1-containing complexes by using proA-TEV-Rpt1, in which Rpt1's N-terminal end contains a protein A affinity tag followed by a TEV protease cleavage site (proA-TEV-Rpt1), as described previously[147]. 4-6L of yeast culture was grown in YPD overnight to an $OD_{600}$ of 15-20, harvested and ground in liquid nitrogen, and the ground powders hydrated in an equivalent volume of buffer 3 (50 mM Tris-HCl [pH 7.5], 5 mM $MgCl_2$, 1 mM EDTA, 10% glycerol, and 1 mM ATP) supplemented with protease inhibitors. Lysates were pelleted at 4°C and the supernatant incubated with Affinity Gel Rabbit IgG resin (MP Biomedical) for 2 hr at 4 °C. Resins were washed extensively in buffer 3 containing 100 mM NaCl followed by 1 M NaCl. After a final wash with buffer 3, base was eluted by incubating the resin with 1 bed volume of buffer 3 containing TEV protease (Invitrogen) for 1 hr at 30 °C. CP was purified as described previously[207] except that lysis was performed in liquid nitrogen.

## Analysis of base-CP association by native PAGE and in-gel peptidase assay

Affinity-purified base was mixed with CP at 2:1 molar ratio in 10 $\mu$l of buffer 3 at 30 °C for 15 min. The entire reactions were immediately loaded on pre-chilled 3.5% native gels and run for 2.5 hr at 100V at 4 °C[150]. In-gel peptidase assays were conducted as described[150] with an AlphaImager system (ProteinSimple).

# References

1.  Hershko, A. & Ciechanover, A. The ubiquitin system. *Annu Rev Biochem* **67**, 425–479 (1998).

2.  Finley, D. Recognition and processing of ubiquitin-protein conjugates by the proteasome. *Annu Rev Biochem* **78**, 477–513 (2009).

3.  Varshavsky, A. The ubiquitin system, an immense realm. *Annu Rev Biochem* **81**, 167–176 (2012).

4.  Schwartz, A. L. & Ciechanover, A. Targeting proteins for destruction by the ubiquitin system: implications for human pathobiology. *Annu Rev Pharmacol Toxicol* **49**, 73–96 (2009).

5.  Ruschak, A. M., Slassi, M., Kay, L. E. & Schimmer, A. D. Novel proteasome inhibitors to overcome bortezomib resistance. *J Natl Cancer Inst* **103**, 1007–1017 (2011).

6.  Stein, M. L. & Groll, M. Applied techniques for mining natural proteasome inhibitors. *BBA-Mol Cell Res.* DOI:10.1016/j.bbamcr.2013.01.017 (2013).

7.  Capili, A. D. & Lima, C. D. Taking it step by step: mechanistic insights from structural studies of ubiquitin/ubiquitin-like protein modification pathways. *Curr Opin Struc Biol* **17**, 726–735 (2007).

8.  Deshaies, R. J. & Joazeiro, C. A. RING domain E3 ubiquitin ligases. *Annu Rev Biochem* **78**, 399–434 (2009).

9.  Schulman, B. A. Twists and turns in ubiquitin-like protein conjugation cascades. *Protein Sci* **20**, 1941–1954 (2011).

10. Liu, F. & Walters, K. J. Multitasking with ubiquitin through multivalent interactions. *Trends Biochem Sci* **35**, 352–360 (2010).

11. Fushman, D. & Wilkinson, K. D. Structure and recognition of polyubiquitin chains of different lengths and linkage. *F1000 Biol Rep* **3**, (2011).

12. Dikic, I., Wakatsuki, S. & Walters, K. J. Ubiquitin-binding domains - from structures to functions. *Nat Rev Mol Cell Bio* **10**, 659–671 (2009).

13. Husnjak, K. & Dikic, I. Ubiquitin-binding proteins: decoders of ubiquitin-mediated cellular functions. *Annu Rev Biochem* **81**, 291–322 (2012).

14. Chen, Z. J. & Sun, L. J. Nonproteolytic functions of ubiquitin in cell signaling. *Mol Cell* **33**, 275–286 (2009).

15. Xu, P. *et al.* Quantitative proteomics reveals the function of unconventional ubiquitin chains in proteasomal degradation. *Cell* **137**, 133–145 (2009).

16. Komander, D. *et al.* Molecular discrimination of structurally equivalent Lys 63-linked and linear polyubiquitin chains. *EMBO Rep* **10**, 466–473 (2009).

17. Varadan, R. *et al.* Solution conformation of Lys63-linked di-ubiquitin chain provides clues to functional diversity of polyubiquitin signaling. *J Biol Chem* **279**, 7055–7063 (2004).

18. Nathan, J. A., Tae Kim, H., Ting, L., Gygi, S. P. & Goldberg, A. L. Why do cellular proteins linked to K63-polyubiquitin chains not associate with proteasomes? *EMBO J* **32**, 552–565 (2013).

19. Dammer, E. B. *et al.* Polyubiquitin linkage profiles in three models of proteolytic stress suggest the etiology of Alzheimer disease. *J Biol Chem* **286**, 10457–10465 (2011).

20. Eytan, E., Ganoth, D., Armon, T. & Hershko, A. ATP-dependent incorporation of 20S protease into the 26S complex that degrades proteins conjugated to ubiquitin. *Proc Natl Acad Sci U.S.A.* **86**, 7751–7755 (1989).

21. Löwe, J. *et al.* Crystal structure of the 20S proteasome from the archaeon T. acidophilum at 3.4 A resolution. *Science* **268**, 533–539 (1995).

22. Groll, M., Ditzel, L., Löwe, J. & Stock, D. Structure of 20S proteasome from yeast at 2.4 A resolution. *Nature* **386**, 463–471 (1997).

23. Seemüller, E. *et al.* Proteasome from Thermoplasma acidophilum: a threonine protease. *Science* **268**, 579–582 (1995).

24. Ruschak, A. M., Religa, T. L., Breuer, S., Witt, S. & Kay, L. E. The proteasome antechamber maintains substrates in an unfolded state. *Nature* **467**, 868–871 (2010).

25. Heinemeyer, W., Fischer, M., Krimmer, T., Stachon, U. & Wolf, D. H. The active sites of the eukaryotic 20S proteasome and their involvement in subunit precursor processing. *J Biol Chem* **272**, 25200–25209 (1997).

26. Groll, M., Berkers, C. R., Ploegh, H. L. & Ovaa, H. Crystal structure of the boronic acid-based proteasome inhibitor bortezomib in complex with the yeast 20S proteasome. *Structure* **14**, 451–456 (2006).

27. Berkers, C. R. *et al.* Activity probe for in vivo profiling of the specificity of proteasome inhibitor bortezomib. *Nat Methods* **2**, 357–362 (2005).

28. Baugh, J. M., Viktorova, E. G. & Pilipenko, E. V Proteasomes can degrade a significant proportion of cellular proteins independent of ubiquitination. *J Mol Biol* **386**, 814–827 (2009).

29. Groll, M. *et al.* A gated channel into the proteasome core particle. *Nat Struct Mol Biol* **7**, 1062–1067 (2000).

30. Köhler, A. *et al.* The substrate translocation channel of the proteasome. *Biochimie* **83**, 325–332 (2001).

31. Religa, T. L., Sprangers, R. & Kay, L. E. Dynamic regulation of archaeal proteasome gate opening as studied by TROSY NMR. *Science* **328**, 98–102 (2010).

32. Stadtmueller, B. M. & Hill, C. P. Proteasome activators. *Mol Cell* **41**, 8–19 (2011).

33. Kish-Trier, E. & Hill, C. P. Structural Biology of the Proteasome. *Annu Rev Biophys* **42**, 29–49 (2013).

34. Ustrell, V., Hoffman, L., Pratt, G. & Rechsteiner, M. PA200, a nuclear proteasome activator involved in DNA repair. *EMBO J* **21**, 3516–3525 (2002).

35. Schmidt, M. *et al.* The HEAT repeat protein Blm10 regulates the yeast proteasome by capping the core particle. *Nat Struct Mol Biol* **12**, 294–303 (2005).

36. Ma, C.-P., Slaughter, C. A. & DeMartino, G. N. Identification, purification, and characterization of a protein activator (PA28) of the 20S proteasome (macropain). *J Biol Chem* **267**, 10515–10523 (1992).

37. Dubiel, W., Pratt, G., Ferrell, K. & Rechsteiner, M. Purification of an 11S regulator of the multicatalytic protease. *J Biol Chem* **267**, 22369–22377 (1992).

38. Chu-Ping, M., Vu, J. H., Proske, R. J., Slaughter, C. A. & DeMartino, G. N. Identification, purification, and characterization of a high molecular weight, ATP-dependent activator (PA700) of the 20S proteasome. *J Biol Chem* **269**, 3539–3547 (1994).

39. Barthelme, D. & Sauer, R. T. Identification of the Cdc48•20S proteasome as an ancient AAA+ proteolytic machine. *Science* **337**, 843–846 (2012).

40. Barthelme, D. & Sauer, R. T. Bipartite determinants mediate an evolutionarily conserved interaction between Cdc48 and the 20S peptidase. *Proc Natl Acad Sci U.S.A.* **110**, 3327–3332 (2013).

41. Smith, D. M. *et al.* Docking of the proteasomal ATPases' carboxyl termini in the 20S proteasome's alpha ring opens the gate for substrate entry. *Mol Cell* **27**, 731–744 (2007).

42. Förster, A., Masters, E. I., Whitby, F. G., Robinson, H. & Hill, C. P. The 1.9 A structure of a proteasome-11S activator complex and implications for proteasome-PAN/PA700 interactions. *Mol Cell* **18**, 589–599 (2005).

43. Sadre-Bazzaz, K., Whitby, F. G., Robinson, H., Formosa, T. & Hill, C. P. Structure of a Blm10 complex reveals common mechanisms for proteasome binding and gate opening. *Mol Cell* **37**, 728–735 (2010).

44. Lasker, K. *et al.* Molecular architecture of the 26S proteasome holocomplex determined by an integrative approach. *Proc Natl Acad Sci U.S.A.* **109**, 1380–1387 (2012).

45. Lander, G. C. *et al.* Complete subunit architecture of the proteasome regulatory particle. *Nature* **482**, 186–191 (2012).

46. Chu-Ping, M., Slaughter, C. A. & DeMartino, G. N. Purification and characterization of a protein inhibitor of the 20S proteasome (macropain). *Biochim Biophys Acta* **1119**, 303–311 (1992).

47. Kusmierczyk, A. R., Kunjappu, M. J., Kim, R. Y. & Hochstrasser, M. A conserved 20S proteasome assembly factor requires a C-terminal HbYX motif for proteasomal precursor binding. *Nat Struct Mol Biol* **18**, 622–629 (2011).

48. Hirano, Y. *et al.* A heterodimeric complex that promotes the assembly of mammalian 20S proteasomes. *Nature* **437**, 1381–1385 (2005).

49.  Stadtmueller, B. M. *et al.* Structure of a proteasome Pba1-Pba2 complex: implications for proteasome assembly, activation, and biological function. *J Biol Chem* **287**, 37371–37382 (2012).

50.  Bader, M. *et al.* A conserved F box regulatory complex controls proteasome activity in *Drosophila*. *Cell* **145**, 371–382 (2011).

51.  Zhang, F. *et al.* Structural insights into the regulatory particle of the proteasome from *Methanocaldococcus jannaschii*. *Mol Cell* **34**, 473–484 (2009).

52.  Bohn, S. *et al.* Structure of the 26S proteasome from *Schizosaccharomyces pombe* at subnanometer resolution. *Proc Natl Acad Sci U.S.A.* **107**, 20992–20997 (2010).

53.  Da Fonseca, P. C. A., He, J. & Morris, E. P. Molecular Model of the Human 26S Proteasome. *Mol Cell* **46**, 54–66 (2012).

54.  Beck, F. *et al.* Near-atomic resolution structural model of the yeast 26S proteasome. *Proc Natl Acad Sci U.S.A.* **109**, 14870–14875 (2012).

55.  Sledz, P. *et al.* Structure of the 26S proteasome with ATP-γS bound provides insights into the mechanism of nucleotide-dependent substrate translocation. *Proc Natl Acad Sci U.S.A.* **110**, 7264–7269 (2013).

56.  Tomko, R. J., Funakoshi, M., Schneider, K., Wang, J. & Hochstrasser, M. Heterohexameric ring arrangement of the eukaryotic proteasomal ATPases: implications for proteasome structure and assembly. *Mol Cell* **38**, 393–403 (2010).

57.  Yu, Y. *et al.* Interactions of PAN's C-termini with archaeal 20S proteasome and implications for the eukaryotic proteasome-ATPase interactions. *EMBO J* **29**, 692–702 (2010).

58.  Park, S. *et al.* Reconfiguration of the proteasome during chaperone-mediated assembly. *Nature* **497**, 512–516 (2013).

59.  Smith, D. M., Fraga, H., Reis, C., Kafri, G. & Goldberg, A. L. ATP binds to proteasomal ATPases in pairs with distinct functional effects, implying an ordered reaction cycle. *Cell* **144**, 526–538 (2011).

60.  Knowlton, J., Johnston, S., Whitby, F. & Realini, C. Structure of the proteasome activator REGα (PA28α). *Nature* **390**, 639–643 (1997).

61. Whitby, F. *et al.* Structural basis for the activation of 20S proteasomes by 11S regulators. *Nature* **408**, 115–120 (2000).

62. Zhang, Z. *et al.* Identification of an activation region in the proteasome activator REGalpha. *Proc Natl Acad Sci U.S.A.* **95**, 2807–2811 (1998).

63. Förster, A., Whitby, F. G. & Hill, C. P. The pore of activated 20S proteasomes has an ordered 7-fold symmetric conformation. *EMBO J* **22**, 4356–4364 (2003).

64. Dick, T., Ruppert, T., Groettrup, M. & Kloetzel, P. Coordinated dual cleavages induced by the proteasome regulator PA28 lead to dominant MHC ligands. *Cell* **86**, 253–262 (1996).

65. Groettrup, M. *et al.* A role for the proteasome regulator PA28alpha in antigen presentation. *Nature* **381**, 166–168 (1996).

66. Dange, T. *et al.* Blm10 protein promotes proteasomal substrate turnover by an active gating mechanism. *J Biol Chem* **286**, 42830–42839 (2011).

67. Savulescu, A. F. & Glickman, M. H. Proteasome activator 200: the heat is on... *Mol Cell Proteomics* **10**, 6890–6898 (2011).

68. Glickman, M. H. *et al.* A subcomplex of the proteasome regulatory particle required for ubiquitin-conjugate degradation and related to the COP9-signalosome and eIF3. *Cell* **94**, 615–623 (1998).

69. Deveraux, Q., Ustrell, V., Pickart, C. & Rechsteiner, M. A 26S protease subunit that binds ubiquitin conjugates. *J Biol Chem* **269**, 7059–7061 (1994).

70. Schreiner, P. *et al.* Ubiquitin docking at the proteasome through a novel pleckstrin-homology domain interaction. *Nature* **453**, 548–552 (2008).

71. Husnjak, K. *et al.* Proteasome subunit Rpn13 is a novel ubiquitin receptor. *Nature* **453**, 481–488 (2008).

72. Yao, T. & Cohen, R. E. A cryptic protease couples deubiquitination and degradation by the proteasome. *Nature* **419**, 403–407 (2002).

73. Verma, R. *et al.* Role of Rpn11 metalloprotease in deubiquitination and degradation by the 26S proteasome. *Science* **298**, 611–615 (2002).

74. Tomko, R. J. & Hochstrasser, M. Incorporation of the Rpn12 subunit couples completion of proteasome regulatory particle lid assembly to lid-base joining. *Mol Cell* **44**, 907–917 (2011).

75. Fukunaga, K., Kudo, T., Toh-e, A., Tanaka, K. & Saeki, Y. Dissection of the assembly pathway of the proteasome lid in Saccharomyces cerevisiae. *Biochem Biophys Res Commun* **396**, 1048–1053 (2010).

76. Pathare, G. R. *et al.* The proteasomal subunit Rpn6 is a molecular clamp holding the core and regulatory subcomplexes together. *Proc Natl Acad Sci U.S.A.* **109**, 149–154 (2012).

77. Kajava, A. V What curves alpha-solenoids? Evidence for an alpha-helical toroid structure of Rpn1 and Rpn2 proteins of the 26 S proteasome. *J Biol Chem* **277**, 49791–49798 (2002).

78. He, J. *et al.* The structure of the 26S proteasome subunit Rpn2 reveals its PC repeat domain as a closed toroid of two concentric α-helical rings. *Structure* **20**, 513–521 (2012).

79. Rosenzweig, R., Osmulski, P. A., Gaczynska, M. & Glickman, M. H. The central unit within the 19S regulatory particle of the proteasome. *Nat Struct Mol Biol* **15**, 573–580 (2008).

80. Rosenzweig, R., Bronner, V., Zhang, D., Fushman, D. & Glickman, M. H. Rpn1 and Rpn2 coordinate ubiquitin processing factors at proteasome. *J Biol Chem* **287**, 14659–14671 (2012).

81. Saeki, Y., Sone, T., Toh-e, A. & Yokosawa, H. Identification of ubiquitin-like protein-binding subunits of the 26S proteasome. *Biochem Biophys Res Commun* **296**, 813–819 (2002).

82. Elsasser, S. *et al.* Proteasome subunit Rpn1 binds ubiquitin-like protein domains. *Nat Cell Biol* **4**, 725–730 (2002).

83. Leggett, D. S. *et al.* Multiple associated proteins regulate proteasome structure and function. *Mol Cell* **10**, 495–507 (2002).

84. Ito, T. *et al.* A comprehensive two-hybrid analysis to explore the yeast protein interactome. *Proc Natl Acad Sci U.S.A.* **98**, 4569–4574 (2001).

85. Hamazaki, J. *et al.* A novel proteasome interacting protein recruits the deubiquitinating enzyme UCH37 to 26S proteasomes. *EMBO J* **25**, 4524–4536 (2006).

86. Gandhi, T. K. B. *et al.* Analysis of the human protein interactome and comparison with yeast, worm and fly interaction datasets. *Nat Genet* **38**, 285–293 (2006).

87. Wang, Q., Young, P. & Walters, K. J. Structure of S5a bound to monoubiquitin provides a model for polyubiquitin recognition. *J Mol Biol* **348**, 727–739 (2005).

88. Zhang, N. *et al.* Structure of the S5a:K48-linked diubiquitin complex and its interactions with Rpn13. *Mol Cell* **35**, 280–290 (2009).

89. Yao, T. *et al.* Proteasome recruitment and activation of the Uch37 deubiquitinating enzyme by Adrm1. *Nat Cell Biol* **8**, 994–1002 (2006).

90. Qiu, X.-B. *et al.* hRpn13/ADRM1/GP110 is a novel proteasome subunit that binds the deubiquitinating enzyme, UCH37. *EMBO J* **25**, 5742–5753 (2006).

91. Chen, X., Lee, B.-H., Finley, D. & Walters, K. J. Structure of proteasome ubiquitin receptor hRpn13 and its activation by the scaffolding protein hRpn2. *Mol Cell* **38**, 404–415 (2010).

92. Hamazaki, J. *et al.* Rpn10-mediated degradation of ubiquitinated proteins is essential for mouse development. *Mol Cell Biol* **27**, 6629–6638 (2007).

93. Al-Shami, A. *et al.* Regulators of the proteasome pathway, Uch37 and Rpn13, play distinct roles in mouse development. *PloS One* **5**, e13654 (2010).

94. Mazumdar, T. *et al.* Regulation of NF-kappaB activity and inducible nitric oxide synthase by regulatory particle non-ATPase subunit 13 (Rpn13). *Proc Natl Acad Sci U.S.A.* **107**, 13854–13859 (2010).

95. Huang, Y. & Ratovitski, E. A. Phosphorylated TP63 induces transcription of RPN13, leading to NOS2 protein degradation. *J Biol Chem* **285**, 41422–41431 (2010).

96. Mayor, T., Lipford, J. R., Graumann, J., Smith, G. T. & Deshaies, R. J. Analysis of polyubiquitin conjugates reveals that the Rpn10 substrate receptor contributes to the turnover of multiple proteasome targets. *Mol Cell Proteomics* **4**, 741–751 (2005).

97. Chandra, A., Chen, L. & Madura, K. Synthetic lethality of rpn11-1 rpn10Δ is linked to altered proteasome assembly and activity. *Curr Genet* **56**, 543–557 (2010).

98. Lam, Y. A., Lawson, T. G., Velayutham, M., Zweier, J. L. & Pickart, C. M. A proteasomal ATPase subunit recognizes the polyubiquitin degradation signal. *Nature* **416**, 763–767 (2002).

99. Archer, C. T. *et al.* Physical and functional interactions of monoubiquitylated transactivators with the proteasome. *J Biol Chem* **283**, 21789–21798 (2008).

100. Sims, J. J., Haririnia, A., Dickinson, B. C., Fushman, D. & Cohen, R. E. Avid interactions underlie the Lys63-linked polyubiquitin binding specificities observed for UBA domains. *Nat Struct Mol Biol* **16**, 883–889 (2009).

101. Bertolaet, B. *et al.* UBA domains of DNA damage-inducible proteins interact with ubiquitin. *Nat Struct Biol* **8**, 417–422 (2001).

102. Wilkinson, C. R. *et al.* Proteins containing the UBA domain are able to bind to multi-ubiquitin chains. *Nat Cell Biol* **3**, 939–943 (2001).

103. Raasi, S., Varadan, R., Fushman, D. & Pickart, C. M. Diverse polyubiquitin interaction properties of ubiquitin-associated domains. *Nat Struct Mol Biol* **12**, 708–714 (2005).

104. Raasi, S. & Pickart, C. M. Rad23 ubiquitin-associated domains (UBA) inhibit 26 S proteasome-catalyzed proteolysis by sequestering lysine 48-linked polyubiquitin chains. *J Biol Chem* **278**, 8951–8959 (2003).

105. Varadan, R., Assfalg, M., Raasi, S., Pickart, C. & Fushman, D. Structural determinants for selective recognition of a Lys48-linked polyubiquitin chain by a UBA domain. *Mol Cell* **18**, 687–698 (2005).

106. Zhang, D., Raasi, S. & Fushman, D. Affinity makes the difference: nonselective interaction of the UBA domain of Ubiquilin-1 with monomeric ubiquitin and polyubiquitin chains. *J Mol Biol* **377**, 162–180 (2008).

107. Hiyama, H. *et al.* Interaction of hHR23 with S5a. The ubiquitin-like domain of hHR23 mediates interaction with S5a subunit of 26 S proteasome. *J Biol Chem* **274**, 28019–28025 (1999).

108. Walters, K. J., Kleijnen, M. F., Goh, A. M., Wagner, G. & Howley, P. M. Structural studies of the interaction between ubiquitin family proteins and proteasome subunit S5a. *Biochemistry* **41**, 1767–1777 (2002).

109. Wang, X. *et al.* Mass spectrometric characterization of the affinity-purified human 26S proteasome complex. *Biochemistry* **46**, 3553–3565 (2007).

110. Ng, J. M. Y. *et al.* Developmental defects and male sterility in mice lacking the ubiquitin-like DNA repair gene mHR23B. *Mol Cell Biol* **22**, 1233–1245 (2002).

111. Walters, K. J., Lech, P. J., Goh, A. M., Wang, Q. & Howley, P. M. DNA-repair protein hHR23a alters its protein structure upon binding proteasomal subunit S5a. *Proc Natl Acad Sci U.S.A.* **100**, 12694–12699 (2003).

112. Raasi, S., Orlov, I., Fleming, K. G. & Pickart, C. M. Binding of polyubiquitin chains to ubiquitin-associated (UBA) domains of HHR23A. *J Mol Biol* **341**, 1367–1379 (2004).

113. Verma, R., Oania, R., Graumann, J. & Deshaies, R. J. Multiubiquitin chain receptors define a layer of substrate selectivity in the ubiquitin-proteasome system. *Cell* **118**, 99–110 (2004).

114. Fishbain, S., Prakash, S., Herrig, A., Elsasser, S. & Matouschek, A. Rad23 escapes degradation because it lacks a proteasome initiation region. *Nat Commun* **2**, (2011).

115. Díaz-Martínez, L. A., Kang, Y., Walters, K. J. & Clarke, D. J. Yeast UBL-UBA proteins have partially redundant functions in cell cycle control. *Cell Div* **1**, (2006).

116. Medicherla, B., Kostova, Z., Schaefer, A. & Wolf, D. H. A genomic screen identifies Dsk2p and Rad23p as essential components of ER-associated degradation. *EMBO Rep* **5**, 692–697 (2004).

117. Kang, Y. *et al.* UBL/UBA ubiquitin receptor proteins bind a common tetraubiquitin chain. *J Mol Biol* **356**, 1027–1035 (2006).

118. Zhang, D. *et al.* Together, Rpn10 and Dsk2 can serve as a polyubiquitin chain-length sensor. *Mol Cell* **36**, 1018–1033 (2009).

119. Kang, Y., Zhang, N., Koepp, D. M. & Walters, K. J. Ubiquitin receptor proteins hHR23a and hPLIC2 interact. *J Mol Biol* **365**, 1093–1101 (2007).

120. Schauber, C. *et al.* Rad23 links DNA repair to the ubiquitin/proteasome pathway. *Nature* **391**, 715–718 (1998).

121. Mah, A. L., Perry, G., Smith, M. A. & Monteiro, M. J. Identification of ubiquilin, a novel presenilin interactor that increases presenilin protein accumulation. *J Cell Biol* **151**, 847–862 (2000).

122. Lenkinski, R. E., Chen, D. M., Glickson, J. D. & Goldstein, G. Nuclear magnetic resonance studies of the denaturation of ubiquitin. *Biochim Biophys Acta* **494**, 126–130 (1977).

123. Henderson, A., Erales, J., Hoyt, M. A. & Coffino, P. Dependence of proteasome processing rate on substrate unfolding. *J Biol Chem* **286**, 17495–17502 (2011).

124. Maytal-Kivity, V., Reis, N., Hofmann, K. & Glickman, M. H. MPN+, a putative catalytic motif found in a subset of MPN domain proteins from eukaryotes and prokaryotes, is critical for Rpn11 function. *BMC Biochem* **3**, (2002).

125. Peth, A., Uchiki, T. & Goldberg, A. L. ATP-dependent steps in the binding of ubiquitin conjugates to the 26S proteasome that commit to degradation. *Mol Cell* **40**, 671–681 (2010).

126. Rinaldi, T. *et al.* Participation of the proteasomal lid subunit Rpn11 in mitochondrial morphology and function is mapped to a distinct C-terminal domain. *Biochem J* **381**, 275–285 (2004).

127. Verma, R. *et al.* Proteasomal proteomics: identification of nucleotide-sensitive proteasome-interacting proteins by mass spectrometric analysis of affinity-purified proteasomes. *Mol Biol Cell* **11**, 3425–3439 (2000).

128. Lam, Y. A., Xu, W., DeMartino, G. N. & Cohen, R. E. Editing of ubiquitin conjugates by an isopeptidase in the 26S proteasome. *Nature* **385**, 737–740 (1997).

129. Hanna, J. *et al.* Deubiquitinating enzyme Ubp6 functions noncatalytically to delay proteasomal degradation. *Cell* **127**, 99–111 (2006).

130. Sakata, E. *et al.* The catalytic activity of Ubp6 enhances maturation of the proteasomal regulatory particle. *Mol Cell* **42**, 637–649 (2011).

131. Peth, A., Besche, H. C. & Goldberg, A. L. Ubiquitinated proteins activate the proteasome by binding to Usp14/Ubp6, which causes 20S gate opening. *Mol Cell* **36**, 794–804 (2009).

132. Prakash, S., Tian, L., Ratliff, K. S., Lehotzky, R. E. & Matouschek, A. An unstructured initiation site is required for efficient proteasome-mediated degradation. *Nat Struct Mol Biol* **11**, 830–837 (2004).

133. Zhang, F. *et al.* Mechanism of substrate unfolding and translocation by the regulatory particle of the proteasome from *Methanocaldococcus jannaschii*. *Mol Cell* **34**, 485–496 (2009).

134. Wang, J. *et al.* Crystal structures of the HslVU peptidase–ATPase complex reveal an ATP-dependent proteolysis mechanism. *Structure* **9**, 177–184 (2001).

135. Hinnerwisch, J., Fenton, W. A., Furtak, K. J., Farr, G. W. & Horwich, A. L. Loops in the central channel of ClpA chaperone mediate protein binding, unfolding, and translocation. *Cell* **121**, 1029–1041 (2005).

136. Bohon, J., Jennings, L. D., Phillips, C. M., Licht, S. & Chance, M. R. Synchrotron protein footprinting supports substrate translocation by ClpA via ATP-induced movements of the D2 loop. *Structure* **16**, 1157–1165 (2008).

137. Maillard, R. A. *et al.* ClpX(P) generates mechanical force to unfold and translocate its protein substrates. *Cell* **145**, 459–469 (2011).

138. Stinson, B. M. *et al.* Nucleotide binding and conformational switching in the hexameric ring of a AAA+ machine. *Cell* **153**, 628–639 (2013).

139. Erales, J., Hoyt, M. A., Troll, F. & Coffino, P. Functional asymmetries of proteasome translocase pore. *J Biol Chem* **287**, 18535–18543 (2012).

140. Gillette, T. G., Kumar, B., Thompson, D., Slaughter, C. A. & DeMartino, G. N. Differential roles of the COOH termini of AAA subunits of PA700 (19S regulator) in asymmetric assembly and activation of the 26S proteasome. *J Biol Chem* **283**, 31813–31822 (2008).

141. Kim, Y.-C. & DeMartino, G. N. C termini of proteasomal ATPases play nonequivalent roles in cellular assembly of mammalian 26 S proteasome. *J Biol Chem* **286**, 26652–26666 (2011).

142. Djuranovic, S. *et al.* Structure and activity of the N-terminal substrate recognition domains in proteasomal ATPases. *Mol Cell* **34**, 580–590 (2009).

143. Takagi, K. *et al.* Structural basis for specific recognition of Rpt1, an ATPase subunit of the 26S proteasome, by a proteasome-dedicated chaperone Hsm3. *J Biol Chem* **287**, 12172–12182 (2012).

144. Barrault, M.-B. *et al.* Dual functions of the Hsm3 protein in chaperoning and scaffolding regulatory particle subunits during the proteasome assembly. *Proc Natl Acad Sci U.S.A.* **109**, E1001–E1010 (2012).

145. Nakamura, Y. *et al.* Structural basis for the recognition between the regulatory particles Nas6 and Rpt3 of the yeast 26S proteasome. *Biochem Biophys Res Commun* **359**, 503–509 (2007).

146. Ehlinger, A. *et al.* Conformational dynamics of the Rpt6 ATPase in proteasome assembly and Rpn14 binding. *Structure* **21**, 753–765 (2013).

147. Park, S. *et al.* Hexameric assembly of the proteasomal ATPases is templated through their C termini. *Nature* **459**, 866–870 (2009).

148. Ruschak, A. M. & Kay, L. E. Proteasome allostery as a population shift between interchanging conformers. *Proc Natl Acad Sci U.S.A.* **109**, E3454–E3462 (2012).

149. Harris, J. L., Alper, P. B., Li, J., Rechsteiner, M. & Backes, B. J. Substrate specificity of the human proteasome. *Chem Biol* **8**, 1131–1141 (2001).

150. Roelofs, J. *et al.* Chaperone-mediated pathway of proteasome regulatory particle assembly. *Nature* **459**, 861–865 (2009).

151. Funakoshi, M., Tomko, R. J., Kobayashi, H. & Hochstrasser, M. Multiple assembly chaperones govern biogenesis of the proteasome regulatory particle base. *Cell* **137**, 887–899 (2009).

152. Kaneko, T. *et al.* Assembly pathway of the mammalian proteasome base subcomplex is mediated by multiple specific chaperones. *Cell* **137**, 914–925 (2009).

153. Saeki, Y., Toh-E, A., Kudo, T., Kawamura, H. & Tanaka, K. Multiple proteasome-interacting proteins assist the assembly of the yeast 19S regulatory particle. *Cell* **137**, 900–913 (2009).

154. Le Tallec, B., Barrault, M.-B., Guérois, R., Carré, T. & Peyroche, A. Hsm3/S5b participates in the assembly pathway of the 19S regulatory particle of the proteasome. *Mol Cell* **33**, 389–399 (2009).

155. Kim, S. *et al.* Crystal structure of yeast Rpn14, a chaperone of the 19S regulatory particle of the proteasome. *J Biol Chem* **285**, 15159–15166 (2010).

156. Thompson, D., Hakala, K. & DeMartino, G. N. Subcomplexes of PA700, the 19S regulator of the 26S proteasome, reveal relative roles of AAA subunits in 26S proteasome assembly and activation and ATPase activity. *J Biol Chem* **284**, 24891–24903 (2009).

157. Isono, E. *et al.* The Assembly Pathway of the 19S Regulatory Particle of the Yeast 26S Proteasome. *Mol Biol Cell* **18**, 569–580 (2007).

158. Saeki, Y., Toh-e, A. & Yokosawa, H. Rapid isolation and characterization of the yeast proteasome regulatory complex. *Biochem Biophys Res Commun* **273**, 509–515 (2000).

159. Kusmierczyk, A. R., Kunjappu, M. J., Funakoshi, M. & Hochstrasser, M. A multimeric assembly factor controls the formation of alternative 20S proteasomes. *Nat Struct Mol Biol* **15**, 237–244 (2008).

160. Riedinger, C. *et al.* Structure of Rpn10 and its interactions with polyubiquitin chains and the proteasome subunit Rpn12. *J Biol Chem* **285**, 33992–34003 (2010).

161. Boehringer, J. *et al.* Structural and functional characterization of Rpn12 identifies residues required for Rpn10 proteasome incorporation. *Biochem J* **448**, 55–65 (2012).

162. Kikuchi, J. *et al.* Co- and post-translational modifications of the 26S proteasome in yeast. *Proteomics* **10**, 2769–2779 (2010).

163. Djakovic, S. N. *et al.* Phosphorylation of Rpt6 regulates synaptic strength in hippocampal neurons. *J Neurosci* **32**, 5126–5131 (2012).

164. Kimura, A., Kato, Y. & Hirano, H. N-myristoylation of the Rpt2 subunit regulates intracellular localization of the yeast 26S proteasome. *Biochemistry* **51**, 8856–8866 (2012).

165. Hoyt, M. A. *et al.* Glycine-alanine repeats impair proper substrate unfolding by the proteasome. *EMBO J* **25**, 1720–1729 (2006).

166. Kraut, D. A. & Matouschek, A. Proteasomal degradation from internal sites favors partial proteolysis via remote domain stabilization. *ACS Chem Biol* **6**, 1087–1095 (2011).

167. Tomko, R. J. & Hochstrasser, M. Order of the proteasomal ATPases and eukaryotic proteasome assembly. *Cell Biochem Biophys* **60**, 13–20 (2011).

168. Saeki, Y. & Tanaka, K. Assembly and function of the proteasome. *Methods Mol Biol* **832**, 315–337 (2012).

169. Murzin, A. G. OB(oligonucleotide/oligosaccharide binding)-fold: common structural and functional solution for non-homologous sequences. *EMBO J* **12**, 861–867 (1993).

170. Tian, G. *et al.* An asymmetric interface between the regulatory and core particles of the proteasome. *Nat Struct Mol Biol* **18**, 1259–1267 (2011).

171. Kisselev, A. F., Van der Linden, W. A. & Overkleeft, H. S. Proteasome inhibitors: an expanding army attacking a unique target. *Chem Biol* **19**, 99–115 (2012).

172. Glickman, M. H., Rubin, D. M. & Fried, V. A. The regulatory particle of the *Saccharomyces cerevisiae* proteasome. *Mol Cell Biol* **18**, 3149–3162 (1998).

173. Rabl, J. *et al.* Mechanism of gate opening in the 20S proteasome by the proteasomal ATPases. *Mol Cell* **30**, 360–368 (2008).

174. Horwitz, A. A. *et al.* ATP-induced structural transitions in PAN, the proteasome-regulatory ATPase complex in Archaea. *J Biol Chem* **282**, 22921–22929 (2007).

175. Montelione, G. T. & Wagner, G. 2D Chemical exchange NMR spectroscopy by proton-detected heteronuclear correlation. *J Am Chem Soc* **111**, 3096–3098 (1989).

176. Shen, Y. *et al.* Consistent blind protein structure generation from NMR chemical shift data. *Proc Natl Acad Sci U.S.A.* **105**, 4685–4690 (2008).

177. Rohl, C. A., Strauss, C. E. M., Misura, K. M. S. & Baker, D. Protein structure prediction using Rosetta. *Methods Enzymol* **383**, 66–93 (2004).

178. Wishart, D. S. & Sykes, B. D. The 13C chemical-shift index: a simple method for the identification of protein secondary structure using 13C chemical-shift data. *J Biomol NMR* **4**, 171–180 (1994).

179. d'Auvergne, E. J. & Gooley, P. R. Optimisation of NMR dynamic models I. Minimisation algorithms and their performance within the model-free and Brownian rotational diffusion spaces. *J Biomol NMR* **40**, 107–119 (2008).

180. d'Auvergne, E. J. & Gooley, P. R. Optimisation of NMR dynamic models II. A new methodology for the dual optimisation of the model-free parameters and the Brownian rotational diffusion tensor. *J Biomol NMR* **40**, 121–133 (2008).

181. Pace, C. N. & Scholtz, J. M. A helix propensity scale based on experimental studies of peptides and proteins. *Biophys J* **75**, 422–427 (1998).

182. De la Torre, J. G., Navarro, S., Lopez Martinez, M. C., Diaz, F. G. & Lopez Cascales, J. J. HYDRO: a computer program for the prediction of hydrodynamic properties of macromolecules. *Biophys J* **67**, 530–531 (1994).

183. De la Torre, J. G., Echenique, G. D. R. & Ortega, A. Improved calculation of rotational diffusion and intrinsic viscosity of bead models for macromolecules and nanoparticles. *J Phys Chem B* **111**, 955–961 (2007).

184. Fahmy, A. & Wagner, G. TreeDock: A tool for protein docking based on minimizing van der Waals energies. *J Am Chem Soc* **124**, 1241–1250 (2002).

185. Park, S., Kim, W., Tian, G., Gygi, S. P. & Finley, D. Structural defects in the regulatory particle-core particle interface of the proteasome induce a novel proteasome stress response. *J Biol Chem* **286**, 36652–36666 (2011).

186. Ciechanover, A. The ubiquitin-proteasome proteolytic pathway. *Cell* **79**, 13–21 (1994).

187. Rock, K. L. & Goldberg, A. L. Degradation of cell proteins and the generation of MHC class I-presented peptides. *Annu Rev Immunol* **17**, 739–779 (1999).

188. Ciechanover, A., Finley, D. & Varshavsky, A. Ubiquitin dependence of selective protein degradation demonstrated in the mammalian cell cycle mutant ts85. *Cell* **37**, 57–66 (1984).

189. Finley, D., Ciechanover, A. & Varshavsky, A. Thermolability of ubiquitin-activating enzyme from the mammalian cell cycle mutant ts85. *Cell* **37**, 43–55 (1984).

190. Wang, Q., Goh, A. M., Howley, P. M. & Walters, K. J. Ubiquitin recognition by the DNA repair protein hHR23a. *Biochemistry* **42**, 13529–13535 (2003).

191. Wilkinson, C. R. *et al.* Analysis of a gene encoding Rpn10 of the fission yeast proteasome reveals that the polyubiquitin-binding site of this subunit is essential when Rpn12/Mts3 activity is compromised. *J Biol Chem* **275**, 15182–15192 (2000).

192. Matiuhin, Y. *et al.* Extraproteasomal Rpn10 restricts access of the polyubiquitin-binding protein Dsk2 to proteasome. *Mol Cell* **32**, 415–425 (2008).

193. Van Nocker, S. *et al.* The multiubiquitin-chain-binding protein Mcb1 is a component of the 26S proteasome in *Saccharomyces cerevisiae* and plays a nonessential, substrate-specific role in protein turnover. *Mol Cell Biol* **16**, 6020–6028 (1996).

194. Szlanka, T. *et al.* Deletion of proteasomal subunit S5a/Rpn10/p54 causes lethality, multiple mitotic defects and overexpression of proteasomal genes in *Drosophila melanogaster*. *J Cell Sci* **116**, 1023–1033 (2003).

195. Kang, Y., Chen, X., Lary, J. W., Cole, J. L. & Walters, K. J. Defining how ubiquitin receptors hHR23a and S5a bind polyubiquitin. *J Mol Biol* **369**, 168–176 (2007).

196. Fushman, D., Varadan, R., Assfalg, M. & Walker, O. Determining domain orientation in macromolecules by using spin-relaxation and residual dipolar coupling measurements. *Prog Nucl Mag Res Sp* **44**, 189–214 (2004).

197. Thrower, J. S., Hoffman, L., Rechsteiner, M. & Pickart, C. M. Recognition of the polyubiquitin proteolytic signal. *EMBO J* **19**, 94–102 (2000).

198. Hofmann, R. M. & Pickart, C. M. In vitro assembly and recognition of Lys-63 polyubiquitin chains. *J Biol Chem* **276**, 27936–27943 (2001).

199. Ryu, K.-S. *et al.* Binding surface mapping of intra- and interdomain interactions among hHR23B, ubiquitin, and polyubiquitin binding site 2 of S5a. *J Biol Chem* **278**, 36621–36627 (2003).

200. Lee, S. Y.-C., De la Mota-Peynado, A. & Roelofs, J. Loss of Rpt5 protein interactions with the core particle and Nas2 protein causes the formation of faulty proteasomes that are inhibited by Ecm29 protein. *J Biol Chem* **286**, 36641–36651 (2011).

201. Pickart, C. M. & Raasi, S. Controlled synthesis of polyubiquitin chains. *Method Enzymol* **399**, 21–36 (2005).

202. Lipari, G. & Szabo, A. Model-free approach to the interpretation of nuclear magnetic resonance relaxation in macromolecules. 1. Theory and range of validity. *J Am Chem Soc* **104**, 4546–4559 (1982).

203. Fahmy, A. & Wagner, G. Optimization of van der Waals energy for protein side-chain placement and design. *Biophys J* **101**, 1690–1698 (2011).

204. Bochtler, M. *et al.* The structures of HsIU and the ATP-dependent protease HsIU-HsIV. *Nature* **403**, 800–805 (2000).

205. Schuck, P. Size-distribution analysis of macromolecules by sedimentation velocity ultracentrifugation and Lamm equation modeling. *Biophys J* **78**, 1606–1619 (2000).

206. Stafford, W. F. & Sherwood, P. J. Analysis of heterologous interacting systems by sedimentation velocity: curve fitting algorithms for estimation of sedimentation coefficients, equilibrium and kinetic constants. *Biophys Chem* **108**, 231–243 (2004).

207. Leggett, D., Glickman, M. & Finley, D. Purification of proteasomes, proteasome subcomplexes, and proteasome-associated proteins from budding yeast. *Methods Mol Biol* **301**, 57–70 (2005).

# Appendix

## Rpt6-C peptide backbone chemical shift assignments for 4-helix bundle and partially unfolded states

| Residue | 4-helix bundle | | | | | Partially Unfolded | | | | |
|---|---|---|---|---|---|---|---|---|---|---|
| | Cα | Cβ | C′ | N | HN | Cα | Cβ | C′ | N | HN |
| 318 | | | | | - | | | | | - |
| 319 | | | | | - | | | | | - |
| 320 | | | | | | | | | | |
| 321 | | | | | | | | | | |
| 322 | 54.9 | | 180.6 | 121.9 | 8.203 | | | | | |
| 323 | 54.6 | | 180.9 | 120.98 | 7.946 | | | | | |
| 324 | 60 | | 177.8 | 118.12 | 8.295 | | | | | |
| 325 | 55.3 | 17.2 | 179.3 | 120.94 | 8.565 | | | | | |
| 326 | 58.4 | 29.1 | 178.1 | 119.06 | 7.707 | | | | | |
| 327 | 65.1 | 38.1 | 178.5 | 120 | 7.772 | | | | | |
| 328 | 58 | 42.6 | 177.9 | 119.53 | 8.153 | | | | | |
| 329 | 59.6 | | 178.8 | 121.22 | 8.125 | | | | | |
| 330 | 65 | | 179.6 | 119.47 | 8.163 | | | | | |
| 331 | 59.2 | 30.4 | 176.7 | 116.25 | 8.17 | | | | | |
| 332 | 59.1 | 64.9 | 176.2 | 113.44 | 8.08 | | | | | |
| 333 | 59 | 30.2 | 177.2 | 121.87 | 7.211 | | | | | |
| 334 | 55.6 | 31.9 | 176.9 | 115.78 | 8.214 | | | | | |
| 335 | 55.2 | | 174.7 | | | | | | | |
| 336 | 52 | 37.9 | 173.9 | 120.47 | 8.93 | **53.4** | | | **119.57** | **8.445** |
| 337 | 54.4 | 42.6 | 178 | 123.28 | 8.366 | | | | | |
| 338 | 63 | 70 | 174.4 | 116.72 | 8.251 | | | | | |
| 339 | 57.6 | 29.8 | 175 | 124.68 | 8.434 | **58.4** | **31.9** | | **115.26** | **8.331** |
| 340 | 44.25 | - | 174.9 | 111.09 | 8.794 | **45.2** | **-** | **174.1** | **111.09** | **8.483** |
| 341 | 61.5 | 38.1 | 174.2 | 121.4 | 7.311 | **61.2** | | | **119.45** | **7.951** |
| 342 | 51 | 38.4 | 175.9 | 126.56 | 9.186 | | | | | |
| 343 | 56.5 | 41 | 179.2 | 123.28 | 8.728 | | | | | |
| 344 | 59.5 | 32.7 | 177.9 | 121.4 | 8.172 | | | | | |
| 345 | 58.3 | 32.3 | 179.2 | 117.66 | 7.304 | | | | | |
| 346 | 66.2 | 31 | 177.1 | 117.66 | 6.822 | **62.2** | | | **120.98** | **8.063** |
| 347 | 55.1 | | 181.3 | 119.86 | 8.06 | | | | | |
| 348 | 58.9 | 29.9 | 177.4 | 119.06 | 8.388 | | | | | |
| 349 | 56.8 | 32.8 | 176.9 | 116.77 | 7.392 | **56.2** | | | **121.36** | **8.216** |
| 350 | 55.5 | 30.4 | 176.7 | 116.25 | 7.103 | | | | | |

| Residue | Cα | Cβ | C′ | N | HN | Cα | Cβ | C′ | N | HN |
|---|---|---|---|---|---|---|---|---|---|---|
| 351 | 55.3 | 40.4 | 178.7 | 118.12 | 7.666 | | | | | |
| 352 | 45.4 | - | 174.5 | 112.03 | 8.433 | | | | | |
| 353 | 59.2 | 29.4 | 174.2 | 117.19 | 7.687 | | | | | |
| 354 | 56.8 | 65.8 | 176.7 | 118.12 | 9.342 | 56.1 | | | | |
| 355 | 47.6 | - | 176.5 | 108.75 | 9.144 | 45.2 | - | 173.9 | 109.4 | 8.391 |
| 356 | 54.6 | 19.3 | 180.5 | 123.85 | 8.271 | 52.4 | 24.6 | 177.4 | 123.28 | 8.139 |
| 357 | 56.7 | 40.9 | 177.8 | 120 | 7.868 | 54.1 | 41 | 176.3 | 119.06 | 8.322 |
| 358 | 66.7 | 31.3 | 179.3 | 119.06 | 7.748 | 62.3 | 32.6 | 176.2 | 120 | 7.964 |
| 359 | 60.1 | 32.1 | 179.2 | 119.06 | 7.735 | 56.2 | 32.9 | 177.1 | 124.07 | 8.346 |
| 360 | 46.9 | - | 176.4 | 106.88 | 8.168 | 45.1 | - | 173.9 | 109.47 | 8.322 |
| 361 | 66.7 | | 177.22 | 122.51 | 8.222 | 62.1 | 32.8 | 176.1 | 119.06 | 8.006 |
| 362 | 64.2 | 27.1 | 176.7 | 117.23 | 7.577 | 58.4 | 28.1 | 175 | 123.17 | 8.538 |
| 363 | 65.9 | 68.8 | 177.3 | 115.46 | 8.043 | 61.8 | 70.3 | 174.7 | 116.73 | 8.321 |
| 364 | 58.4 | | 177.4 | 121.65 | 8.376 | 56.9 | 30.1 | 176.6 | 122.81 | 8.456 |
| 365 | 55.2 | 18.9 | 179.3 | 122.34 | 8.423 | 53.1 | 19.1 | 178.6 | 124.04 | 8.321 |
| 366 | 46.6 | - | 176.7 | 99.96 | 7.426 | 45.1 | - | 174.7 | 107.27 | 8.321 |
| 367 | 57.5 | 31.2 | 178.9 | 121.4 | 7.661 | | | | | |
| 368 | 61.9 | 39.5 | 178.4 | 120.94 | 8.045 | | | | | |
| 369 | 55.5 | 18.5 | 179.8 | 120.47 | 7.256 | 52.7 | | 176.1 | 123.44 | 8.004 |
| 370 | 57.9 | 42.3 | 182 | 117.66 | 7.713 | | | | | |
| 371 | 59.2 | 30.2 | 178.1 | 120.74 | 8.414 | | | | | |
| 372 | 55.6 | 29.9 | 174.6 | 116.72 | 7.358 | | | | | |
| 373 | 56.7 | 26.5 | 175.3 | 115.31 | 8.109 | | | | | |
| 374 | 55.3 | 33.7 | 176.3 | 117.66 | 8.18 | | | | | |
| 375 | 61.8 | 38.7 | 176 | 117.19 | 8.242 | | | | | |
| 376 | 55.4 | 32 | 176.1 | 117.19 | 7.492 | 55.7 | | | 123.15 | 8.071 |
| 377 | 61.5 | 33 | 176.8 | 123.28 | 8.567 | | | | | |
| 378 | 60.2 | 72.7 | 175.9 | 119.06 | 9.783 | 61.7 | | 174.5 | 117.12 | 8.315 |
| 379 | 59.3 | | 178.4 | 120.47 | 9.186 | 55.9 | | | 122.08 | 8.494 |
| 380 | 60.2 | 28.8 | 178.2 | 117.66 | 8.485 | | | | | |
| 381 | 58 | 40.2 | 179 | 120.94 | 7.738 | | | | | |
| 382 | 62.9 | 38.7 | 178.1 | 115.31 | 7.461 | | | | | |
| 383 | 60.3 | 29.2 | 180.4 | 118.59 | 8.457 | | | | | |
| 384 | 57.4 | 41.2 | 179.8 | 121.87 | 8.594 | 55.4 | 42.4 | 177.4 | 121.72 | 7.993 |
| 385 | 55.4 | 20.5 | 179.5 | 122.44 | 7.878 | 52.6 | 19 | 178 | 123.75 | 8.056 |
| 386 | 66.8 | 31.9 | 177.8 | 118.12 | 8.576 | 62.7 | 32.6 | 176.9 | 117.87 | 7.926 |
| 387 | 46.9 | - | 175.6 | 105 | 7.578 | 45.3 | - | 174.1 | 111.09 | 8.293 |
| 388 | 58.6 | 33 | 179.1 | 120.47 | 7.719 | 56.2 | | 176.8 | 120.42 | 8.001 |
| 389 | 65.1 | 32.7 | 177.9 | 118.16 | 8.153 | 63.4 | | | 121.69 | 8.063 |
| 390 | 56.3 | 31.3 | 177.3 | 116.06 | 8.346 | 56.4 | | | 116.25 | 8.335 |

| Residue | Cα | Cβ | C′ | N | HN | Cα | Cβ | C′ | N | HN |
|---|---|---|---|---|---|---|---|---|---|---|
| **391** | 53.9 | 38.4 | 175.6 | 117.66 | 7.771 | | | | | |
| **392** | 56.8 | 32.6 | 176.9 | 120.39 | 7.991 | | | | | |
| **393** | 53.6 | 38.6 | 175.6 | 118.59 | 8.359 | | | | | |
| **394** | 56.1 | 29.3 | 176.2 | 120 | 8.241 | | | | | |
| **395** | 56.9 | 29.9 | 176.8 | 121.4 | 8.411 | | | | | |
| **396** | 62.1 | 69.7 | 174.2 | 114.84 | 8.156 | | | | | |
| **397** | 52.6 | 19.1 | 177.6 | 126.12 | 8.234 | | | | | |
| **398** | 61.1 | 38.7 | 176.3 | 119.43 | 8.051 | | | | | |
| **399** | 58.3 | 63.8 | 174.3 | 119.06 | 8.251 | | | | | |
| **400** | 62.3 | 32.4 | 176 | 121.65 | 8.111 | | | | | |
| **401** | 52.7 | 19 | 177.7 | 126.32 | 8.171 | | | | | |
| **402** | 56.1 | 32.9 | 176.1 | 119.8 | 8.089 | | | | | |
| **403** | 54.9 | 42.6 | 176.7 | 122.34 | 8.013 | | | | | |
| **404** | 57.3 | 39.6 | 174.5 | 120.35 | 8.097 | | | | | |
| **405** | 57.5 | 33.8 | 180.9 | 127.07 | 7.76 | | | | | |